TUBULAR STRUCTURES XIV

EDITOR:
LEROY GARDNER

CRC Press
Taylor & Francis Group
A BALKEMA BOOK

TUBULAR STRUCTURES XIV

PROCEEDINGS OF THE 14TH INTERNATIONAL SYMPOSIUM ON TUBULAR STRUCTURES, LONDON, UK, 12–14 SEPTEMBER 2012

Tubular Structures XIV

Editor

Leroy Gardner
Department of Civil and Environmental Engineering, Imperial College London, UK

CRC Press
Taylor & Francis Group
Boca Raton London New York Leiden

CRC Press is an imprint of the
Taylor & Francis Group, an **informa** business
A BALKEMA BOOK

CRC Press
Taylor & Francis Group
6000 Broken Sound Parkway NW, Suite 300
Boca Raton, FL 33487-2742

© 2012 by Taylor & Francis Group, LLC
CRC Press is an imprint of Taylor & Francis Group, an Informa business

No claim to original U.S. Government works
Version Date: 2012919

International Standard Book Number-13: 978-0-203-07310-0 (eBook - PDF)

This book contains information obtained from authentic and highly regarded sources. Reasonable efforts have been made to publish reliable data and information, but the author and publisher cannot assume responsibility for the validity of all materials or the consequences of their use. The authors and publishers have attempted to trace the copyright holders of all material reproduced in this publication and apologize to copyright holders if permission to publish in this form has not been obtained. If any copyright material has not been acknowledged please write and let us know so we may rectify in any future reprint.

Except as permitted under U.S. Copyright Law, no part of this book may be reprinted, reproduced, transmitted, or utilized in any form by any electronic, mechanical, or other means, now known or hereafter invented, including photocopying, microfilming, and recording, or in any information storage or retrieval system, without written permission from the publishers.

For permission to photocopy or use material electronically from this work, please access www.copyright.com (http://www.copyright.com/) or contact the Copyright Clearance Center, Inc. (CCC), 222 Rosewood Drive, Danvers, MA 01923, 978-750-8400. CCC is a not-for-profit organization that provides licenses and registration for a variety of users. For organizations that have been granted a photocopy license by the CCC, a separate system of payment has been arranged.

Trademark Notice: Product or corporate names may be trademarks or registered trademarks, and are used only for identification and explanation without intent to infringe.

Visit the Taylor & Francis Web site at
http://www.taylorandfrancis.com

and the CRC Press Web site at
http://www.crcpress.com

Tubular Structures XIV – Gardner (Ed.)
© 2012 Taylor & Francis Group, London, ISBN 978-0-415-62137-3

Table of contents

Connections

Elliptical hollow sections

Fatigue and fracture

Stainless steel

Fire

Trusses and arches

Structural behaviour

Tubular Structures XIV – Gardner (Ed.)
© 2012 Taylor & Francis Group, London, ISBN 978-0-415-62137-3

Preface

This book contains the papers presented at the *14th International Symposium on Tubular Structures* (ISTS14) held in London, UK, from September 12th to 14th, 2012. The Symposium, now regarded as the key international forum for the presentation and discussion of research, developments and applications in the field of tubular structures, was organised by Imperial College London in collaboration with the International Institute of Welding Subcommission XV-E and the Comité International pour le Développement et l'Étude de la Construction Tubulaire (CIDECT). The 13 previous symposia, held between 1984 and 2010, are described in the "Publications of the previous symposia on tubular structures" section of this book. Throughout its 28-year history the frequency, location and technical content of all the symposia has been determined by the IIW Subcommission XV-E on Tubular Structures.

The Symposium was sponsored by CIDECT, Tata Steel Tubes, Vallourec & Mannesmann Tubes (V&M), s^2 (space solutions) and Stalatube OY. It is their generous support that enabled the Symposium to take place and made it possible to continue the tradition of allowing presenting authors of papers to attend the Symposium without payment of registration fees.

A total of 95 technical papers, each of which has been reviewed by two international experts in the field, are included in the proceedings. One of these papers relates to the invited 'Kurobane Lecture', given, at this Symposium, by Prof. Xiao-Ling Zhao from the Monash University, Australia. Prof. Zhao was selected by the IIW Subcommission XV-E. The Kurobane Lecture is the International Symposium on Tubular Structures Keynote Address which was inaugurated at the ISTS8 in 1998. The Symposium also featured a special session to mark the 50th Anniversary of CIDECT, with structural and architectural contributions.

The editor would like to express his sincere gratitude to the reviewers of the papers for their hard work and expert opinions. The editor also wishes to thank the international programme committee and the local organising committee. Particular thanks are owed to Katherine Cashell, Jeanette Abela, Ulrika Wernmark, Stephanie O'Mahony and Betty Yue for their much appreciated efforts.

The information provided in this publication is the sole responsibility of the individual authors. It does not reflect the opinion of the editor, supporting associations, organisations or sponsors, and they are not responsible for any use that might be made of information appearing in this publication. Anyone making use of the contents of this book assumes all liability arising from such use.

The editor hopes that the contemporary applications, case studies, concepts, insights, overviews, research summaries, analyses and product developments described in this book provide some inspiration to architects, developers, contractors, engineers and fabricators to build ever more innovative and competitive tubular structures. This archival volume of the current "state of the art" will also serve as excellent reference material to academics, researchers, trade associations and manufacturers of hollow sections in the future.

Leroy Gardner
Editor
Imperial College London
2012

Tubular Structures XIV – Gardner (Ed.)
© 2012 Taylor & Francis Group, London, ISBN 978-0-415-62137-3

Publications of previous international symposia on tubular structures

B. Young (Ed.) 2010. *Tubular Structures XIII*, 13th International Symposium on Tubular Structures, Hong Kong, China, 2010. Boca Raton/London/New York/Leiden: CRC Press/Balkema.

Z.Y. Shen, Y.Y. Chen & X.Z. Zhao (Eds.) 2009. *Tubular Structures XII*, 12th International Symposium on Tubular Structures, Shanghai, China, 2008. Boca Raton/London/New York/Leiden: CRC Press/Balkema.

J.A. Packer & S. Willibald (Eds.) 2006. *Tubular Structures XI*, 11th International Symposium and IIW International Conference on Tubular Structures, Québec, Canada, 2006. London/Leiden/New York: Taylor & Francis (including A.A. Balkema Publishers).

M.A. Jaurrieta, A. Alonso & J.A. Chica (Eds.) 2003, *Tubular Structures X*, 10th International Symposium on Tubular Structures, Madrid, Spain, 2003. Rotterdam: A.A. Balkema Publishers.

R. Puthli & S. Herion (Eds.) 2001. *Tubular Structures IX*, 9th International Symposium on Tubular Structures, Düsseldorf, Germany, 2001. Rotterdam: A.A. Balkema Publishers.

Y.S. Choo & G.J. van der Vegte (Eds.) 1998. *Tubular Structures VIII*, 8th International Symposium on Tubular Structures, Singapore, 1998. Rotterdam: A.A. Balkema Publishers.

J. Farkas & K. Jármai (Eds.) 1996. *Tubular Structures VII*, 7th International Symposium on Tubular Structures, Miskolc, Hungary, 1996. Rotterdam: A.A. Balkema Publishers.

P. Grundy, A. Holgate & B. Wong (Eds.) 1994. *Tubular Structures VI*, 6th International Symposium on Tubular Structures, Melbourne, Australia, 1994. Rotterdam: A.A. Balkema Publishers.

M.G. Coutie & G. Davies (Eds.) 1993. *Tubular Structures V*. 5th International Symposium on Tubular Structures, Nottingham, United Kingdom, 1993. London/Glasgow/NewYork/Tokyo/Melbourne/Madras: E & FN Spon.

J. Wardenier & E. Panjeh Shahi (Eds.) 1991. *Tubular Structures*, 4th International Symposium on Tubular Structures, Delft, The Netherlands, 1991. Delft: Delft University Press.

E. Niemi & P. Mäkeläinen (Eds.) 1990. *Tubular Structures*, 3rd International Symposium on Tubular Structures, Lappeenranta, Finland, 1989. Essex: Elsevier Science Publishers Ltd.

Y. Kurobane & Y. Makino (Eds.) 1987. *Safety Criteria in Design of Tubular Structures*, 2nd International Symposium on Tubular Structures, Tokyo, Japan, 1986. Tokyo: Architectural Institute of Japan, IIW.

International Institute of Welding 1984. *Welding of Tubular Structures/Soudage des Structures Tubulaires*, 1st International Symposium on Tubular Structures, Boston, USA, 1984. Oxford/New York/Toronto/Sydney/Paris/Frankfurt: Pergamon Press.

Tubular Structures XIV – Gardner (Ed.)
© 2012 Taylor & Francis Group, London, ISBN 978-0-415-62137-3

Organisation

This volume contains the Proceedings of the 14th International Symposium on Tubular Structures – ISTS14 held in London, UK, from 12th to 14th September 2012. ISTS14 has been organised by Imperial College London, the International Institute of Welding (IIW) Subcommission XV-E and Comité International pour le Développement et l'Étude de la Construction Tubulaire (CIDECT).

INTERNATIONAL PROGRAMME COMMITTEE

J.A. Packer, *Chair*
University of Toronto, Toronto, Canada

M.A. Bradford
University of New South Wales, Sydney, Australia

Y.Y. Chen
Tongji University, Shanghai, China

S.P. Chiew
Nanyang Technological University, Singapore

Y.S. Choo
National University of Singapore, Singapore

L. Gardner
Imperial College London, UK

S. Herion
Karlsruhe Institute of Technology, Germany

G. Iglesias
Instituto para la Construccion Tubular, Spain

J.P. Jaspart
University of Liège, Belgium

M. Lefranc
Force Technology Norway, Sandvika, Norway

S. Maddox
The Welding Institute, Cambridge, UK

G. Marquis, *Chair of IIW Commission XIII*
The Aalto University School of Science and Technology, Finland

P.W. Marshall
MHP Systems Engineering, Houston, US

A.C. Nussbaumer
Ecole Polytechnique Fédérale de Lausanne, Switzerland

R.S. Puthli
Karlsruhe Institute of Technology, Germany

T. Schlafly
American Institute of Steel Construction, US

G.J. van der Vegte
Delft University of Technology, The Netherlands

J. Wardenier
Delft University of Technology and National University of Singapore, The Netherlands and Singapore

B. Young
The University of Hong Kong, Hong Kong, China

X.L. Zhao, *Chair of IIW Subcommission XV-E*
Monash University, Melbourne, Australia

LOCAL ORGANISING COMMITTEE

L. Gardner, *Chair*
Imperial College London, UK

J.M. Abela
Flint and Neill, UK

K.A. Cashell
The Steel Construction Institute, UK

T.M. Chan
University of Warwick, UK

A.Y. Elghazouli
Imperial College London, UK

D. Lam
University of Bradford, UK

T. Mustard
TATA Steel, UK

D.A. Nethercot
Imperial College London, UK

M.L. Romero
Universidad Politécnica de Valencia, Spain

M.A. Serrano
Universidad de Oviedo, Spain

M.A. Wadee
Imperial College London, UK

Y.C. Wang
University of Manchester, UK

P. Watson
TATA Steel, UK

S. Welch
TATA Steel, UK

S. Whitfield
TATA Steel, UK

© 2012 Taylor & Francis Group, London, ISBN 978-0-415-62137-3

Acknowledgements

The Organising Committee wish to express their sincere gratitude for the financial assistance from the following organisations: IIW (International Institute of Welding), CIDECT (Comité International pour le Développement et l'Étude de la Construction Tubulaire), Tata Steel Tubes, Vallourec & Mannesmann Tubes (V&M), s^2 (space solutions) and Stalatube OY.

The technical assistance of the IIW Subcommission XV-E is gratefully acknowledged. We are also thankful to the International Programme Committee as well as the members of the Local Organising Committee. Finally, the editor (who also served as a reviewer) wants to acknowledge the kind assistance of the following reviewers:

J.M. Abela
M.A. Bradford
D. Camotim
K.A. Cashell
R. Chacon
S. L. Chan
T.M. Chan
Y.Y. Chen
S.P. Chiew
Y.S. Choo
M. Eekhout
A.Y. Elghazouli
S. Herion
G. Iglesias
J. Krampen
D. Lam
M. Lefranc
R. Liew
P.W. Marshall
O. Mirza
T. Mustard
D.A. Nethercot
A.C. Nussbaumer
K. Ochi
J.A. Packer
R.S. Puthli
P. Ritakallio
M.L. Romero
B. Rossi
T. Schlafly
M.A. Serrano
N. Silvestre
M.A. Wadee
Y.C. Wang
P. Watson
J. Wardenier
S. Welch
S. Whitfield
T. Wilkinson
B. Young
X.L. Zhao

Leroy Gardner
Editor
Imperial College London

ISTS Kurobane lecture

Tubular Structures XIV – Gardner (Ed.)
© 2012 Taylor & Francis Group, London, ISBN 978-0-415-62137-3

Hybrid hollow structural sections

X.L. Zhao
Department of Civil Engineering, Monash University, Clayton, Australia

ABSTRACT: This paper gives a summary of recent developments in Hybrid Hollow Structural Sections (HSS). They are in the form of: concrete filled HSS; concrete filled double skin HSS; FRP (fibre reinforced polymer) strengthened HSS with/without concrete filling; FRP, concrete and HSS double skin sections. The existing research, main findings and future work are presented.

1 INTRODUCTION

Different abbreviations were used in the literature to describe various types of metal profile with a hollow tubular cross-section, such as SHS for Square Hollow Section, RHS for Rectangular Hollow Section, CHS for Circular Hollow Section, EHS for Elliptical Hollow Section, OHS for Oval Hollow Section and HSS for Hollow Structural Section. The abbreviation "HSS" is adopted in this paper to represent the general term **H**ollow **S**tructural **S**ection.

HSS could be used together with other materials to form hybrid HSS. For example, they could be in the form of concrete filled HSS, concrete filled double skin HSS, FRP (fibre reinforced polymer) strengthened HSS with/without concrete filling, FRP-concrete-HSS double skin sections.

There is an increasing trend in using concrete-filled HSS in recent decades, such as in industrial buildings, structural frames and supports, electricity transmission poles, spatial construction, high-rise or super high-rise buildings and bridge structures (Zhao et al. 2010a).

It is well known that hollow structural sections have many advantages over conventional open sections, such as excellent strength properties (compression, bending and torsion), lower drag coefficients, less painting area, aesthetic merits and the potential of void filling (Wardenier et al. 2010). Compared with unfilled tubes, concrete-filled tubes demonstrate increased load carrying capacity, ductility, energy absorption during earthquakes as well as increased fire resistance. For example, for a column with an effective buckling length L_e of 5 m, mass of steel section of 60 kg/m and concrete core strength of 40 MPa, the compression capacity increases about 50% due to concrete-filling. The increase in rotation capacity under pure bending due to concrete filling was found to be 300% (Zhao and Grzebieta 1999). For concrete-filled RHS subjected to large deformation cyclic bending the failure modes changed from localized cracking to an outward folding mechanism. The fire resistance of unprotected CHS or RHS columns is normally found to be less than 30 minutes (Twilt et al. 1996). Concrete filling can increase the fire resistance up to 2 or 3 hours (Han et al. 2003a, Lu et al. 2010).

FRP (fibre reinforced polymer) has high strength to weight ratio, resistance to corrosion and usually to environmental degradation (Hollaway and Teng 2008). While FRP has been widely used in strengthening aircraft and more recently concrete structures (e.g. Teng et al. 2002, Baker et al. 2002, Rizkalla et al. 2003, Oehlers and Seracino 2004), it has not been widely applied to steel structures. The knowledge of repairing aircraft cannot be directly applied to steel structures in the Civil, Offshore and Mining industry because the materials used are very different. The existing knowledge of CFRP-concrete composite systems may not be applicable to CFRP-steel systems because of the distinct difference between the debonding mechanism of a CFRP-steel system and a CFRP-concrete system, and the unique failure modes for steel members and connections.

It has been shown (Hollaway and Cadei 2002, Zhao and Zhang 2007, Schnerch et al. 2007) that FRP has great potential to strengthen steel structures including HSS. The benefit of using FRP together with hollow structural sections is summarized in Table 1. It is clear that FRP can improve the performance of HSS in terms of strength, ductility, energy absorption and fatigue life.

The existing research, main findings and future work on hybrid HSS are presented in this paper.

2 HOLLOW STRUCTURAL SECTIONS AND CONCRETE

2.1 *Concrete filled HSS*

2.1.1 *Existing research and main findings*

2.1.1.1 *General*

The major research on CFST members and connections was summarized in CIDECT Design Guides No.4 (Twilt et al. 1996), No.5 (Bergmann et al. 1995),

Table 1. Improved performance of HSS due to FRP strengthening.

Configuration and FRP used (Young's Modulus)	Improved performance	Reference
CHS and RHS beams in bending, CFRP sheet (from 50 GPa to 270 GPa)	• Increased moment capacity and ductility in general • For circular hollow sections, slender sections (which cannot reach first yield due to local buckling) could become non-compact sections (which can reach plastic moment capacity)	Haedir et al. (2009), Photiou et al. (2006), Seica and Packer (2007)
CHS and RHS columns in compression, CFRP sheet (230 GPa) and GFRP sheet (80 GPa)	• Compression strength increases about 20% to 70% if CFRP is used • Compression strength increases about 5% to 10% if GFRP is used • Increased energy absorption under large deformation compression force	Shaat and Fam (2006), Bambach and Elchalakani (2007), Teng and Hu (2007), Haedir and Zhao (2011)
RHS subject to concentrated forces through a bearing plate, CFRP Plate (165 GPa)	• Web buckling capacity of cold-formed rectangular hollow sections (RHS) increases about 1.5 to 2.5 times • Web buckling capacity of aluminium RHS increases up to 3.5 times • Web buckling capacity of stainless steel RHS increases up to 50%	Zhao et al. (2006), Wu et al. (2012), Islam and Young (2010, 2011)
RHS subject to concentrated forces through a welded branch, GFRP plate (12.4 GPa)	Web buckling capacity increases about 50%.	Fam and Aguilera (2012)
Welded VHS tubes in tension, CFRP sheet (230 GPa)	Recovered the full yield capacity, which was 50% lost due to HAZ softening, of welded very high strength steel tubes.	Jiao and Zhao (2004)
Welded aluminium K-joints under static load, GFRP sheet (30 GPa) and CFRP sheet (79 GPa)	• Recovered the full connection capacity of aluminium K-joints if CFRP is used or about 80% connection capacity if GFRP is used. • The retrofitted connection with GFRP reinforcement achieved 1.17 to 1.25 times the capacity of the welded aluminum connection without any visible cracks.	Fam et al. (2006) Pantelides et al. (2003)
Welded cross-beam connections subject to fatigue loading, CFRP sheet (230 GPa)	Fatigue life extends to twice the original fatigue life.	Xiao and Zhao (2012)
Welded aluminium K-joints subject to fatigue loading, GFRP sheet (30 GPa)	The repaired connections exceeded the fatigue limit of the aluminium welded connections with no known cracks. The repaired connections with 90% of the weld removed satisfied the constant amplitude fatigue limit threshold.	Nadauld and Pantelides (2007)
CFST columns, CFRP sheet (65 GPa)	• The static strength increased by 55% and 140% when the number of CFRP layers was 2 and 4 respectively • Increased ductility to resist cyclic loading	Xiao et al. (2005)
CFST columns, CFRP sheet (247 GPa)	Recovered certain compression strength of concrete-filled tubes after exposure to fire	Tao et al. (2007a, 2008)
Hybrid FRP–concrete–steel double skin columns, GFRP tube (80 GPa)	The local buckling of the inner steel tube is either delayed or suppressed by the surrounding concrete, leading to a very ductile response.	Teng et al. (2007)

No.7 (Dutta et al. 1998) and No.9 (Kurobane et al. 2005), Wang (2002), Nethercot (2003), Wardenier et al. (2010) and Zhao et al. (2010a). A list of comprehensive references has been given in Zhao et al. (2010a). A brief summary of the design of CFST members using different standards is given in this section in terms of bending, compression, combined actions and fire resistance.

2.1.1.2 *CFST members in bending*

The nominal moment capacity given in the following standards BS5400 (2005), AS5100 (2004), EC4 (2004), DBJ13-51 (2003) is based on simple plastic theory although slightly different stress distributions are adopted. The difference in the nominal moment capacities among the 4 standards mentioned above is found to be less than 2.5% for some typical HSS and concrete (Zhao et al. 2010a). The design capacity difference varies from 7% to 24%, which is mainly due to different material property factors or capacity factors adopted in different standards. The nominal moment capacity for concrete filled CHS and RHS beams can be estimated as follows:

$$M_{CFST,CHS} = 4 \cdot f_y \cdot t \cdot r_m^2 \cdot \cos\gamma_0 + \frac{2}{3} \cdot f_c \cdot r_i^3 \cdot \cos^3\gamma_0 \quad (1a)$$

$$r_m = \frac{d-t}{2} \quad (1b)$$

$$r_i = \frac{d-2 \cdot t}{2} \quad (1c)$$

$$\gamma_0 = \frac{\pi}{2} \cdot F_{CHS} \quad (1d)$$

$$F_{CHS} \approx \frac{\frac{1}{8} \cdot \frac{f_c}{f_y} \cdot \frac{d}{t}}{1 + \frac{1}{4} \cdot \frac{f_c}{f_y} \cdot \frac{d}{t}} \quad (1e)$$

$$M_{CFST,RHS} = f_y \cdot t \cdot \left[B \cdot (D-t) + \frac{1}{2} \cdot (D - 2 \cdot t)^2 \right]$$

$$+ f_y \cdot t \cdot \frac{1}{2} \cdot (D - 2 \cdot t)^2 \cdot (1 - F_{RHS})^2$$

$$+ \frac{1}{2} \cdot (B - 2 \cdot t) \cdot d_n^2 \cdot f_c \quad (2a)$$

$$d_n = \left(\frac{D - 2 \cdot t}{2} \right) \cdot F_{RHS} \quad (2b)$$

$$F_{RHS} \approx \frac{1}{1 + \frac{1}{4} \cdot \frac{f_c}{f_y} \cdot \frac{B}{t}} \quad (2c)$$

where f_y is the yield stress of HSS, f_c is concrete cylinder strength, d, D, B and t are defined in Figure 1.

2.1.1.3 *CFST members in compression*

Different standards (e.g. AIJ 1997, AISC 2010, ACI 2002, BS5400, EC4, DBJ13-51) have different approaches in dealing with the design of CFST compressive section capacity, as shown in Table 2.

It was found by Zhao et al. (2010a) that the nominal section capacity predicted by BS5400 is slightly higher than those from AS5100 (2004), EC4, DBJ13-51, whereas the difference in nominal capacities among the other 3 standards is within 4% for some typical sections. The difference between the design section capacities varies from 1% to 20% among the standards due to different material property factors or capacity factors adopted in different standards.

For CFST column design the approach is very similar, i.e. section capacity (N_s) multiplied by a reduction factor (φ).

$$N_c = \varphi N_s \quad (3)$$

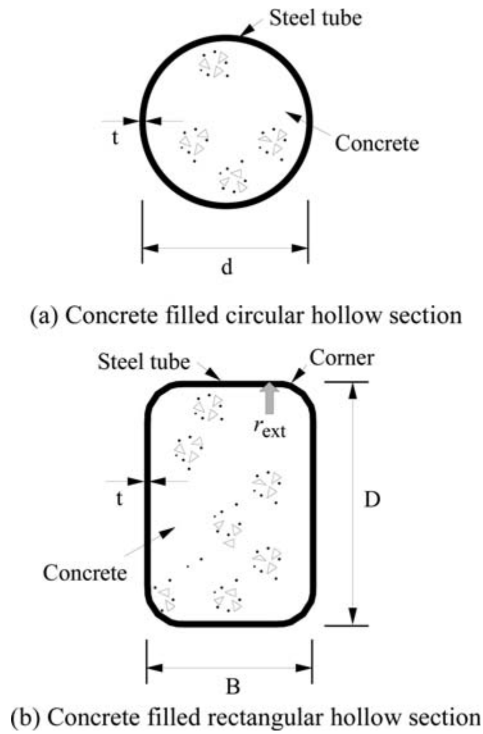

Figure 1. Concrete filled Hollow Structural Section (HSS).

Different column curves are adopted in different standards to determine the reduction factor φ which is basically a function of column slenderness, except for BS5400 where an extra reduction factor of 0.85 needs to be considered. The column slenderness depends mainly on the column length, boundary conditions at column ends and yield stress. Some typical column curves are summarized in Zhao et al. (2010a). The maximum difference in column design capacity among the four standards mentioned above is about 10% to 20% for some typical sections.

2.1.1.4 *CFST members subject to combined bending and compression*

The stress distribution in CFST members subjected to combined bending and compression (also called CFST beam-columns) has four typical cases corresponding to various level of axial force versus the level of bending moment. The four typical stress distributions determine four typical locations of the neutral axis in CFST beam-columns, which in turn correspond to the four key points (A, B, C and D) in the interaction diagrams defined in Figure 2. The interaction diagram for an unfilled HSS beam-column is also shown in Figure 2 as a dashed line connecting points A and B. The part CDB in the interaction diagram is unique for CFST members due to the contribution of concrete.

Three straight lines (AC, CD and DB) are adopted in Eurocode 4 to simplify the interaction diagram. In DBJ13-51, a combination of a straight line (AC)

Table 2. Design approaches for section capacity of CFST HSS.

Code	Method	Confinement considered (Yes or No)	Concrete strength (Cube or Cylinder)
AIJ	Superposition	No	Cylinder
AISC	Equivalent steel section with modified yield stress	No	Cylinder
ACI	RC method by converting steel tube into equivalent "reinforced bars".	No	Cylinder
BS5400	Composite section with modified concrete strength	Yes	Cube
EC4	Composite section with modified concrete strength	Yes	Cylinder
DBJ13-51	Treat the whole section as one material with modified stress	Yes	Cube

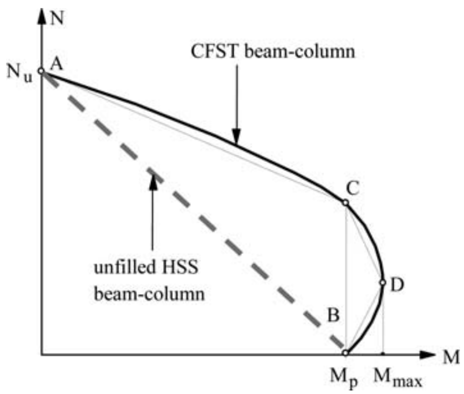

Figure 2. Schematic view of interaction diagram.

and a curve (CDB) is adopted. In BS5400 it is specified that the maximum bending moment should not exceed the ultimate moment capacity of CFST members subject to pure bending. Therefore the interaction diagram in BS5400 only consists of two parts (AC which is a straight line for CFST RHS and a curve for CFST CHS, and CB which is a vertical cut-off line). The turning point C in EC4 and BS5400 has the same value, whereas a different value is adopted in DBJ13-51. DBJ13-51 also gives two separate interaction diagrams, one for section capacity and the other for member capacity in a non-dimensional format. Design examples can be found in Zhao et al. (2010a).

2.1.1.5 *Fire resistance of CFST columns*

Three levels of assessment of fire resistance of unprotected CFST columns were presented in CIDECT Design Guide No. 4 (Twilt et al. 1995). Level 1 assessment utilizes a simple design table to determine the minimum cross-sectional dimensions, reinforcement ratios and location of reinforcement bars to satisfy a certain degree of utilization (μ) and fire resistance (R30 minutes to R180 minutes). Level 2 assessment utilizes the concept of a buckling curve for CFST columns for different fire classes. It recommends a buckling curve for given values of tube size, steel grade, fire class, concrete grade and the amount of reinforcement. The effective buckling length factor of columns in braced frames is between 0.5 and 0.7 depending on the boundary conditions (Twilt et al. 1995). A conservative value of 0.7 may be used for estimating the bucking length of columns on the top floor and for the columns at the edge of a building with only one adjacent beam. The validity range of level 2 assessment can be summarised as follows: Fire classes are R60, R90 and R120, Concrete grades C20, C30 and C40, CHS diameter $d = 219$ to 406 mm and thickness $t = 4.5$ to 6.3 mm, SHS width $B = 180$ to 400 mm and thickness $t = 6.3$ to 10 mm. Level 3 assessment includes a complete thermal and mechanical analysis with real boundary conditions. This is the most sophisticated level. It requires expert knowledge and time in handling necessary computer programs.

The preferred solution in China to achieve sufficient fire resistance is to use plain concrete-filled tubes with external fire protection rather than using steel bar or fibre reinforced concrete. The formulae in DBJ13-51 to calculate the thickness of fire protection materials are based on the research by Han et al. (2003a, 2003b), which can be expressed as a function of fire load ratio, fire resistance, perimeter of the column and column slenderness. It was demonstrated by Han and Yang (2007) that the protection thickness could be reduced from 50 mm (based on conventional code for fire protection of steel columns) to 10 mm (based on DBJ13-51) for two high rise buildings: SEG Plaza (291.6 m in height) and Wuhan International Stock Centre (242.9 m in height) requiring 180 minutes of fire resistance, due to concrete-filling.

An extensive research program was carried out in North America on CFST HSS columns under fire (Lie and Chabot 1990, Kodur and Lie 1996, Lie and Stringer 1994, Kodur 1998, 1999), with three types of concrete-filling, namely plain concrete, steel bar-reinforced concrete and steel fibre-reinforced concrete. A formula was proposed (Lie and Stringer 1994, Kodur 1999) to calculate the fire resistance of CFST columns as shown in Eq. (6).

$$R = f\frac{(f_c' + 20)}{(KL - 1000)} D^2 \sqrt{\frac{D}{P}} \tag{4}$$

where R is the fire resistance in minutes, f_c' is the specified 28-day cylinder concrete strength in MPa, D is the outside diameter or width of the column in mm, P is the applied axial load in kN, K is the effective length factor, L is the column length in mm and f is a parameter that depends on the type of concrete filling (plain, bar-reinforced or fibre-reinforced), the cross-sectional shape (circular or square), the type of aggregate (carbonate or siliceous), the percentage of steel reinforcement (p_r) and the thickness of concrete cover. Values of the parameter f are summarized in Table 7.5 of Zhao et al. (2010a).

2.1.2 *Future work*

The future work in CFST HSS is needed in the following areas: (i) new materials such as stainless steel tubes, high strength steel tubes filled with self-consolidating concrete, geopolymeric recycled concrete and ultra high strength concrete (e.g. Uy 2008, Lu et al. 2009, Uy et al. 2011, Shi et al. 2012, Liew et al. 2012); (ii) new structural elements such as EHS, very slender CFST columns, tapered CFST columns and CFST fabricated section utilizing very high strength steel tubes as corners (e.g. Yang et al. 2008, Zhao and Packer 2009, Espinos et al. 2011, Han et al. 2010, An et al. 2012, Mashiri et al. 2011); (iii) connections and frames (e.g. Kurobane et al. 2005, Nie et al. 2006, Herrera et al.2008, Han et al. 2008, 2009, Wang et al. 2009); (iv) fatigue resistance of CFST joints (e.g. Udomworarat et al. 2000, Gu et al. 2008, Tong et al. 2008, Mashiri and Zhao 2010); (v) earthquake followed by fire (e.g. Song et al. 2012); and (vi) CFST subject to impact and blast loading as well as progressive collapse (e.g. Bambach et al. 2008, Fujikura et al. 2008, Remennikov et al. 2011, Qu et al. 2011, Kang et al. 2012, Nethercot 2009).

2.2 *Concrete filled double skin HSS*

2.2.1 *Existing research and main findings*

Concrete filled double skin hollow structural sections have four possible combinations of CHS and RHS as the outer and inner tubes. Two examples are shown in Figure 3.

Most of the existing research on CFDST has been summarized in Zhao and Han (2006) and Chapter 9.4 of Zhao et al. (2010a).

The ultimate moment capacity of CFDST (M_{CFDST}) can be estimated using the sum of the section capacity of an unfilled inner tube (M_{inner}) and that of an outer tube with concrete component, i.e.

$$M_{CFDST} = M_{inner} + M_{outer-with-concrete} \tag{5}$$

where $M_{outer\text{-}with\text{-}concrete}$ can be derived in a similar manner as that for CFST, i.e. adopting simple plastic

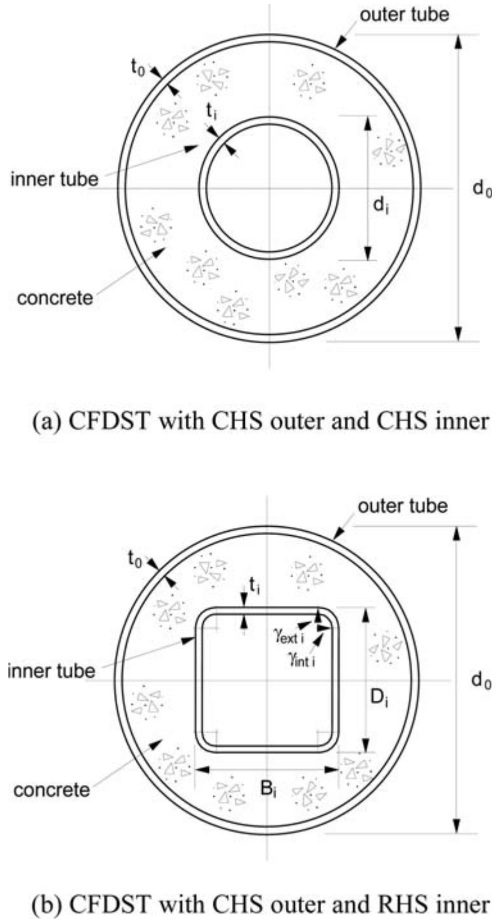

(a) CFDST with CHS outer and CHS inner

(b) CFDST with CHS outer and RHS inner

Figure 3. Concrete filled double skin Hollow Structural Section (HSS).

theory to find out the position of the neutral axis, then adding the moment contribution of each force through the cross-section. Formulae for M_{CFDST} were given in Zhao and Choi (2010) for four possible combinations of CHS and RHS as the outer and inner tubes.

For CFDST sections in compression, local buckling is delayed or eliminated, with a significant increase in load carrying capacity and ductility compared with those of the outer tube alone, as shown in Figure 4. The section capacity of a CFDST can be estimated using the superposition method; i.e. a sum of capacities of the outer tube, inner tube and concrete.

For CFDST subject to combined bending and compressive forces, the interaction formulae were derived by Han et al. (2004), Tao et al. (2004). They are similar to those given by Han et al. (2001) for concrete-filled beam-columns. They were summarised in Chapter 9.4.2.3 of Zhao et al. (2010a).

If other conditions are kept the same, the fire endurance of CFDST columns was found to be slightly better than tubular columns fully filled with concrete

(i) CHS outer with d_o/t_o of 55

(ii) CFDST with d_o/t_o of 55
(a) Failure mode

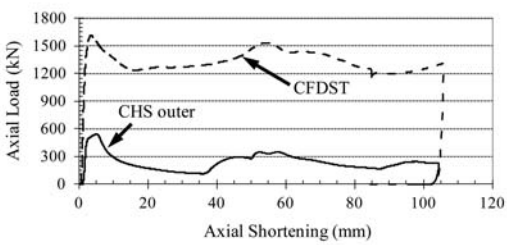

(b) Axial load versus shortening curve (with d_o/t_o of 55)

Figure 4. Typical behaviour of CFDST in compression versus that of outer steel tube (adapted from Zhao et al. 2010b).

(Yang and Han 2008, Lu et al. 2010). This is mainly because of the relatively low temperature in the inner steel tube. Therefore the fire resistance of a CFDST column could be conservatively estimated by treating it as a CFST column.

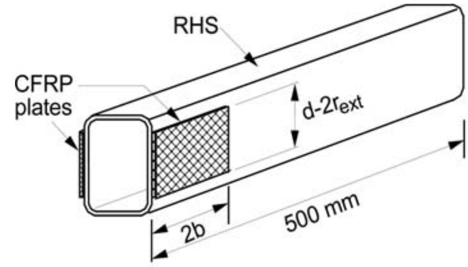

(a)Type O (Outside web strengthening)

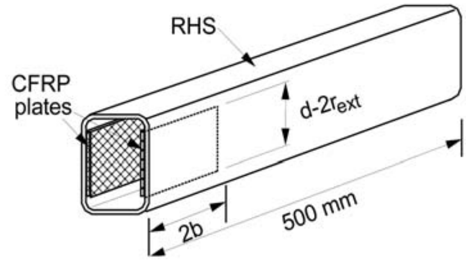

(b) Type I (Inside web strengthening)

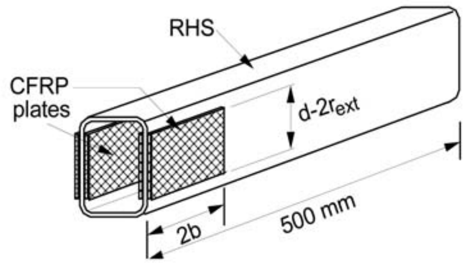

(c)Type B (Both sides strengthening)

Figure 5. Types of strengthening for Rectangular Hollow Section (RHS) webs (adapted from Zhao et al. 2006).

2.2.2 *Future work*

The future work described in Section 2.1.2 for CFST HSS equally applies to CFDST HSS with additional references relevant to CFDST subject to dynamic loading shown below: e.g. Nakanishi et al. (1999), Han et al. (2006) and Corbett et al. (1990).

3 HOLLOW STRUCTURAL SECTION MEMBERS AND FRP

3.1 *CFRP strengthened RHS webs*

Web crippling failure becomes critical at the loading points or supports of beams where concentrated forces are applied. Zhao et al. (2006) conducted a study on FRP strengthening of cold-formed rectangular hollow sections (RHS) subject to an end bearing force. Three types of strengthening scheme were adopted as shown in Figure 5.

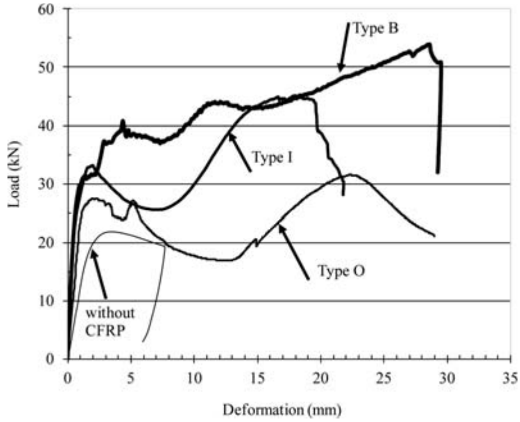

Figure 6. Typical load deformation curves for cold-formed RHS $100 \times 50 \times 2$ with various types of strengthening (adapted from Zhao et al. 2006).

Typical load-deformation behaviour is presented in Figure 6, which clearly demonstrates the increased web crippling capacity and ductility. The main reasons for the improved behaviour are the increased restraint against web rotation and the change of failure mode from web bucking to web yielding. Design formulae were proposed (Zhao et al. 2006) to predict the improved web buckling capacity, which are similar to those for un-strengthened webs, but with reduced effective length factor. Similar research was also conducted on aluminium RHS and stainless steel RHS by Wu et al. (2012) and Islam and Young (2010, 2011). Recently Fam and Aguilera (2012) carried out tests on GFRP (glass fibre reinforced polymer) strengthened RHS webs in a welded T-joint.

3.2 *CFRP strengthened HSS in compression*

Hybrid GFRP-CHS columns were studied by Teng and Hu (2007), whereas CFRP-CHS columns were investigated by Haedir and Zhao (2011). The "elephant foot" buckling mode in CHS is delayed or eliminated by FRP. More increase in ultimate load carrying capacity was found with CFRP than that with GFRP.

Tests were carried out on hybrid CFRP-SHS columns by Shaat and Fam (2006). Failure of retrofitted SHS columns was via overall buckling followed by secondary local buckling associated with delamination and crushing of the CFRP. Bambach and Elchalakani (2007) conducted quasi-static tests on CFRP reinforced SHS under large deformation axial compression. Multiple folding mechanisms were observed (see Figure 7) with an increased ultimate strength and energy absorption. The FE work by Shaat and Fam (2007) revealed that the axial strength of CFRP-SHS columns is not sensitive to initial imperfection of SHS. Bambach and Elchalakani (2007) applied a plastic mechanism analysis to reasonably predict the unloading curves of such hybrid columns.

Figure 7. Typical failure mode of SHS and CFRP-SHS subject to large deformation axial loading (Bambach and Elchalakani 2007).

It should be noted that different combinations of longitudinal and transverse fibres were adopted in the above studies.

The design of CFRP-SHS and CFRP-CHS columns was presented in Bambach et al. (2009a) and Haedir and Zhao (2011).

3.3 *CFRP strengthened HSS in bending*

Haedir et al. (2009) carried out tests on CFRP-CHS beams in pure bending. Both longitudinal and transverse CFRP sheets were applied. It was found that the longitudinal CFRP layers contributed more to the increase in moment capacity, whereas the hoop layers played a more important role in restraining or delaying the local buckling. Slender CHS could become a non-compact CHS when strengthened by CFRP. The rotation capacity of non-compact CHS also increased significantly. Analytical models for determining the ultimate moment capacity and for predicting the moment-curvature response of CFRP-reinforced steel CHS beams were developed by Haedir et al. (2011). The nonlinear model accounted for material properties of the steel and CFRP, volume fractions of the fibre and adhesive, amount of CFRP, and a wider range of section slenderness. Design rules for predicting the strength of composite CHS under bending were also proposed (Haedir and Zhao 2012). Similar work was done by Seica and Packer (2007), where curing of the specimens was performed both in air and in seawater. A slightly lower increase in the ultimate moment capacity was observed for specimens cured in seawater.

Photiou et al. (2006) conducted a study on CFRP and GFRP strengthening of artificially degraded steel RHS beams. The degrading was done through machining the thickness of the tension flange. All the upgraded beams reached the plastic collapse load of the original undamaged RHS beams. It was recorded that the steel beams can be deformed well into their plastic regions. However it is difficult to quantify the achieved rotation capacity since the non-dimensional moment-curvature curves were not reported in the paper.

3.4 *Future work*

There is a need to conduct more tests to cover wider ranges of parameters, such as steel tubular section sizes, CFRP modulus, adhesive types and thickness. There is a lack of detailed FE simulation of web buckling with FRP strengthening (Fernando et al. 2009). More research is needed to understand the behaviour of FRP strengthened HSS subject to impact and blast loading (Bambach et al. 2009b), as well as harsh environmental conditions (Seica and Packer 2007).

4 HOLLOW STRUCTURAL SECTION JOINTS AND FRP

4.1 *CFRP strengthened welded VHS joints*

There is a significant (up to 50%) strength reduction in the HAZ (heat affected zone) of very high strength (VHS) tubes after welding. Jiao and Zhao (2004) investigated the behaviour of CFRP strengthened butt-welded VHS tubes. Significant strength increase was obtained for CFRP strengthened butt-welded VHS tubes. The full yield capacity of VHS steel tubes was recovered when the bond length reachedabout 50 mm.

4.2 *FRP strengthened aluminium CHS K-joints*

Welded aluminum K-joints with different damage levels (e.g. about 25%, 65% and 100% of the total welded length) were repaired by using GFRP (Pantelides et al. 2003). The repaired joints with a damage level up to 65% reached capacities about 20% higher than those without cracks, whereas the repaired joints with a damage level of 100% recovered 95 to 99% of the original capacity. A similar study was carried out by Fam et al. (2006) on using CFRP and GFRP to repair cracked welded aluminum K-joints with a damage level of 90%. The full strength of the welded joints could be restored if CFRP was used, whereas about 80% of the capacity was restored by using GFRP.

Nadauld and Pantelides (2007) studied the fatigue performance of GFRP-strengthened aluminium K-joints with partially fractured branch-to-chord welds. The repaired joints exceeded the fatigue limit of the welded aluminium K-joints without damage. The same type of K-joints with 90% of the weld removed were repaired using GFRP. Such repaired joints satisfied the constant amplitude fatigue limit threshold. A cumulative damage index was established which led to a fatigue reduction factor for the rehabilitation design of cracked aluminum connections using GFRP composites.

4.3 *Future work*

There is a need to develop strengthening techniques for various types of welded HSS joints subject to fatigue loading, such as cross-beam joints (Xiao and Zhao 2012), cast steel to HSS joints. Theoretical modeling and numerical simulation are also necessary.

5 HOLLOW STRUCTURAL SECTION, CONCRETE AND FRP

5.1 *CFRP strengthened CFST*

Xiao et al. (2005) studied CFST columns confined by CFRP at critical locations to avoid plastic hinges, hence soft storey behaviour, under earthquake loading. A gap (made with 1-mm-thick soft foam tapes affixed on the surface of the steel tube) was introduced between the CFRP and the tubular column to delay the engagement of the CFRP, to achieve both increased strength and ductility. The work on using CFRP to strengthen CFST SHS and CHS columns is still very limited although attempts were made by some researchers (Tao et al. 2007b, Sun et al. 2008, Park et al. 2010). Research has been undertaken (Tao et al. 2008) to determine the effectiveness of using FRP composites to repair damaged CFST columns, particularly for damage due to fire exposure. These results revealed that CFRP gave reasonable repair for specimens with a low level of exposure to fire.

5.2 *Hybrid double skin section*

Teng et al. (2007) developed a hybrid FRP–concrete–steel double-skin tubular column (see Figure 8 for an example). The test results confirmed that the concrete in the new column is very effectively confined by the two tubes and the local buckling of the inner

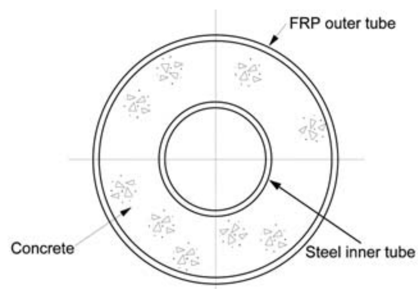

(a) FRP-concrete-steel hybrid double skin section (without eccentricity)

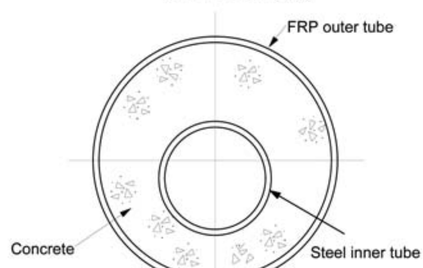

(b) FRP-concrete-steel hybrid double skin section (with eccentricity)

Figure 8. Schematic view of FRP-concrete-steel double skin section, e.g. CHS FRP as outer tube and steel CHS as inner tube (adapted from Teng et al. 2007).

steel tube is either delayed or suppressed by the surrounding concrete, leading to a very ductile response. When such hybrid sections are used as beams, the inner steel tube could be shifted towards the tensile side (see Figure 8(b)). Such beams were found to have a very ductile behaviour. The GFRP tube enhances the structural behaviour by providing both confinement to the concrete and additional shear resistance.

5.3 *Future work*

More tests are needed on FRP-CFST columns and FRP-concrete-HSS hybrid columns with wider ranges of parameters. There is a need to develop analytical models, numerical simulation and a design guide for such hybrid sections under static and dynamic loading (Shan et al. 2007).

6 CONCLUSIONS

This paper has presented a summary of recent developments in hybrid hollow structural sections (HSS) in the form of: concrete filled HSS; concrete filled double skin HSS; FRP strengthened HSS with/without concrete filling; FRP, concrete and HSS double skin sections. The benefits of hybrid HSS include increased strength, ductility, fire resistance, energy absorption and fatigue life. The existing research, main findings and future work for each type of HSS have been described. A comprehensive list of references in this field has been given.

ACKNOWLEDGEMENT

The author wishes to thank the following professors in the field of hollow structural sections and FRP strengthening for their advice, collaboration and friendship: Prof. Greg Hancock at the University of Sydney, Prof. Jeff Packer at the University of Toronto, Prof. Jaap Wardenier at Delft University of Technology, Prof. Lin-Hai Han at Tsinghua University, Prof. Le-Wei Tong at Tongji University, Prof. Qing-Yuan Wang at Sichuan University, Prof. Jin-Guang Teng at Hong Kong Polytechnic University, Prof. Sami Rizkalla at North Carolina State University and Prof. Len Hollaway at Surrey University. The encouragement and support from members of IIW XV-E subcommission and CIDECT are deeply appreciated. The author wishes to dedicate this paper to the late Professor Yoshi Kurobane who made such a significant contribution to the research into hollow structural sections.

REFERENCES

ACI. 2002. *Building code requirements for structural concrete and commentary*. ACI 318M-02, Michigan: American Concrete Institute.

AIJ. 1997. *Recommendations for design and construction of concrete filled steel tubular structures.* Tokyo: Architectural Institute of Japan.

AISC. 2010. *Specification for structural steel buildings*. ANSI/AISC 360-10, Chicago: American Institute of Steel Construction.

An, Y.F., Han, X.L. & Zhao, X.L. 2012. Behaviour and design calculations on very slender thin-walled CFST columns. *Thin-Walled Structures* 53(6): 161–175.

AS5100. 2004. *Bridge design – Steel and composite construction*. Australian Standard AS 5100, Sydney: Standards Australia.

Baker, A.A., Rose, L.R.F. & Jones, R. 2002. *Advances in the bonded composite repair of metallic aircraft structure*. Amsterdam: Elsevier.

Bambach, M.R. & Elchalakani M. 2007. Plastic mechanism analysis of steel SHS strengthened with CFRP under large axial deformation. *Thin-Walled Structures* 45(2): 159–170.

Bambach, M.R., Jama, H., Zhao, X.L. & Grzebieta, R.H. 2008. Hollow and concrete filled steel hollow sections under transverse impact loads. *Engineering Structures* 30(10): 2859–2870.

Bambach, M.R., Jama, H. & Elchalakani, M. 2009a. Axial capacity and design of thin-walled steel SHS strengthened with CFRP. *Thin-Walled Structures* 47(10): 1112–1121.

Bambach, M.R., Elchlakani, M. & Zhao, X.L. 2009b. Composite steel–CFRP SHS tubes under axial impact. *Composite Structures* 87(3): 282–292.

Bergmann, R., Matsui, C., Meinsma, C. & Dutta, D. 1995. *Design guide for concrete filled hollow section columns under static and seismic loading*. Köln: TÜV-Verlag.

BS5400. 2005. *Steel, concrete and composite bridges*. BS5400, Part 5: Code of practice for design of composite bridges. London: British Standards Institution.

Corbett, G., Reid, S. & Al-Hassani, S. 1990. Resistance of steel-concrete sandwich tubes to penetration. *International Journal of Impact Engineering* 9(2): 191–203.

DBJ13-51. 2003. *Technical specification for concrete-filled steel tubular structures*. Fuzhou: The Construction Department of Fujian Province.

Dutta, D., Wardenier, J., Yeomans, N., Sakae, K., Bucak, Ö & Packer, J.A. 1998. *Design guide for fabrication, assembly and erection of hollow section structures*. Köln: TÜV-Verlag.

EC 4. 2004. *Design of composite steel and concrete structures – Part 1.1: General rules and rules for buildings.* EN 1994-1-1:2004, December 2004, Brussels: European Committee for Standardization.

Espinos, A., Gardner, L., Romero, M.L. & Hospitaler, A. 2011. Fire behaviour of concrete filled elliptical steel columns. *Thin-Walled Structures* 49(2): 239–255.

Fam, A., Witt, S. & Rizkalla, S. 2006. Repair of damaged aluminum truss joints of highway overhead sign structures using FRP. *Construction and Building Materials* 20(10): 948–956.

Fam, A. & Aguilera, J. 2012. Strengthening T-joints of thin-walled rectangular hollow steel sections (HSS) using GFRP plates. *FRP International* 8(6): 3–6.

Fernando, D., Yu, T., Teng J.G. & Zhao X.L. 2009. CFRP strengthening of rectangular steel tubes subjected to end bearing loads: effect of adhesive properties and finite element modelling. *Thin-Walled Structures* 47(10): 1020–1028.

Fujikura, S., Bruneau, M., & Lopez-Garcia, D. 2008. Experimental investigation of multihazard resistant bridge piers having concrete-filled steel tube under blast loading. *Journal of Bridge Engineering* 13(6): 586–594.

Gu, M., Tong, L.W., Zhao, X.L. & Lin, X.G. 2008. Stress intensity factors of surface cracks in welded T-joints between CHS brace and concrete-filled chord. *Proceedings of the 12th International Symposium on Tubular Structures*, Shanghai, China, October, pp. 359–366.

Haedir, J., Bambach, M.R., Zhao X.L. & Grzebieta R.H. 2009. Strength of circular hollow sections (CHS) tubular beams externally reinforced by carbon FRP sheets in pure bending. *Thin-Walled Structures* 47 (10): 1136–1147.

Haedir J. & Zhao, X.L. 2011. Design of short CFRP-reinforced steel tubular columns. *Journal of Constructional Steel Research* 67(3): 497–509.

Haedir J., Zhao, X.L., Grzebieta,R. H. & Bambach, M. 2011. Non-linear analysis to predict the moment-curvature response of CFRP-strengthened steel CHS tubular beams. *Thin-Walled Structures* 49(8): 997–1006.

Haedir J. & Zhao, X.L. 2012. Design of CFRP-strengthened steel CHS tubular beams. *Journal of Constructional Steel Research* in press, doi: 10.1016/j.jcsr.2011.12.004

Han, L.H., Zhao, X.L, Yang, Y.F. & Feng, J.B. 2003a. Experimental study and calculation of fire resistance of concrete-filled hollow section columns. *Journal of Structural Engineering* 129(3): 346–356.

Han, L.H., Yang, Y.F. & Xu, L. 2003b. An experimental study and calculations on the fire resistance of concrete-filled SHS and columns. *Journal of Constructional Steel Research* 59(6): 427–452.

Han, L.H., Tao, Z. & Zhao, X.L. 2004. Concrete-filled double skin (SHS outer and CHS inner) steel tubular beam-columns. *Thin-Walled Structures* 42(9): 1329–1355.

Han, L.H., Huang, H., Tao, Z. & Zhao, X.L. 2006. Concrete-filled double skin steel tubular (CFDST) beam-columns subjected to cyclic bending. *Engineering Structures* 28(12): 1698–1714.

Han, L.H. & Yang, Y.F. 2007. *Modern technology of concrete-filled steel tubular structures*. Beijing: China Architecture and Building Press.

Han, L.H., Wang, W.D. & Zhao, X.L. 2008. Behaviour of steel beam to concrete-filled SHS column frames: Finite element model and verifications. *Engineering Structures* 30(6): 1647–1658.

Han, L.H., Li, W. & Uy, B. 2009. Seismic behaviour of concrete-filled steel tubular frame to RC shear wall high-rise mixture structures. *Journal of Constructional Steel Research* 65(7): 1249–1260.

Han, L.H., Ren, Q.X. & Li, W. 2010. Tests on inclined, tapered and STS concrete-filled steel tubular (CFST) stub columns. *Journal of Constructional Steel Research* 66(10): 1186–1195.

Han, L.H., Zhao, X.L. & Tao, Z. 2001. Test and mechanics model for concrete-filled SHS stub columns, columns, and beam-columns. *Steel and Composite Structures* 1(1): 51–74.

Herrera, R.A., Ricles, J.M., & Sause, R. 2008. Seismic performance evaluation of a large-scale composite MRF using pseudodynamic testing. *Journal of Structural Engineering* 134(2): 279–288.

Hollaway, L.C. & Cadei, J. 2002. Progress in the technique of upgrading metallic structures with advanced polymer composites. *Progress in Structural Engineering and Materials* 4(2): 131–148.

Hollaway, L.C. & Teng., J.C. 2008. *Strengthening and rehabilitation of civil infrastructures using fiber-reinforced polymer (FRP) composites*. Cambridge: Woodhead Publishing.

Islam, S.M.Z. & Young, B. 2010. Effects of different adhesive and FRP on strengthening of stainless steel tubular structural members. *Proceedings of the 13th International Symposium on Tubular Structures*, Hong Kong, China, December, pp.273–280.

Islam, S.M.Z. & Young, B. 2011. FRP Strengthened aluminium tubular sections subjected to web crippling. *Thin-Walled Structures* 49(11): 1392–1403.

Jiao, H. & Zhao, X.L. 2004. CFRP strengthened butt-welded very high strength (VHS) circular steel tubes. *Thin-Walled Structures* 42(7): 963–978.

Kang, K.W., Lee, S.C. & Liew, J.Y.R. 2012. Analysis of steel-concrete composite column subject to blast. *Structures and Buildings*, ICE Proceedings, in press.

Kodur, V.K.R. & Lie, T.T. 1996. Fire resistance of circular steel columns filled with fibre-reinforced concrete. *Journal of Structural Engineering* 122(7): 776–782.

Kodur, V.K.R. 1998. Design equations for evaluating fire resistance of SFRC-filled HSS columns. *Journal of Structural Engineering* 124(6): 671–677.

Kodur, V.K.R. 1999. Performance-based fire resistance design of concrete-filled steel columns. *Journal of Constructional Steel Research* 51(1): 21–36.

Kurobane, Y., Packer, J.A., Wardenier, J. & Yeomans, N. 2005. *Design guide for structural hollow section column connections*. Köln: TÜV-Verlag.

Lie, T.T. & Chabot, M. 1990. A method to predict the fire resistance of circular concrete filled hollow steel columns. *Journal of Fire Protection Engineering* 2(6): 111–126.

Lie, T.T. & Stringer, D.C. 1994. Calculation of the fire resistance of steel hollow structural section columns filled with plain concrete. *Canadian Journal of Civil Engineering* 21(3): 382–385.

Liew, J.Y.R., Xiong, D.X. & Xiong, M.X. 2012. Experimental investigation on ultra-high strength concrete filled steel tube columns. *Proceedings of the 14th International Symposium on Tubular Structures*, London, UK, September.

Lu, H., Zhao, X.L. & Han, L.H. 2009. Fire behaviour of high strength self-consolidating concrete filled steel tubular stub columns. *Journal of Constructional Steel Research* 65(10–11): 1995–2010.

Lu, H., Han, L.H. & Zhao, X.L. 2010. Fire performance of self-consolidating concrete filled double skin steel tubular columns: Experiments. *Fire Safety Journal* 45(2): 106–115.

Mashiri, F.R. & Zhao, X.L. 2010. Square hollow section (SHS) T-joints with concrete-filled chords subjected to in-plane fatigue loading in the brace. *Thin-Walled Structures* 48(2): 150–158.

Mashiri, F.R., Uy, B. & Naderloo, H. 2011. Concrete-filled VHS-to-mild steel plate fabricated section stub column tests. *Proceedings of the 6th International Symposium on Steel Structures*, Seoul, Korea, November, pp. 913–918.

Nadauld, J. & Pantelides, C.P. 2007. Rehabilitation of cracked aluminium connections with GFRP composites for fatigue stresses. *Journal of Composite Construction* 11(3): 328–335.

Nakanishi, K., Kitada, T. & Nakai, H. 1999. Experimental study on ultimate strength and ductility of concrete filled steel columns under strong earthquakes. *Journal of Constructional Steel Research* 51(3): 297–319.

Nethercot, D.A. 2003. *Composite construction*, London: Spon Press.

Nethercot, D.A. 2009. Enhancing the robustness of steel and composite buildings. *Proceedings of the 6th International Conference on Advances in Steel Structures*, Hong Kong, China, December, pp.105–122.

Nie, J.G., Qin, K. & Xiao, Y. 2006. Push-over analysis of the seismic behavior of a concrete-filled rectangular tubular frame structure. *Tsinghua Science and Technology* 11(1): 124–130.

Oehlers, D.J. & Seracino, R. 2004. *Design of FRP and steel plated RC structures – retrofitting beams and slabs for strength, stiffness and ductility*. Oxford: Elsevier.

Pantelides, C.P., Nadauld, J. & Cercone, L. 2003. Repair of cracked aluminium overhead sign structures with glass fiber reinforced polymer composites. *Journal of Composite Construction* 7(2): 118–126.

Park, J.W., Hong, Y.K. & Choi, S.M. 2010. Behaviors of concrete filled square steel tubes confined by carbon fiber sheets (CFS) under compression and cyclic loads. *Steel & Composite Structures* 10(2): 187–205.

Photiou, N.K., Hollaway, L.C. & Chryssanthopoulos, M.K. 2006. Strengthening of an artificially degraded steel beam utilizing a carbon/glass composite system. *Construction and Building Materials* 20(1–2): 11–21.

Qu, H.Y., Li, G.Q., Chen, S.W., Sun, J.Y. & Sozen, M.A. 2011. Analysis of circular concrete-filled steel tube specimen under lateral impact. *Advances in Structural Engineering – An International Journal* 14(7): 941–952.

Remennikov, A.M., Kong, SY. & Uy, B. 2011. Response of foam- and concrete-filled square steel tubes under low-velocity impact loading. *Journal of Performance of Constructed Facilities* 25(7): 373–381.

Rizkalla, S., Hassan, T. & Hassan, N. 2003. Design recommendations for the use of FRP for reinforcement and strengthening of concrete structures. *Progress in Structural Engineering and Materials* 5(1): 16–28.

Schnerch, D., Dawood, M., Rizkalla, S. & Sumner, E. 2007. Proposed design guidelines for strengthening steel bridges with FRP materials. *Construction and Building Materials* 21(7): 1001–1010.

Seica, M.V. & Packer, J.A. 2007. FRP materials for the rehabilitation of tubular steel structures, for underwater applications. *Composite Structures* 80(3): 440–450.

Shaat, A. & Fam, A. 2006. Axial loading tests on CFRP-retrofitted short and long HSS steel columns. *Canadian Journal of Civil Engineering* 33(6): 458–470.

Shaat, A. & Fam, A. 2007. Fiber-element model for slender HSS columns retrofitted with bonded high-modulus composites. *Journal of Structural Engineering* 133(1): 85–95.

Shan, J.H., Chen, R., Zhang, W.X., Xiao, Y., YI, W.J. & Lu, F.Y. 2007. Behavior of concrete filled tubes and confined concrete filled tubes under high speed impact. *Advances in Structural Engineering – An International Journal* 10(2): 209–218.

Shi, X.S., Wang, Q.Y., Zhao, X.L. & Collins, F. 2012. Experimental study on strength and ductility of steel tubular stub columns filled with geopolymeric recycled concrete. *Proceedings of the 14th International Symposium on Tubular Structures*, London, UK, September.

Song, Q.Y., Heidarpour, A., Zhao, X.L. & Han, L.H. 2012. FE modelling of flexible I-beam to square hollow section column connections subjected to earthquake and subsequent fire. *Proceedings of the 14th International Symposium on Tubular Structures*, London, UK, September.

Sun, G.S., Zhao, Y.H. and Gu, W. 2008. Stability of concrete filled CFRP-steel tube under axial compression. *Proceedings of the 12th International Symposium on Tubular Structures*, Shanghai, China, October, pp. 111–116.

Tao, Z., Han, L.H. & Zhao, X.L. 2004. Behaviour of concrete-filled double skin CHS steel tubular stub columns and beam-columns. *Journal of Constructional Steel Research* 60(8): 1129–1158.

Tao, Z., Han, L.H. & Wang, L.L. 2007a. Compressive and flexural behaviour of CFRP-repaired concrete-filled steel tubes after exposure to fire. *Journal of Constructional Steel Research* 63(8): 1116–1126.

Tao, Z., Han, L.H. & Zhuang, J.P. 2007b. Axial loading behaviour of CFRP strengthened concrete-filled steel tubular stub columns. *Advances in Structural Engineering – An International Journal* 10(1): 37–46.

Tao, Z., Han, L.H. & Zhuang, J.P. 2008. Cyclic performance of fire-damaged concrete-filled steel tubular beam-columns repaired with CFRP wraps.*Journal of Constructional Steel Research* 64(1): 37–50.

Teng, J.G., Chen, J.F., Smith, S.T. & Lam, L. 2002. *FRP – strengthened RC structures*, West Sussex: John Wiley & Sons, Ltd.

Teng, J.G. & Hu. Y.M. 2007. Behaviour of FRP-jacketed circular steel tubes and cylindrical shells under axial compression. *Construction and Building Materials* 21(6): 827–838.

Teng, J.G., Yu, T., Wong, Y.L & Dong, S.L. 2007. Hybrid FRP–concrete–steel tubular columns: Concept and behaviour. *Construction and Building Materials* 21(6): 846–854.

Tong, L.W., Sun, C.Q., Chen, Y.Y, Zhao, X.L., Shen, B. & Liu, C.B. 2008. Experimental comparison in hot spot stress between CFCHS and CHS K-joints with gap. *Proceedings of the 12th International Symposium on Tubular Structures*, Shanghai, China, October, pp. 389–395.

Twilt, L., Hass, R., Klingsch, W., Edwards, M. & Dutta, D. 1996. *Design guide for structural hollow section columns exposed to fire*. Köln: TÜV-Verlag.

Udomworarat, P., Miki, C., Ichikawa, A., Sasaki, E., Sakamoto, T., Mitsuki, K. & Hasaka, T. 2000. Fatigue and ultimate strengths of concrete filled tubular K-joints on truss girder. *Journal of Structural Engineering* (Japan Society of Civil Engineers) 46(3): 1627–1635.

Uy, B. 2008. Stability and ductility of high performance steel sections with concrete infill. *Journal of Constructional Steel Research* 64(7–8): 748–754.

Uy, B. Tao, Z & Han, L.H. 2011. Behaviour of short and slender concrete filled stainless steel tubular columns. *Journal of Constructional Steel Research* 67(3): 360–378.W

Wang, W.D., Han, L.H. & Zhao, X.L. 2009. Analytical behaviour of frames with steel beams to concrete-filled steel tubular column. *Journal of Constructional Steel Research* 65(3): 497–508.

Wang, Y.C. 2002. *Steel and composite structures: Behaviour and design for fire safety*. London: Taylor & Francis.

Wardenier, J., Packer, J.A., Zhao, X.L. & van der Vegte, G.J. 2010. *Hollow sections in structural applications*, Delft: Bouwen met Staal.

Wu, C., Zhao, X.L., Duan, W.H. & Phipat, P. 2012. Improved end bearing capacities of sharp-corner aluminium tubular sections with CFRP strengthening.*Journal of Structural Stability and Dynamics* 12(1): 109–130.

Xiao, Y., He, W.H. & Choi, K.K. 2005. Confined concrete-filled tubular columns. *Journal of Structural Engineering* 131(3): 488–497.

Xiao, Z.G. & Zhao, X.L. 2012. CFRP repaired welded thin-walled cross-beam connections subject to in-plane fatigue loading. *International Journal of Structural Stability and Dynamics* 12(1): 195–211.

Yang, H., Lam, D. & Gardner, L. 2008. Testing and analysis of concrete-filled elliptical hollow sections. *Engineering Structures* 30(12): 3771–3781.

Yang, Y.F. & Han, L.H. 2008. Concrete-filled double-skin tubular columns under fire. *Magazine of Concrete Research* 60(3): 211–222.

Zhao X.L. & Grzebieta R. 1999. Void-filled SHS beams subjected to large deformation cyclic bending. *Journal of Structural Engineering* 125(9): 1020–1027.

Zhao, X.L. & Han, L.H. 2006. Double skin composite construction.*Progress in Structural Engineering and Materials* 8(3): 93–102.
Zhao, X.L., Fernando, D. & Al-Mahaidi, R. 2006. CFRP strengthened RHS subjected to transverse end bearing force. *Engineering Structures* 28(11): 1555–1565.
Zhao, X.L. & Zhang, L. 2007. State of the art review on FRP strengthened steel structures. *Engineering Structures* 29(8): 1808–1823.
Zhao, X.L. & Packer, J.A. 2009, Tests and design of concrete-filled elliptical hollow section stub columns. *Thin-Walled Structures* 47(6–7): 617–628.
Zhao, X.L. & Choi, A. 2010. Moment capacity of concrete filled double skin tubes. *Proceedings of the 13th International Symposium on Tubular Structures*, Hong Kong, China, December, pp. 583–590.
Zhao, X.L., Han, L.H. & Lu, H. 2010a. *Concrete filled tubular members and connections*. London: Taylor & Francis.
Zhao, X.L., Tong, L.W. & Yang, X.Y. 2010b. CFDST stub columns subjected to large deformation axial loading. *Engineering Structures* 32(3): 692–703.

CIDECT 50^{th} anniversary session papers

Tubular Structures XIV – Gardner (Ed.)
© 2012 Taylor & Francis Group, London, ISBN 978-0-415-62137-3

Tubular steel structures in architecture

M. Eekhout
Faculty of Architecture, Delft University of Technology, Director of Octatube, Delft, The Netherlands

ABSTRACT: The aesthetics of tubular structures are a major contribution to their architectural image, but as designers strive for a heightened spatial enlightenment, designs are requiring ever more complex structural solutions and high standards in their elements and components. New designs are helped by combinations of intelligent detailing, by the application of computerized 3D design, by engineering improvements in materials, by fabrication techniques and by assembly procedures. More attention is now paid to the integration with other components of the building, such as roof cladding, glass façades, panelled walls, climate installations, etc. The building as a technical artefact becomes increasingly complicated in its making and in its functioning. In the last decades Western European architectural ideas have been received with high expectations around the world. The computer and the internet have changed the behaviour and potentialities of architects. In earlier days it were books only to stimulate getting acquainted with foreign architecture, assisted by glossy magazines. The internet sites have even accelerated this. But the core of the developments is forced by design in tubular structures. When seen over a longer period, certain changes are apparent.

1 1991 STANSTED AIRPORT TERMINAL BUILDING, NORMAN FOSTER

The design of the Stansted Airport Terminal building is overwhelmed by the spreading arms of the roof structure, which is based on 36 modules in tubular structure. The outside modules are standing trees of tubular structure, which keep up intermediate roof modules of the same size that are connected along their edges. The 4 spreading arms carry the perimeter of a tubular triangulated framework shell visible as a vaulted ceiling. During the construction the 4 arms were held together by ties, which are connected in a very crucial joint, on the site called the 'Jesus joint'. The primary tubular structure module is concentrated on ground level of the terminal in 4 CHS columns, welded in a majestic framework, which penetrates the lower stories through voids. The roof structures are clad in metal, but the tops are covered in glass to obtain overhead daylight of the terminal space, softened by perforated metal sheeting. The large overhead volume gives the building the feeling of one unifying space with smaller activities.

Figure 1. Stansted Airport, London.

2 1991 AIRPORT PASSENGER TERMINAL STUTTGART, GERKAN, MARG UNDER PARTNER

The sloped roof of this terminal building is supported by a forest of steel trees, which are composed of circular tubes in a tree-like arrangement of stems, thicker

Figure 2. Passengers Terminal, Stuttgart.

and thinner branches that finally hold up the roof. The structure is characterised by welded intermediate steel castings to make a streamlined and natural transition from the smaller tubes into the thicker tubes and finally into the lower stems.

3 1992 EL ALAMILLO BRIDGE, SEVILLE, CALATRAVA

The prominent harp-like suspension bridge by Santiago Calatrava was built for the Olympic games of 1992 in Barcelona. The bridge was held up by 13 guy cables attached to the prominent and purpose made steel tubular section. The actual counterbalance to the cables and loads from the deck and cables is formed by filling the steel mast with concrete. Mainly the upper half acts as a counter ballast. Dutch architect Ben van Berkel would later (1996) design a similar cable stayed bridge in Rotterdam, the Erasmus bridge or 'The Swan', which is more facetted in form, made as a purpose made hollow section and instead of deadweight the counter balance was brought by two mayor stabilising cables at the back.

4 1993 WATERLOO INTERNATIONAL TRAIN TERMINAL, LONDON, NICOLAS GRIMSHAW

The high speed terminal train station nears the centre of London was designed by Nicolas Grimshaw as a large urban shed and inaugurated in 1993. The form the the structure had to follow the rails, which are in London partly historic and partly quite condensed and unavoidable curved in plan. In cross section the structure is a truss with three pins. The left truss has a suspended cladding, the other half an upper cladding. Cladding is in metal decking and glass. The form of the roof circular in plan with a large radius and the cross section with many different corners resulted in a construction system that had flexibility in form to allow for all possible geometrical deviations. Recently the Eurostar ceased to frequent Waterloo.

Figure 3. El Alamillo Bridge, Seville.

5 1994 KANZAI AIRPORT TERMINAL, OSAKA, RENZO PIANO, OVE ARUP

This airport in an densely populated urban area has been built on an artificial island, of which the underground was expected to deform considerably. This has been taken into account in the engineering plans of layout, schemes and details.

The architect's plan for a long building and overviewable terminal volume resulted in a king-size hall where departure and arrivals are separated horizontally. The tubular steel structure in an elegant arched form hovers over space. The structure itself has elegant details, some of them were made in cast steel and welded.

The three-dimensional trusses govern space, and between them are ceiling membranes in a similar shape, which lead the flow of air through the volume. The details of the building have been set on rubber bearings. Other precautions were taken as compensations against earthquakes. The Kobe earthquake of 1995 did no damage at all and the terminal complex emerged unscathed.

Figure 4. Waterloo station, London.

Figure 5. Partial façade Kanzai Airport.

6 1996 NEUE MESSE LEIPZIG, GERKAN MARG UND PARTNER, IAN RITCHIE

A 90 meters span tubular structure in which the main trusses span in the 90 m span direction above the glass cladding below. The cladding is suspended via tubular purlins in 2 directions from which the spiders are connecting the laminated clear glass panels. The height of 30 m caused a natural flow of air to ventilate as a chimney through space. Lower entrance ventilation, upper ridge exhaust ventilation.

7 1997 FREMONT STREET EXPERIENCE, LAS VEGAS, JON JERDE

A glass clad regular space frame in the form of a cylindrical barrel vault that easily could have span with the space frame alone.

The lower chord of the space frame has been enriched with a light penetrating sun screen, which unifies the space frame, takes the technical character down a bit. One wonders why tubular columns are at all positioned underneath a cylindrical space frame vault? The reason is more architectonical than functional/technical. The indoor atmosphere increased.

Figure 6. Interior passenger Terminal Kanzai Airport.

Figure 7. Neue Messe, Leipzig.

8 1997, STADE DE FRANCE, PARIS, MZRC

This tubular structures roof acts structurally as a saucer which is suspended upward and stabilised downward. From the outside it is a flat saucer. The interior displays a grid of CHS profiles, interconnected. the grid of flat trusses continues over the free playing field and hardly gives any shadow and covering. The floating character of this stadium overwhelms the A1 drivers alongside the building.

9 1998 LAW COURTS BORDEAUX, RICHARD ROGERS

A rather traditional set-up of trusses on columns with barrel-vaulted undulating roofs in between tem, mainly in tubular structures but now is a complex late-modern building with stone covered lower floors in concrete and upper volume in tubular steel enveloped with glass. Detailing is modern and state of the art. The conical space contains a court room. High Tech in an urban environment.

Figure 8. Fremont Street, Las Vegas.

Figure 9. Interior State de France, Paris.

Figure 10. Law Courts, Bordeaux.

Figure 11, 12. Oriente station & shopping centre, Lisbon.

10 1998 ORIENTE TRAIN STADIUM, LISBON, CALATRAVA

This train station has a minority in circular tubes and a majority of specially made steel ribs. Visually very much attraction looking and at the time of the Expo of Lisbon it was the entrance to the world. The welcoming gesture speaks for itself. The adjacent shopping centre continues the spatial experience.

11 2000 EDEN PROJECT, NICOLAS GRIMSHAW

The covering of the Eden project in Bodelva, Cornwall UK, contains two large greenhouses where public botanical gardens are located. The geometry of the domes is derived from regular polyhedra, intersecting in this case as giant soap bubbles. The space frames used are quite regular thanks to the Pre-High-Tech studies of the late Richard Buckminster Fuller. The

Figure 13. Eden Project, Cornwall.

Figure 14. British Museum, London.

lengths of the space frame members varies around 4 to 5 metres. The cushions have a diameter of 4 to 9 metre diameter. Cushions are made as triple layered ETFE cushions, with two air-inflated chambers.

12 2000 BRITISH MUSEUM ATRIUM ROOF, LONDON, NORMAN FOSTER

The inner courtyard of 92 × 72 metres with the elliptical, slightly asymmetrically positioned Library. In this building Karl Marx wrote his 'Das Kapital' as he could not afford a private writing place. This atrium covering has the form of a squared asymmetrical donut and has been designed, engineered and made on site as a shell grid of a triangulated single skin space frame.

Because of the visual flow of material elements and glass panels, the path was chosen for a strong bur simple single layer of RHS square hollow sections. They

Figure 15. Millenium Dome/O2 Dome, London.

were welded on site on the RHS profiles, after having been positions exactly in situ by 3D surveying apparatus. Quite in contradiction to the development in space frame world, this space frame was not regular or repetitive. That is the reason why all corners were snubbed off in a workshop off-site, coded and positioned and clicked on place. Only after the positioning of all tubes the welding could begin, which had to take care of many distortions in the overall shell.

13 2000 MILLENIUM DOME, LONDON, RICHARD ROGERS, BURO HAPPOLD

The Millennium Dome was a public project to show British awareness of the turn of the century. Like the Millennium bridge it attracted a lot of attention. It became world's largest tent structure. Prominent features are the tubular mast poles sticking out of the Teflon coated membrane fabric. Diameter of the dome is 365 meter. Long after the change of millennium the dome got another function: called the O2 dome after the sponsoring telecom company, it serves now as the temple for pop artists. Michael Jackson contracted 50 shows 'This is it' here, but deceased some weeks before the start.

14 2001 MEDIATHEQUE SENDAI, MIYAGI, JAPAN, TOYO ITO

A five stories public building made of steel structures by a ship building company, with characteristic tubular columns, all in a different but outstanding form. Through these tubular circles of columns stairs and elevators are designed. This vertical traffic gives a unobstructed view of the different stories.

15 2003 TOWN HALL ALPHEN AAN DE RIJN, NL, ERICK VAN EGERAAT

This first official Dutch and permanent Free Form building has a very irregular shape, yet almost all elements and components in its geometry are geometrically defined as they are part of a torus, cone, cylinder etc. In the beginning of the Free Form technology it caused a struggle between the designing parties and

Figure 16. Mediatheque, Japan.

Figure 17. Town Hall Alphen aan de Rijn.

the producing and building parties as the designers overlooked the geometrical complexities.

Yet the lessons were learned within an additional year of design development and the building from then on was only built up of similar elements in different form, positioned in different click points. The architect requested individualized screened glass panels. All elliptical façade tubes had a different height, some even in a crooked form near a prominent stair (wedding stair): *'industrialisation in lots of one'*. (Janssen & Boorn, 2002)

16 2004 FEDERATION SQUARE MELBOURNE, LAB ARCHITECTURE

An open environment on a well known place in the city amidst older 'heritage' buildings often accumulates tensions amongst the public. It becomes a topic of intense debate. Such was the case with the 'Fed' Square. The total assembly positions itself counter to the conservative parties. The theatre is the most outspoken part of those buildings in a fuzzy tubular network geometry with an even more complex glass covering. Fuzzy networks in 'down under'. For the 2008 Olympic Games in Beijing architect PTW Architects, CSCEC and Arup would design an indoor swimming pool stadium with a similar roof and façade

Figure 18. Interior Town Hall, Alphen.

Figure 19. Federation Square, Melbourne.

system with 'fuzzy logic' in tubular structures covered with inflatable cushions.

17 2006 BARAJAS AIRPORT TERMINALS, MADRID, RICHARD ROGERS / ANTONIO LAMELA

The new Barajas Terminals form together the international airport of Madrid, one of the largest in Europe and certainly one of more spacier airports to date. The construction exists of tapered tubular columns in changing colours indicating the gates, on concrete frames in a very smoothened design modus. The steel roof plane with bamboo ceiling undulates over the long double Y-stilts construction. The length of the terminals, the wideness, the gentle gestures of the columns

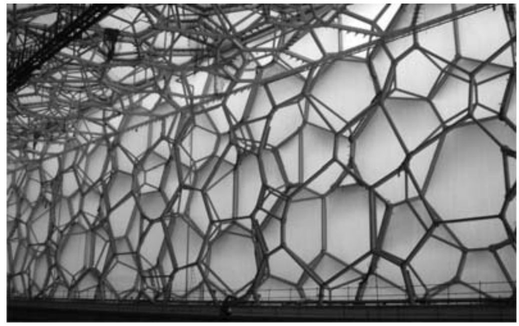

Figure 20. Swimming stadion, Beijing.

Figure 21. Terminal 4 Barajas Airport, Madrid.

and the changing colours of the stilts make these terminals almost a modern version of grand cathedral spaces and unique in the world.

18 2005 NATURAL MUSEUM, LEEUWARDEN, NL, JELLE DE JONG

This museum of Natural History was housed in a 17th/19th century building in the city centre and had to be covered to extend its museum collection and public meeting possibilities. After a design competition the architect made a design based on an experienced lightweight steel tubular grid, clad with insulated glass panels, stabilized by stainless steel rods from 4 long masts, penetrating trough the glass plane.

The masts stabilize the roof plane upward or downward snow, deadweight and wind forces and downward for upwind. The roof scheme is a table structure, independent form the existing buildings. The roof edges are chosen on the top of the tiled roofs, but only a thin rubber flap makes the cover, no forces are allowed on the existing building, the edges around have ventilating windows. The roof structure of the horizontal glass plane and the 4 prominent masted poles were accepted by the monument commission as an extreme structural state of the art positioning to the old buildings.

Figure 22. Natural Museum, Leeuwarden, NL.

Figure 23. The Cockpit, Utrecht.

19 2005 SOUND BARRIER / ‘COCKPIT’ CAR SHOWROOM A2 UTRECHT, NL, KAS OOSTERHUIS

This 1.500 meters long sound barrier along the A2 near Utrecht, NL and 180m long car Hessing showroom of exclusive cars has a fluent Free Form design which blends well in the short time this building is seen from driving the highway. The cross sectional shape changes during the entire length, is triangulated in a space frame and only the cockpit has a tubular space frame with clearly over-designed tubular members. Glazing follows the triangulation of the design grid.

20 2005 ALLIANZ STADIUM, MÜNCHEN, HERZOG + DE MEURON

This lightweight showing stadium is covered with EFTE cushions along all of its facades, illuminating

Figure 24. Allianz Arena, Munich.

Figure 25. Evo Restaurant, Barcelona.

in different colours: White for neutral football games, red when Bayern München plays and blue when 1860 München plays. The light is an integral message for the stadium that often is used in the darker hours of the day. The tubular structure of the football stadium functions as it should, serving the function of roof without attracting much attention.

21 2006 EVO RESTAURANT, HOTELES HESPERIA, BARCELONA, RICHARD ROGERS

The Evo restaurant sits as a gigantic diamond on the high Hesperia Hotel in Barcelona and has been designed as an expensive icon in the silhouette of the high rise building. The menus are suited for the elite. The view out is phantastic. The restaurant has a diameter of 22 m and has a network geometry dome structure made of slender RHS tubes, welded on site, that is to say: on the ground level. The entire diamond shaped restaurant has been lifted with a giant crane in its position.

Figure 26. BMW World, Munich.

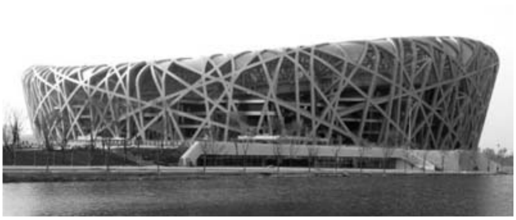

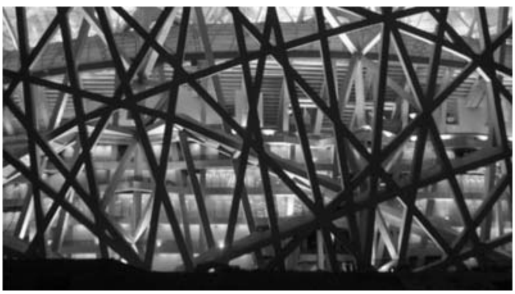

Figure 27, 28. Olympic Stadium, Beijing.

22 2007 BMW WELT MUNICH, COOP HIMMELBLAU

This building serves mainly as a rich environment from which the lucky owners of new BMW cars can get their brand new cars and drive into the future. The building has some prominent sides. One of them is the double cone, made of a tubular network which by its turning movement twists the entire building visually. (Himmelblau, 2010)

23 2008 BIRD NEST INDOOR SPORT STADIUM, BEIJING, HERZOG + DE MEURON / OVE ARUP

The Bird nest stadium is the apotheosis of the use of tubular structures to date in the world. It used 8x more steel than an average stadium of the same size, elsewhere causing the world's price of steel to skyrocket for a while. The design was very outspoken, had the looks of a giant Chinese woven reed basket, and is considered as a prime example of a Free Form building. It was mainly used 14 days in its life in the summer of 2008, but it was on all television sets over the entire world and had a function as public advertisement of China as a country organising the 2008 Olympics.

24 CONCLUSION

While the first 15 years, half a professional generation, of tubular structures were mainly colored by high tech architecture, the latter 15 years after that were colored by prominent free form architecture projects. Kanzai Airport was the turning point: both high tech and free form. This was the time that the computer penetrated design offices and that accurate designing and engineering of complicated structures and free form structures became possible. Before that it was only confined to a few specialists who had advanced computer programs and were used to deal with components in large variety of form and dimensions. Since then, however, computer programs are commercially available for designers and engineers. What stays is the wish of the architect to make surprising buildings with 3-dimensional structures to make the spatial gestures. Tubular structures have proven to be flexible and versatile enough for this purpose.

REFERENCES

Jansen, J & Boorn, 2002, Stadhuis Alphen aan de Rijn, TU Eindhoven.

Mönninger, M., 2010, Coop Himmel(b)lau Complete Works 1968–2010, Taschen.

Eekhout, M., 2011, Tubular Structures in Architecture, Cidect Geneva & TU Delft.

Tubular Structures XIV – Gardner (Ed.)
© 2012 Taylor & Francis Group, London, ISBN 978-0-415-62137-3

Design and erection of the London Eye and the Wembley National Stadium arch

A.P. Mann
Senior Consultant, Jacobs, UK

ABSTRACT: Since the Millennium, the London skyline has acquired two prominent structures: the London Eye and the Wembley Stadium arch. Both are very large lattice structures and both are made up of tubular element substructures. Although serving quite different functions, both structures posed similar design challenges not least in the need to consider global buckling modes. Partly because of that demand, the need to assure tolerances was also very important for each. Given their huge sizes, these was an especial need to consider processes of node fabrication, sub-assembly and final erection into position.

1 LONDON EYE

1.1 *Introduction*

Since the Millennium, the London skyline has acquired two prominent and now well known structures: the London Eye and the Wembley arch. Although serving very different purposes, both structures share certain features. Firstly, and generically, they are both large span tubular structures acting primarily in compression. Secondly, they both support or incorporate cables and thirdly, considerations of fabrication, sub assembly and erection were highly significant for both projects and there was a certain commonality between their construction approaches.

The London Eye rim was designed, fabricated and erected by Hollandia based in Rotterdam. The Wembley Arch was designed by Mott MacDonald and fabricated by Cleveland Bridge (Darlington). Cleveland Bridge were also responsible for the erection engineering. The paper's author acted as third party for site works on both projects and acknowledges here the great skill of the design and construct teams.

1.2 *London Eye function*

Figure 1 shows the Eye. The Eye's rim (about 132 m across) is a triangular lattice using tubes for all its members. On the outside, the rim supports 32 passenger capsules and the total self weight is transmitted down from the rim via cables to the central hub and thence to ground. Laterally, wind acts on the capsules plus the exposed surface of the rim and this load is also carried via the spoke cables back to the hub. To transmit lateral loading, the spoke cables are inclined out of plane (Figure 2). Moreover, for efficiency and to avoid cable slackening, all cables are pre stressed. By this means the 'tension cables' carry tension and the 'compression cables' carry compression, by relief of tension. One down side is of course the inevitability of placing the rim in a permanent state of circumferential compression (though this does confer some advantages). Arithmetically, the cable prestress is quite large such that the total compression induced in the rim is also large; this being the summation of prestress plus gravity and wind loads with the prestress contribution being dominant.

Figure 1. London Eye rim.

The rim's mode of failure is then one of global buckling having the classic four quadrant mode shape buckling form under excess axial load. For stability and to limit interaction it was essential to compute the elastic critical buckling load and keep it high in relation to individual member capacities.

Figure 2. Eye rim with spoke cables.

An interesting question in assessing capacity is to consider what the partial load factor on prestress loading should be. Self evidently there is uncertainty in both gravity and wind loads which partly justifies their relevant factors: it is conceivable that either of them in practice (especially the wind load) could be higher than computed. However, the prestress load is put in to a defined and measured amount and can actually only reduce with time – the reduction being linked to losses via by cable creep although the spoke cables are periodically 'tuned up'. Philosophically, if the rim were to buckle, the dominant driving force (the prestress) would be shed, whereas of course gravity loading remains always active which again brings into question what partial load factor is appropriate. Although these are interesting asides, in practice the prestress was treated as dead load though arguably this was conservative.

Given that the dominant loads are axial and that global buckling is a significant issue, it also follows that the global structural tolerances (out of plane) are matters to be addressed positively. During design, active consideration was given to tolerances. There are several sources of dimensional variation: the rim might not be plane, and the wheel might not be round and the hub might not be in the centre of whatever shape the rim ended up. All of these separate tolerance topics have implications not only for rim structural capacity but also for wheel functionality. The concern was compounded because building the rim was a 'one off' so pragmatically no one could be totally sure what tolerances were achievable. There is little point in any design demanding a tight tolerance if the contactor struggles to enforce it. Moreover following construction, the team would have the problem of determining what to do if the tolerances had not been achieved.

To investigate alignment effects during the design stage, various simulations were run with cables at differing prestress values to see what possible misalignments might be generated, these included variation on absolute prestress values, plus tension variations between individual spoke cables. Thereafter, other simulations were run with different misalignments to assess global buckling sensitivity. Fortunately these studies suggested firstly that alignment would not be overly affected by variations in cable prestress and secondly (again fortunately) that buckling capacity was not much affected over a range of sensible misalignment presumptions or of cable stress variations.

There are however other practical consequences of tolerance. A key point to note is that functionally the Eye works by being in continuous motion and requiring passengers to board a continually moving wheel (it is in fact the safety and practicality of that boarding process which governs wheel speed). Thus a key interface is that between the Boarding Platform surface and the steps of the capsules both vertically and laterally. Excess vertical steps would create a trip hazard, while excess horizontal gaps would create foot trap hazards. The target therefore was to keep the gap between the Boarding Platform edge and the capsule steps not so tight as to risk a clash and not so wide as to risk a foot trap hazard. For both these reasons, rim planarity, rim circularity and rim concentricity were important objectives.

To further assure horizontal alignment, the rim is guided through horizontal restraint rollers set either side of the Boarding Platform. Consequently, the structural implication of this is that the wheel is 'forced' into line during each rotation to a degree linked to its out-of-plane tolerance. Hence there is a fatigue loading case with a cycle of loading (in and out) once for each revolution. Acceptable alignment in the vertical direction was to some extent achieved by controlling wheel circularity (and assuring the hub was in the centre) via control of the cable tensioning (and the assembly/erection methodology was important in this respect) and partly by providing some adjustability in the attachment points of the capsules to the rim. In practice, step variations are not very much. There is also a height variation between summer and winter due to thermal changes but as the thermal mass of the structure is so high, this has not, in practice, been a problem. If necessary, the Boarding Platform surface can be adjusted up and down since it is supported on jacks but this is rarely done.

As the rim rotates, it does ovalise to some extent and this also creates some fatigue loading in plane. That is not a major problem, not least since the entire rim is permanently in compression. Fatigue cracking can initiate in welded zones even when steel is in compression (cracks being propagated by residual stress) but as the rim is in high imposed compression any consequences would not be so important and cracks would be unlikely to propagate. In practice no cracking has been detected (there are annual inspections). As the rim rotates, the forces in the cables do change though not to a huge amount but such changes also impose fatigue cycling on the cable end node supports so these too are designed for local stress fluctuations.

Local fatigue issues occur at the capsule attachment points because these structural parts undergo one complete reversal of load with each wheel rotation. It will be observed (Figure 1) that each capsule has four support points and that there is bracing between the separate support points. This is deliberate for although the structure is designed for fatigue, very high assurance is required against potential capsule loss. Hence the philosophy was to provide a highly redundant attachment structure such that any single support could be lost with the capsule still remaining in position.

Generally then the structural design of the rim is fairly complex. There is a global buckling problem to be resolved taking the dominant loads as pre stress. Then superimposed on that there are global and local fatigue issues linked to a number of causes. The design also has close links to functionality in that tolerances are important for a number of reasons. Finally, taking account of erection methodology, there is a key erection load case to consider.

1.3 *Interface with drive system and electrical pick up*

The rim has an interface with the wheel drive system which is shown in Figure 3. Fixed to the side of the rim there is a running strip coated with a friction surface (see also Figure 4). This strip is gripped by the drive wheels top and bottom and as these wheels are turned by their motors so the sandwiched strip is pushed along and the whole wheel rotates. Neither the rim nor the running strip are circular but are instead made up of a series of straights. The implication of this is that the drive wheel sets have to move up and down (and be capable of moving in and out) with wheel rotation. To do this, they are fixed to articulated arms. As this movement capability is in all circumstances necessary, the actual rim circularity tolerance is not that important from a drive perspective; tolerances being much less than the movements inherent in having a segmental driving surface. There is a separate interface with the electrical pick up system and the horizontal and vertical rim tolerances governed the amount of articulation that had to be built into the pick up supports.

1.4 *Detailing*

A key requirement of the rim design was aesthetics. The intention was always that whatever was built had to look good. For this reason, the bulk of connections

Figure 3. Eye rim interface with drive system.

Figure 4. Eye rim nodes and running strip.

on the truss are fully welded with the architect taking a keen interest in their appearance. The design of the nodes required considerations of:

- Appearance
- Strength
- Fatigue resistance
- Practicality
- Facilities for mass production in jigs

There are different types of nodes, normal types accommodating triangular bracing and the type that anchors the cables. A typical truss junction can be seen in Figure 4.

1.5 *Assembly*

As the contractor Hollandia was based in Rotterdam, the entire structure was shop fabricated there and shipped direct to the London site. The rim itself came in four quadrants each of these coming over the sea and up the Thames on barges. Figure 5 shows a rim section on the quay in Holland ready to be loaded onto its barge. These four segment were then fitted together on site. At site, the inner chord remained bolted between quadrants whilst the outer chord was site welded. Thereafter, the spoke cables were added and tensioned up. How this was achieved whilst maintaining

Figure 5. Eye rim segment ready to be loaded onto a barge.

circularity will be appreciated from a description of the erection methodology.

1.6 *Erection*

A significant imperative for the project was rapid completion for the wheel had to be in place by Millennium eve. As time was really short, this was a significant factor in the thinking devoted to the erection method. Other considerations were that site space for assembly was extremely restricted. It is possible to erect wheels vertically but this requires some significant temporary works to maintain alignment and traditionally vertical erection methodology has been used where rims have rigid spokes rather than cables. Moreover, a vertical erection method in London would have meant a large amount of working at height along with the risk of dropping tools onto rights of way below. Given that space was available on the river, Hollandia decided to assemble the rim flat over the water surface and then jack the whole rim up into its vertical plane from that position.

Of course there are pros and cons with any erection method. In favour, fortunately the Thames happens to be about twice the rim diameter opposite Jubilee gardens and also fortunately, the navigable passage runs along the opposite bank. Thus it was possible to pile into the river on the garden's side to form temporary support platforms to hold the rim temporarily. The four segments of rim were supported on these platforms (Figure 6). Whilst in this horizontal plane, cables were added and tensioned up so this was much easier than it would have been to add cables in the vertical plane with all the added risk of uncertainty in achieving circularity. On the down side, to match the erection methodology, it was necessary to articulate the A frame (column support) top and bottom and to adjust the hinge support position upwards at the A frame bottom so as to allow the frame to be in an alignment that cleared the river wall and fitted up to the rim on its river supports. This demand may be appreciated from Figure 7. Structurally, it will also be appreciated from

Figure 6. Eye rim temporarily supported above the river.

Figure 7. Eye erection.

Figure 8. Eye rim out of plane umbrella of support cables.

the erection picture of Figure 7 that at the moment of lift off, the rim weight was at its most eccentric relative to the foundations and therefore this moment dictated the maximum up lift imposed on the rear foundation and the foundation design was actually governed by that condition. Additionally, at the moment of lift off, the rim was loaded out of plane and to counteract this was restrained out of plane by an umbrella of temporary cables anchored onto a disc mounted at the rear of the spindle: this array can be seen in Figure 8.

Figure 9. Wembley arch over the stadium.

Figure 10. Arch with roof hanging below and over pitch trusses.

Erection of the rim from horizontal to vertical was a spectacular event and took place in one day hence part of the justification for its adoption. Technically the moment of lift was the moment of greatest stress for much of the structure though this ran counter to popular instinct which probably thought higher elevations would be more critical.

2 WEMBLEY ARCH

The Wembley arch spanning 315 m purports to be one of the longest in the world for a building. Overall, the arch is 140 m high (about the same as the Eye) and the 'tube' is ~7 m diameter. Total self weight is about 1,750 tonnes of steel. The arch is spectacular, visible from a long way off and a signature for the stadium (Figure 9). Its function is to support the roof below (hung on cables) but perhaps surprisingly, it supports not only the roof directly below but a good proportion of the roof on the opposite side of the pitch since that roof is partly supported on trusses which span right across the pitch to carry a moving roof (these trusses can be seen in Figure 10).

Figure 11. Arch before erection with 5 turning masts in position.

Structurally, as for the Eye, the arch is a lattice structure made up of tubular sub elements. It is mostly in compression so again, as for the Eye, global buckling is a major consideration as is buckling of the individual tubes from which it is made. Out of plane wind load is carried again via inclined cables and they have enough gravity stress for wind generated 'compression' to be carried by relief of tension. As the arch is obviously in high compression it has the standard potential buckling modes of failure. Restraint out-of-plane is partly provided by orthogonal cable restraint but there is also an in – plane, side sway, buckling mode resisted by arch in plane stiffness. Because buckling is a dominant design factor, out of plane alignment tolerance was also a significant factor and the contract specification dictated limits for that. During erection, measures had to be deployed to keep the planarity alignment acceptable. Unlike the Eye rim, there are no significant fatigue issues to counter.

2.1 *Nodes*

Aesthetics was clearly important so became a significant influence on the nodal form adopted: all nodes are welded with considerable geometrical complexity belied by their smooth clean appearance post fabrication (some of the complexity is linked to sequence of assembly such that access is retained to complete internal welding).

There were four broad groups of nodes:

- Standard node intersections tube to tube
- Interface with cross arch diaphragms
- Nodes to attach to cables which support the roof
- Nodes to attach cables used for erection purposes

Many of these can be seen in Figure 11.

- Nodes which attach to temporary cables

2.2 *Assembly*

As with all large structures, the practicalities of assembly are key for planning and inseparable from the

Figure 12. Arch assembly: Sub units being lifted into position.

Figure 13. Arch erection with base pinned.

adopted erection methodology. As for the Eye, the plan was to assemble the arch on the ground and then hoist it up. Thus the strategy was for the arch to be made up of sub units which were then assembled into an arch shape (laid out horizontally) on stillages in a position ready for hoisting. Because even the sub units were large, fabrication shops had to be built on site.

This assembly process involved first of all making up 41 diaphragms partly factory welded but then delivered to site in thirds for final assembly (these diaphragms can be seen as the 'verticals' in Figure 11). Thereafter, these were erected in jigs (one diaphragm at each end) and the tubes in between were welded into place. These tubes had been pre cut and profiled in Cleveland Bridge's Darlington factory. These completed sub units were then moved by crawler crane (Figure 12) onto the pitch stillages in hit and miss patterns for the other tubes completing the arch to be welded in between.

2.3 *Erection*

Figures 11 and 13 shows the erection methodology. Although in principle this followed the same strategy as lifting the Eye there were differences. But firstly there are similarities: a key one was the need to introduce a proper pin at the arch base to allow articulation out of plane. The was quite complicated since in the final condition, the arch was required to be pin based so as to be capable of articulation *in-plane* (i.e. at 90° to the erection rotation). The base detail to permit this can be seen in Figure 14. Another similarity is the need to be hauled up on cables so nodal attachment points were required for temporary cables detailed so as to be geometrically clear of the cables used finally for supporting the roof. Again, and like the Eye rim, there were erection load cases of in-plane and out-of-plane loading, a need to maintain alignment consistent with the buckling mode of failure and a critical load case just at lift off.

A difference to the Eye erection is that significant temporary works were required to facilitate the lift. Figures 11 and 13 show the use of five turning masts each of which pulled on the arch to raise it. The cables

Figure 14. Erection pin at arch base.

Figure 15. Strand jacks for pulling up turning masts.

pulling the turning mast up were rotated by shortening attachment cables through strand jacks (Figure 15). Noting there are five turning masts, each with different cable lengths from their heads down to the arch (Figures 11 and 13), it may be appreciated that at any stage of the lift, the amount of force in each cable differed to a degree linked to the system stiffness. It was not possible to pull all five masts in unison and even if they had been so pulled, differing cable stresses and hence differing cable extensions would have created

Figure 16. Arch going 'over the top'.

an arch out of plane deviation. To overcome this, there had to be a sequence of incrementally defined steps. Moreover as the force in each mast system varied, the increment at each point varied. The consequence of this is that cable pulling was a selected mixture of both applied force and applied displacement with the driver for displacement being to keep the arch in plane at all stages or at least within tolerance limits of misalignment. To control this a mathematical model of the whole process was developed and from this a defined sequence of jacking steps was evaluated for each of the five turning masts.

For both the Arch and the Eye rim, the whole erection process was monitored continuously in terms of predicted force on the lifting system(s) and predicted displacement at defined points with survey checks made at each increment to assure that the lifting forces and measured displacements were what was expected against the mathematical models. The whole operation had to be controlled in this manner with a personnel command and control strategy.

A further difference between lifting the arch and lifting the Eye rim is that on the arch, the tilt went further than vertical and as the arch went 'over the top' loads were transferred at that point from pulling cables to restraining cables. (Figure 16).

Both the rim and the arch underwent changes of shape between their unstressed position on the ground and their erected position in the air. As part of the pre-erection engineering it was necessary in both cases to study what those shape changes would be (say under self weight) and determine if preset was required to offset the changes so that the as-built structures conformed to design intent shape.

3 CONCLUSIONS

These are two iconic tubular structures and both presented great challenges in terms of design, fabrication, assembly and erection. A key observation from each is that any design overall needs to consider all the practicalities of assembly and erection if it is to be complete. The reason is obviously that structural capacity is linked to the ability to detail the nodes and the ability to achieve sensible alignments. Furthermore the manner of erection in both these case studies had a significant effect on the detailing, and the manner of erection in both cases imposed significant stresses during the erection phase. In both cases, those erection conditions were enough to influence sizing i.e. the erection condition was at least as important as the permanent condition.

Tubular structures offer great advantages when appearance is a major demand and they offer major advantages when dominant loads are compressive. However, as experienced designers understand, the completeness of design, the practicalities of assembly and costs are all very strongly influenced, if not dominated, by the practicability of making the nodes not least the amount of welding within them. That in turn is very strongly influenced not just by the apparent demands of achieving strength but by the simple geometric demands of weld length and weld volume enforced by the geometry of the tube intersections. It is really the nodes and their configuration that govern the overall design of the members and not the other way around. Altogether, if a design is to achieve a satisfactory outcome in terms of material, functionality, appearance, ease of assembly and erection then there must be an iterative process of development involving skill inputs from several specialists

FURTHER READING

Berenbak J, Lanser A, Mann AP. 2001. The British Airways London Eye. Parts 2 Structure. *The Structural Engineer* 79 (2): 19–28.

Mann AP, Thompson N, Smits C. 2001. Building the British Airways London Eye. *ICE Proceedings, Institution of Civil Engineers,* 144(2): 60–72.

Composite construction

Tubular Structures XIV – Gardner (Ed.)
© 2012 Taylor & Francis Group, London, ISBN 978-0-415-62137-3

Local buckling in Concrete-Filled circular Tubes (CFT)

R. Chacón, E. Mirambell & E. Real
Technical University of Catalonia UPC, Barcelona, Spain

ABSTRACT: Local buckling phenomena in Concrete-Filled Tubes (CFT) is prevented in EN1994 by limiting the slenderness of the steel tubes (D/t) to $90 \cdot \varepsilon^2$. This limitation is inherited from EN1993-1-1 in which slenderness limits are defined for Circular Hollow Sections (CHS). This approach has been tackled by researchers for the case of CHS but has not been studied for CFT to the same extent. This paper describes a series of three-dimensional numerical simulations of CFT subjected to both flexural and axial loads. The three-dimensional simulations provide a phenomenological insight concerning the complex mechanical phenomena involved in local buckling. The results obtained show discrepancies between the EN1994 limitations and the pinpointed phenomenological observations for the case of CFT.

1 INTRODUCTION

Concrete-filled tubes (CFT) are widely used in civil engineering and building construction and consist of a steel tube with a concrete core casted inside. The behavior of CFT has been widely studied and hundreds of tests on CFT subjected to axial and flexural loads are nowadays available in the literature (Goode 2008). Most of the studies have pointed out the beneficial effects of CFT when subjected to different types of loading by comparing their cross-sectional resistance and ductility to pure steel or pure concrete elements. Consensus concerning this matter has been achieved among researchers: due to an enhancement of the confined concrete strength, the resistance of CFT is quite higher than the addition of the resistances of each material when considered separately. The compressive strength is increased due to tri-axial confinement of the concrete core. The susceptibility to local buckling of the steel tube is decreased since the concrete core provides to the steel plate an additional constraint. This constraint prevents the plate to undergo inwards buckling and thus, the critical buckling load of the plate is increased.

Several models of resistance prediction have been proposed (Hatzigeorgiou 2008, Susantha et al. 2001, Johansson 2002) for members with relatively thick steel plates. These models have been compared by several authors (Beck et al. 2009, Oliveira et al. 2010, Chacón et al. 2011) with relevant codes (EN1994 2004, AISC 2005). These comparisons have pinpointed the adequacy of the prediction of the confinement effect onto the ultimate strength of CFT subjected to combined bending and compressive loads.

Moreover, it is understood that CFT columns subjected to bending and/or compressive loads might be prone to local buckling when the D/t ratio of the steel tube is high. The critical buckling loads of the plates belonging to CFT may condition the cross-sectional capacity of the members. The critical buckling mode associated with local instability of a steel plate of a CFT might be labeled as "outwards buckling" since the steel plate is not able to develop inwards waves. As far as known by the authors, no information concerning mathematical developments or eigenvalue analyses of such phenomenon are available in the literature. The cross-sectional resistance of CFT has been traditionally decoupled from the local buckling phenomenon by limiting the D/t ratio of the tube to certain limits.

On the other hand, researchers have pinpointed an existing post-local-buckling strength of slender steel plates which contributes to the ultimate strength of the whole section (Kwon et al. 2011). Several formulae are provided by these authors for the sake of predicting the ultimate strength of the steel plate. These formulae do not require the computation of the effective area of the plate and are derived empirically from a series of experimental tests.

In this paper, the potential local buckling of CFT is studied by means of a fully three dimensional FE-based numerical model in which: i) the concrete core is modeled with solid finite elements and the confinement effect is accounted for and ii) the steel tube is modeled with shell elements and the potential local buckling is taken into account.

The model includes a contact-based formulation in which both entities interact realistically. Full material and geometrical nonlinearity is included. Results concerning the susceptibility to local buckling of the steel plate as well as comparisons with the European code EN1994 are provided at the end of the paper.

In addition, experimental results of CFT subjected to pure compression gathered from the literature are used for comparison purposes.

2 EN1994. DESIGN OF COMPOSITE STEEL AND CONCRETE STRUCTURES

2.1 *General*

EN1994 provides with guidelines for the design of composite columns and compression members with steel grades S235 to S460 and normal weight concrete of strength classes C20/25 to C50/60. These guidelines apply to isolated columns and columns in framed structures where the other structural members are either composite or purely metallic. The steel contribution ratio δ (eq. 1) should fulfill the condition $0{,}2 \leq \delta \leq 0{,}9$.

$$\delta = \frac{A_s \cdot f_y}{A_s \cdot f_y + A_c \cdot f_{ck}} \tag{1}$$

Two methods of design are given: i) a general method whose scope includes members with non-symmetrical or non-uniform cross-sections over the length, ii) a simplified method for members of doubly symmetrical cross-sections.

2.2 *Simplified method*

Only the simplified method is discussed herein. The members must be checked for: cross-sectional resistance, resistance to local buckling and resistance to shear between steel and concrete elements. The cross-sectional resistance must be verified with the well known interaction diagram. The plastic resistance to compression $N_{pl,Rd}$ of a CFT cross-section should be calculated by adding the plastic resistances of its components. Account may be taken of increase in strength of concrete caused by confinement.

The resistance of a cross-section to combined compression and bending and the corresponding interaction curve may be calculated assuming rectangular stress blocks as shown qualitatively in Fig. 1. This diagram can be constructed by varying the neutral axis throughout the cross-section and satisfying the cross-sectional equilibrium with the pair of resulting forces N and M.

Account may be taken of increase in strength of concrete caused by confinement (point A in Fig. 1) This allowance is valid if and only if the relative slenderness of the structural element does not exceed 0,5 and the relative eccentricity of the applied load e/D does not exceed 0,1, being e the eccentricity of loading given by the applied forces M_{Ed}/N_{Ed} and D the diameter of the tube.

2.3 *Local buckling*

Local buckling should be accounted for if the diameter-to-thickness ratio D/t in CFT is greater than $90 \cdot 235/f_y$. The effects of local buckling may be neglected for a steel section if the given limit is not exceeded. If $D/t > 90 \cdot 235/f_y$, full account of local buckling is necessary in all calculations (the designer is recommended to approach this calculation as in shell structures, EN1993-1-6) and the simplified model is no longer valid.

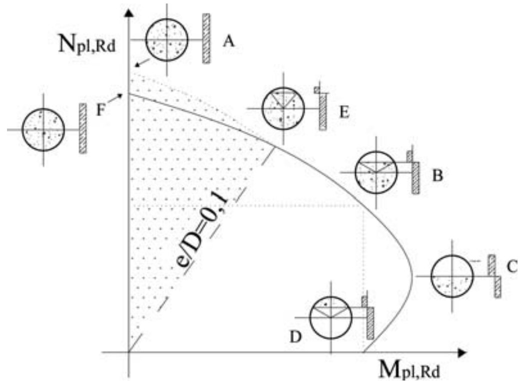

Figure 1. Cross-sectional interaction diagram of a CFT according to EN1994.

3 NUMERICAL MODEL

3.1 *Geometrical modelling*

The structural response of the CFT is modeled by means of the three-dimensional, multi-physics, FE-based Software (Abaqus v10.3, 2011). The concrete core is modeled by using C3D8R solid elements whereas the steel tube is modeled with S4R shell elements.

Both geometries are put together by means of a surface-based contact formulation and meshed separately. This contact formulation reproduces both normal and tangential behaviors between surfaces. For the former, the model allows separation (but no penetration) of adjacent nodes of both entities whereas for the latter, the model is based upon a linear force-slip tangential behavior with a friction coefficient $\mu = 0{,}3$. For both cases tangential and normal stresses are transmitted from one entity another. Thus, the steel tube might induce a certain level of confinement to the concrete or alternatively, the steel plate might undergo local buckling if it is separated from the concrete core. Moreover, it is worth pointing out that symmetries were employed for the sake of reducing the computational cost of the simulations.

3.2 *Constitutive equations*

The concrete core is characterized by a plasticity-based damage model. It assumes that the main two failure mechanisms are tensile cracking and compressive crushing of the concrete material. On the one hand, the model assumes that under uni-axial compression the response is initially linear until the value of failure stress is reached. The maximum stress corresponds to the onset of micro-cracks in the material. The plastic response is characterized by a nonlinear path until the value of f_{ck} is attained and a strain-softening response

Figure 2. Mesh and numerical modelling.

characterizes the material beyond this point. Beyond this stress, the behavior is represented macroscopically with a softening response. On the other hand, the model assumes that the uniaxial tensile response is linear until the value of $f_{ctk} = 0{,}09 \cdot f_{ck}$ is reached (a user-tuneable magnitude). The post-cracking response is characterized by means of values of fracture energy (GFI $\approx$ 0,15 N/mm). The multi-axial behavior is reproduced by means of a scalar damage elasticity set of equations. The uni-axial resistance is increased up to $1{,}16 \cdot f_{ck}$ if the material is subjected to multi-axial stress (also a tuneable magnitude).

The steel tube is characterized by means of elastic-perfectly plastic material. Uni-axially, the material yields once f_y is attained. Multi-axially, the von Mises criterion determines the onset of yielding. No strain hardening is considered in this study.

3.3 *Type of analysis*

The studied phenomenon is strongly nonlinear. Tensile cracking of the concrete, local buckling of the steel plate together with a contact-based formulation must be dealt with coupled. For making the simulations computationally tractable, it has been decided to use an explicit analysis. The procedure solves the equation of motion which relates the inertial forces, the viscous forces and the elastic forces into the same equilibrated system (either static or dynamic).

The rate of load-introduction as well as the mass-scaling of the system is set in such a way the structural problem may be assumed as quasi-static rather than dynamic.

3.4 *Numerical simulations*

The numerical simulations consisted of two load-steps (Fig. 3). It is important to point out that these numerical simulations belong to a vaster study on CFT belonging to integral bridges. Therefore, the numerical simulations were aimed at reproducing the type of forces that the piers from integral bridges are usually subjected to (Chacón et al. 2011). In any case, the internal forces may be summarized in: compressive, bending or a combined action of bending and compression.

- At the first step, an axial load was centrically applied to the CFT. This axial load represents a percentage of the squash load $N_{pl,Rd}$ of the CFT. Eight different values ranging from 0% to 100% of $N_{pl,Rd}$ are included (for the case of 100% of $N_{pl,Rd}$, the CFT fails and the analysis finishes).

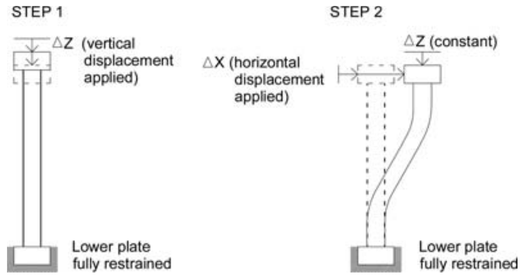

Figure 3. Loading steps in the numerical simulations.

- At the second step, a lateral displacement was applied on the upper cross-section. These displacements assumingly reproduce the non-mechanical (creep, shrinkage, etc) and mechanical deformation (braking, seismic loads) from the bridge deck. The upper cross-section remains horizontal during the whole analysis.
- The resulting internal forces of the CFT can be obtained by applying equilibrium conditions (eq. 2 to 4).

$$\Sigma F_{ver} = 0 \rightarrow N_A = N_B = N \tag{2}$$

$$\Sigma F_{hor} = 0 \rightarrow V_A = V_B = V \tag{3}$$

$$\Sigma M = 0 \rightarrow M_A = M_B = \frac{V \cdot L}{2} + N \cdot \Delta \tag{4}$$

4 NUMERICAL DATABASE

4.1 *Experimental database*

A vast experimental database of 1819 experimental tests is available in the literature (Goode 2008). This database includes tests performed by several authors and provides geometrical, material and ultimate loads information of circular, square and rectangular CFT subjected to axial and/or flexural loads. In this paper, a sample of 526 circular CFT subjected to pure compression excerpted from this database is used for comparison purposes. The sample is chosen in such a way the specimens are not prone to global buckling according to the EN1994 criteria.

4.2 *Numerical database*

A numerical database provided in the present study consists of 192 circular CFT prototypes of total length L = 10,0 meters and outer diameter D = 1,0 meter (L/D = 10) and 112 CFT prototypes with L = 10,0 meters and D = 2,0 meters (L/D = 5). A set of parametric variations of the steel contribution ratio was developed. These specimens were numerically subjected to various combinations of axial and flexural loads. This database has been useful in other studies performed by the authors concerning the ultimate load

Table 1. Geometry of the numerically simulated prototypes.

Element	D (m)	Thickness (mm)	f_y (N/mm^2)	N ($\%N_{plRd}$)	Simulations
L10D1M	1	10-15-20 25-30-35	235–275 355–460	8 cases [0–100]	192
L10D2M	2	20-30-40 50-60-70-80	355–460	8 cases [0–100]	112
				Total	304

Table 2. Additional numerical simulations.

Element	D (m)	Thickness (mm)	f_y (N/mm^2)	Total cses
L10D1M	1	6	235–275	4
	1	8	355–460	4

capacity and ductility of CFT subjected to bending and compressive loads (Chacón et al. 2011) for the particular case of integral bridge piers. Table 1 summarizes the geometrical and material properties of the studied CFT. The steel tube presents variations in thickness as well as in yield strength f_y whereas the concrete core is characterized with an invariable compressive strength $f_{ck} = 30\,N/mm^2$ for all cases. In this study, additional simulations were performed in elements subjected to pure compression with very high D/t ratios. Table 2 depicts the geometries of such prototypes. The length is set to L = 10,0 meters and the outer diameter D = 1,0 meter (L/D = 10).

5 EXPERIMENTAL RESULTS

The sample depicted in sub-section 4.1 includes prototypes subjected to purely compressive loads. The ultimate load capacity of those specimens is provided though information concerning the failure mode of such prototypes is not fully documented.

Figure 4 shows the ultimate load capacity of 526 CFT subjected to pure compression standardized to the EN1994 (in this case, the formulation is applied without accounting for the effect of confinement). The results are plotted against the ratio $(D/t)/(90{\cdot}\varepsilon^2)$. These plots should be read as follows: i) If $N_{exp}/N_{EN1994} < 1{,}0$, the results are not on the safety side, ii) If $(D/t)/(90{\cdot}\varepsilon^2) > 1{,}0$, the CFT should be labeled as susceptible to local buckling (and thus the simplified method would not be valid in the present form). Bold lines indicate the boundaries of the aforementioned regions.

Close inspection of the results leads to twofold conclusions:

- The vast majority of the results are on the safety side (regardless of the susceptibility to local buckling).
- The ultimate load capacity of the allegedly prone to local buckling specimens is generally greater than the EN1994 prediction.

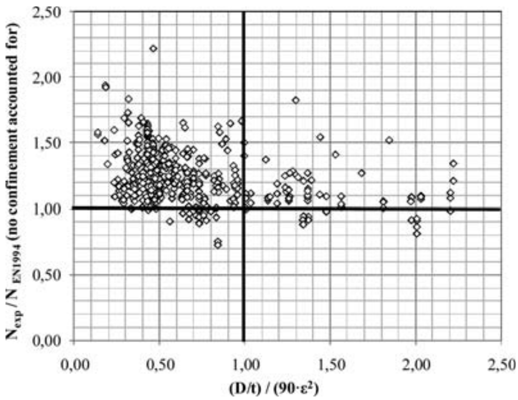

Figure 4. Experimental results as a function of their susceptibility to local buckling (no confinement accounted for).

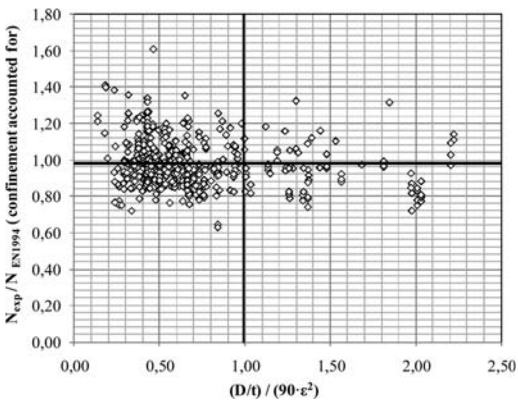

Figure 5. Experimental results as a function of their susceptibility to local buckling (confinement accounted for).

- The D/t limitation provided in EN1994 does not seem to represent the pivotal point beyond which local buckling occurs. However, this plot does neither give information about the possibility that these prototypes undergo local buckling nor, about their potential post-buckling reserve.

Figure 5 shows the ultimate load capacity of 526 CFT subjected to pure compression standardized to the EN1994 (in this case, the formulation is applied accounting for the effect of confinement, point A in Fig 1).

In this case, the vast majority of the results are not on the safety side (regardless of the susceptibility to local buckling). The plot suggests a warning about the validity of the confinement effect provided by EN1994. Similar results have been pinpointed by other authors (Beck et al 2009, Chacón et al 2011).

6 NUMERICAL RESULTS

The experimental results presented in previous sections pinpoint that the susceptibility to local buckling is not reproduced adequately with the limiting ratio D/t. This section provides further information related to the physical phenomenon that clarifies the structural problem to some extent. The results are separated in two sub-sections, namely, pure compression and pure bending. Due to space constraints, the combined bending and compression phenomenon is not treated herein.

6.1 *Pure compression*

CFT subjected to pure compression show different structural response depending on the D/t ratio. Expectedly, the prototypes with high D/t undergo local buckling at early load stages whereas prototypes with low D/t show considerable yielding at failure load. The "axial force" – "longitudinal displacement" curve of the prototype $L = 10$ m, $D = 1$ m and $t = 10$ mm is given in Fig. 6 for various values of steel yield strength f_y. All prototypes presented in this plot should be labeled as "prone to local buckling" according to EN1994. The structural response show different branches. First, all prototypes exhibit an identical linear response. After awhile its slope changes suddenly. This change is identified as a bifurcation point.

At this point, for the prototype with $f_y = 235$ N/mm^2, the steel plate has already reached its yield strength. The slope of the post-bifurcation point branch is very low compared to the linear branch.

For the prototype with $f_y = 460$ N/mm^2, the steel plate has not yet reached its yield strength at the bifurcation point. The slope of the post-buckling branch is considerably high. Eventually, the steel plate yields and the post-buckling slope is degraded to the same level as for the prototype with $f_y = 235$ N/mm^2. For high values of longitudinal displacement, the concrete core crushes (the longitudinal strain reaches $\varepsilon = 0{,}35\%$).

Fig. 7 shows the axial load as a function of the radial displacement of a node located nearby the area of local buckling (Fig. 8 shows this area). The bifurcation point is noticeable (labeled as "buckling" in Fig. 6 and Fig. 7). The change of slope is particularly sharp for the prototype with $f_y = 235$ N/mm^2.

Fig. 8 shows the von Mises stresses of the steel plate in a deformed shape obtained from the numerical simulations. The figure shows a detail of the fully restrained bottom plate of the prototype. The buckling mode is noticeable and additionally, according to the color scale, it is observed that at buckling, the prototype has undergone severe yielding (the units of the von Mises stresses are in N/m^2).

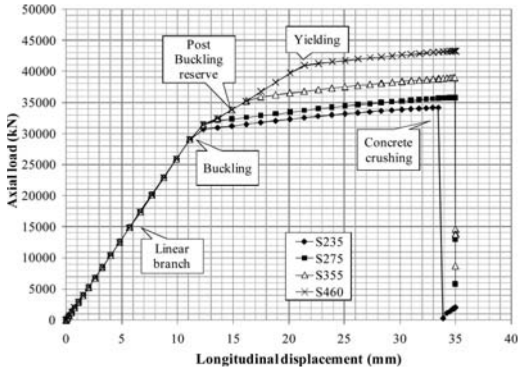

Figure 6. Axial load-longitudinal displacement plot of prototypes with high D/t ratio (D/t = 100).

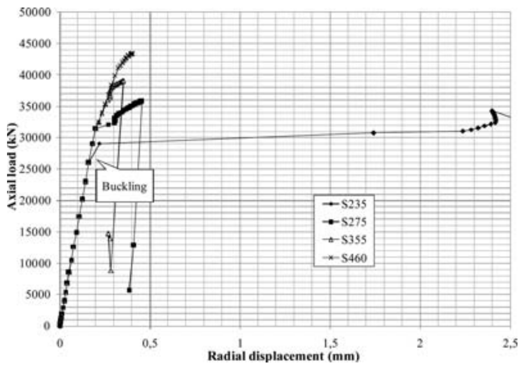

Figure 7. Axial load-radial displacement plot of prototypes with high D/t ratio (D/t = 100).

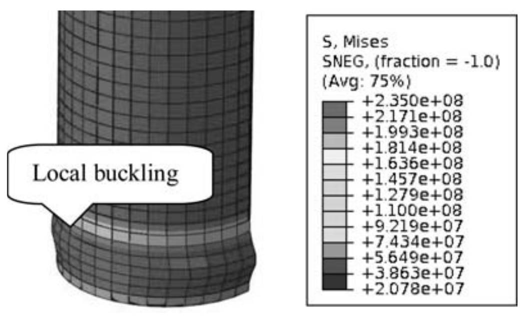

Figure 8. von Mises stresses at bifurcation point for a prototype with high D/t ratio (D/t = 100) and $f_y = 235$ N/mm^2.

On the other hand, Fig 9 shows the axial force-longitudinal displacement curve of the prototype $L = 10$ m, $D = 1$ m and $t = 30$ mm for various values of steel yield strength f_y. All prototypes presented in this plot should not exhibit local buckling according to EN1994. In this case, the structural response shows different stages. First, all prototypes exhibit an

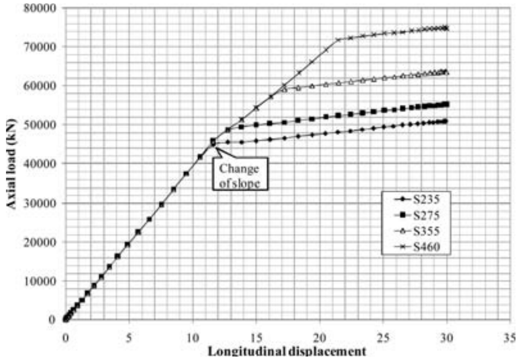

Figure 9. Axial load-longitudinal displacement plot of prototypes with low D/t ratio (D/t = 33.33).

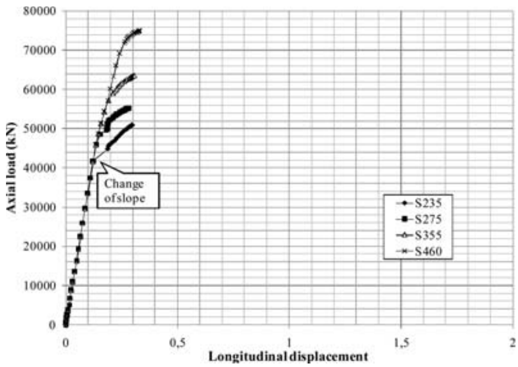

Figure 10. Axial load-radial displacement plot of prototypes with low D/t ratio (D/t = 33.33).

identical linear response. Secondly, the initial linear slope changes. This change is sharper for prototypes with $f_y = 235\,N/mm^2$ than for prototypes with $f_y = 460\,N/mm^2$ in which it is almost unnoticeable.

The main difference between high and low D/t ratios stems in the axial force-radial displacement curve. This radial displacement is shown in Fig. 10 and also exhibits a change of slope. This occurs at considerable higher values than in prototypes with high D/t ratio. Moreover, the change of slope is not as sharp as the one observed with more slender prototypes.

Fig. 11 shows the von Mises stresses (N/m^2) of the steel plate in a deformed shape obtained from the numerical simulations at the point at which the slope changes. No out-of-plane deformation is noticeable. It is also observed that at buckling, the prototype has not yet undergone any noticeable yielding ($f_y = 460\,N/mm^2$).

6.2 *Pure bending*

The numerical simulations of a prototype subjected to pure bending are developed in CFT subjected to lateral displacements at the upper cross-section as shown in Fig. 3. No previous axial force is applied for these cases. A lateral displacement Δ of an element with

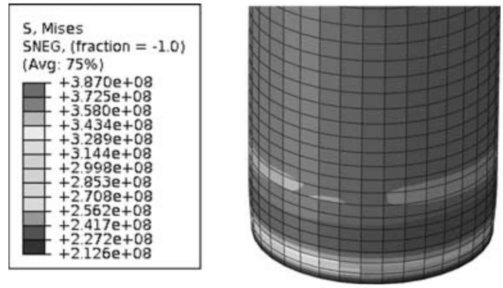

Figure 11. von Mises stresses at the change-of-slope point for a prototype with low D/t ratio (D/t = 33.33) and $f_y = 460\,N/mm^2$.

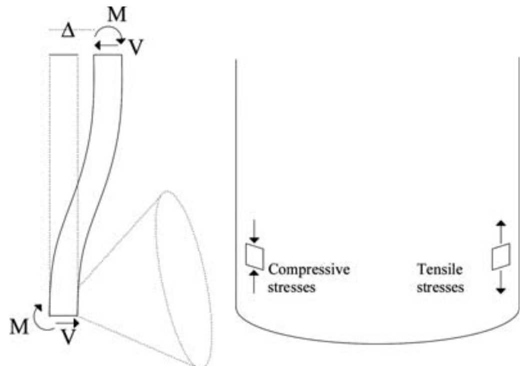

Figure 12. Resulting internal forces.

fully restrained end cross-sections develops internal forces as shown in Fig. 12. The resulting bending moments generate both compressive and tensile stresses in the CFT. These compressive stresses may cause buckling of the steel plate.

In an incremental process, the relationship between the displacement Δ and the resulting bending moment M is initially linear. At high load stages this process might become considerably nonlinear due to various reasons (buckling, yielding, cracking). Fig 13 shows a render from a process of a CFT subjected to an incremental Δ displacement. The render shows a view cut detail of the fully restrained bottom cross-section at which local buckling occurs. The chosen prototype has dimensions L = 10 m, D = 1 m, t = 10 mm. Clear separation between materials is observable.

As a matter of fact, the relative displacement between the concrete core and the steel plate varies throughout the incremental process. Fig. 14 shows the absolute displacement of two nodes (whose position is indicated in Fig. 13) as a function of the step-time of the incremental process. The first node belongs to the concrete core and the second node belongs to the steel plate. Both nodes are adjacent and in absence of local buckling, both nodes are expected to undergo the same level of displacement. In Fig. 14, it is observed that the displacement of both nodes may be separated in three different zones. Zone A, at which both nodes exhibit identical displacement. Zone B, at which

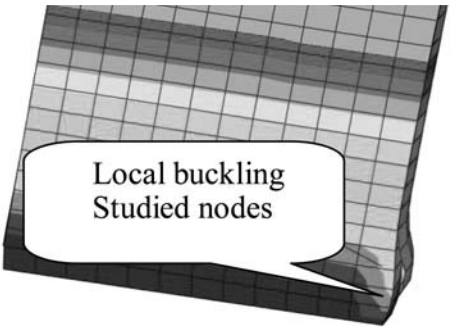

Figure 13. Separation between concrete and steel in the compressed area of the bottom cross-section.

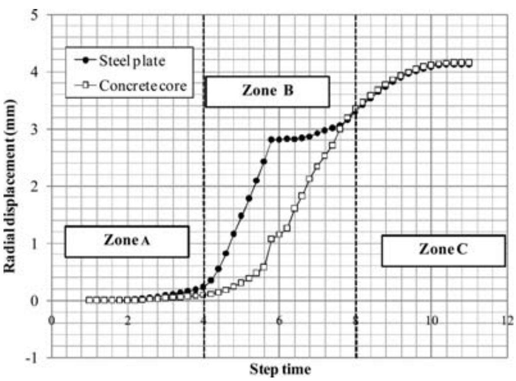

Figure 14. Radial absolute displacement of the nodes located at adjacent positions of the steel plate and concrete core.

there is a clear separation between both nodes (local buckling zone) and Zone C, the post-buckling zone, at which the concrete core exhibits a greater radial deformation (there is no steel plate confining it) and eventually, it reaches again the steel plate. An analysis of such behavior has been performed for all specimens belonging to the database presented in table 1.

Fig. 15 shows the difference between the absolute displacements between both nodes. This difference is labeled as the "relative" displacement between entities. It is observed that at Zone A, the difference is null. At Zone B, the relative displacement reaches a maximum value (1,85 mm for this particular prototype) and eventually, the relative displacement decreases to zero at Zone C.

The magnitude of the maximum relative displacement does not give further information about the potential local buckling of the prototype. If, however, this magnitude is expressed in terms of the plate thickness, further information may be extracted from this measure. Fig. 16 shows the maximum relative displacement between nodes expressed as a percentage of the plate thickness for different CFT (L = 10 m, D = 1 m, varying t [10,15,20,25,30,35] mm). The results are plotted as a function of the D/t ratio. The

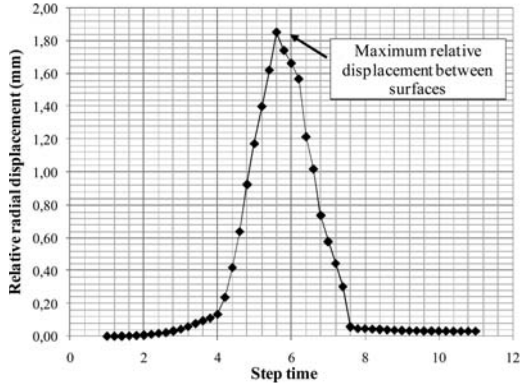

Figure 15. Relative displacement between the nodes located at adjacent positions of the steel plate and concrete core.

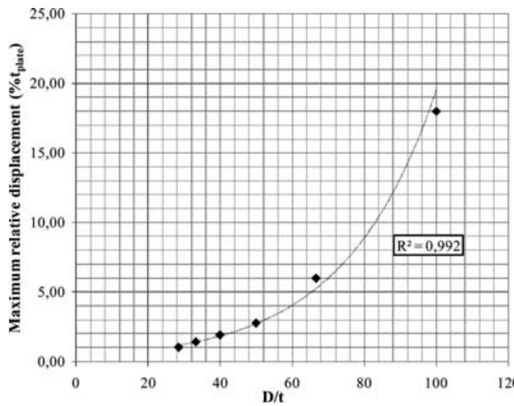

Figure 16. Relative displacement as a function of D/t. L = 10 m. D = 1 m. $f_y = 235$ N/mm^2.

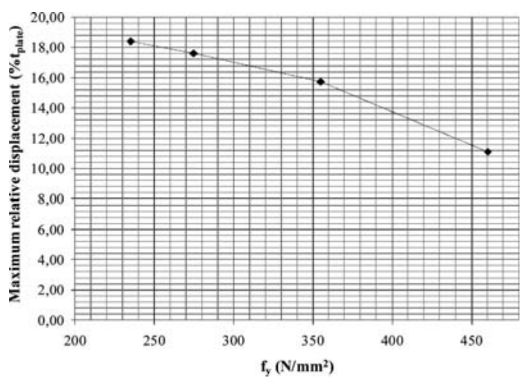

Figure 17. Relative displacement as a function of f_y. L = 10 m. D = 1 m. t = 10 mm. D/t = 100.

relationship between both magnitudes is clearly exponential. A best fit curve is also plotted with the results. This fit is quite accurate according to the regression coefficient R^2=0,992. Noticeably, the higher the D/t ratio, the higher relative displacement between the concrete core and the steel plate is. In terms of the plate thickness, the results vary ranging from 1% to 18% of t.

Expectedly, the prototype that exhibits a greater separation between materials presents a $D/t = 100$. Unexpectedly though, this relative displacement is dependent on the yield strength of the tube f_y in such a way that the higher the f_y, the lower the separation.

This observation contradicts the EN1994 limitation $D/t < 90 \cdot \varepsilon^2$ but is in fully accordance with the results presented in sub-section 6.1 for compressed members.

7 CONCLUSIONS

On the one hand, the experimental results presented in this paper show that the ultimate load capacity of CFT subjected to compressive loads is not particularly sensitive to the susceptibility to local buckling that is defined in EN1994.

On the other hand, the numerical results presented provide a phenomenological insight concerning local buckling in CFT. Failure modes and structural responses of CFT subjected to both compressive and bending loads are described. This insight gives hints about the pre- and post buckling behavior of CFT. Preliminary results show that the EN1994 limitation concerning the susceptibility to local buckling is contradictory to the hitherto observed trends. A more detailed research program concerning this important topic is being performed by the research team.

ACKNOWLEDGMENT

The authors acknowledge the financial support provided by the Spanish Ministerio de Ciencia e Innovación as part of the project 7004/T07-51 "Seguridad y funcionalidad de los puentes integrales frente a acciones accidentales. Investigaciones para el establecimiento de criterios de diseño y construcción".

REFERENCES

Abaqus Simulia V 6.10. Dassault Systemes. RI. USA. 2011

American Iron and Steel Construction (AISC). Specification for steel structural buildings. 2005

Beck A., Oliveira W., Nardim S., El Debs A. 2009. Reliability-based evaluation of design code provisions for circular concrete-filled steel columns. Engineering Structures, Vol 31 (10): 2299–2308.

Chacón R., Mirambell E., Real E. 2011 Strength and Ductility of Concrete-Filled Tube Piers. 6th European Conference on Steel and Composite Structures, Budapest. Eurosteel.

European Committee for Standardisation (ECS). 2004. Eurocode 4: design of composite steel and concrete structures, Part 1-1: general rules and rules for buildings.

Goode C. 2008. Composite columns – 1819 tests on concrete-filled steel tube columns compared to EN1994. *The Structural Engineer.* 18(16): 33–38.

Hatzigeorgiou, G., 2008. Numerical model for the behaviour and capacity of circular CFT columns, Part I: Theory, Engineering Structures, Vol. 30 (6): 1573–1578.

Johansson, M. The efficiency of passive confinement in CFT columns. 2002. Steel and Composite Structures, Vol. 2 (5): 379–396.

Kwon Y., Seo S., Kang D. 2011. Prediction of the squash loads of concrete-filled tubular section coluns with local buckling. Thin-Walled Structures, Vol 49 (1): 85–93.

Oliveira W., Nardim S, El Debs A, El Debs M. 2010. Evaluation of passive confinement in CFT columns. Journal of Constructional Steel Research, Vol 66 (4); 487–495.

Susantha, K., Ge, H., Usami, T. 2001. A capacity prediction procedure for concrete-filled steel columns. Journal of Earthquake Engineering, Vol. 5 (4): 483–520.

Tubular Structures XIV – Gardner (Ed.)
© 2012 Taylor & Francis Group, London, ISBN 978-0-415-62137-3

Concrete filled circular hollow sections under cyclic axial loading

T. Sheehan & T.M. Chan
University of Warwick, UK

ABSTRACT: This paper describes investigations into the structural response of concrete-filled Circular Hollow Sections (CHSs) under cyclic axial loading. The research is based primarily upon laboratory testing. A series of tests on both hot-formed and cold formed concrete-filled CHSs with a non-dimensional global slenderness in the region of 1 were conducted to investigate key structural responses including first cycle peak load, post buckling resistance, reserve strength, ductility level and energy dissipation. Measurements were taken of cross-section geometry, geometric imperfections and material properties. Key test results and sample load-deformation histories are presented. The generated structural performance data will be exploited to calibrate the numerical finite element models which will be used for further parametric studies.

1 INTRODUCTION

A variety of structural systems are used in seismic buildings to provide lateral stability and dissipate energy. Among these, concentrically braced frames are often favoured for simplicity of design. Furthermore, they are more susceptible to ductile failure modes, in contrast to moment frames, which often undergo brittle failure at the connection. Rectangular hollow steel sections are usually selected as bracing members and a significant amount of research has been carried out on these to date, such as Nip et al. (2010), comparing the response of hot-rolled carbon, cold-formed steel and stainless steel sections under cyclic axial loading. In addition to this, several researchers have explored the behavior of concrete-filled steel rectangular sections, such as Broderick et al. (2005), Lee et al. (2000) and Liu & Goel (1988). Concrete-filled tubular braces are becoming increasing popular for this application owing to their excellent strength and ductility in comparison with hollow steel sections. The contribution of concrete enhances the strength of these slender braces in compression, delaying the onset of local buckling and reducing the difference in resistance between compressive and tensile loading.

In practice, circular hollow sections are often overlooked, since more intricate connections are required. However, research to date, such as Elchalakani et al. (2003) and Martinez-Saucedo et al. (2008) have demonstrated that hollow circular steel members are also highly suitable for use as bracing members, as they are not as sensitive to local buckling as rectangular sections owing to the more uniform shape. The advantages of this section could be utilized further by using concrete-filled circular hollow sections as bracing members. The homogeneity of confining pressure on the concrete core and outward pressure on the steel tube provides the optimum cross-section.

Hence, this research will compare the resistance of hollow and concrete-filled circular tubes of both hot-rolled and cold-formed steel. A series of laboratory tests will be carried out, applying a cyclic axial load to each specimen in accordance with ECCS guidelines (1986). Intermediate-length bracing members will be tested, having a non-dimensional slenderness in the region of 1.0 in accordance with BS EN-1993-1-1 (2005) and BS EN 1994-1-1 (2004).

2 EXPERIMENTAL STUDY

2.1 *Introduction*

A series of tensile steel material tests, compressive concrete material tests and column tests under cyclic axial loading were carried out to investigate the structural behaviour of concrete-filled circular hollow sections under cyclic axial loading. All tests were performed in the Structures Laboratory of the School of Engineering, University of Warwick.

2.2 *Tensile coupon tests*

Tensile coupon tests were performed to establish the basic material stress-strain response; this was subsequently utilised during the analysis of the member test results and in the development of numerical models. The tests were carried out in accordance with BS EN ISO 6892-1 (2009).

Two types of steel section were employed for this research: A hot-finished circular tube with a nominal yield stress of 355 N/mm^2 and wall thickness of 3.2 mm (Celsius 355) and a cold-formed tube with a nominal 0.2% proof stress of 355 N/mm^2 and a wall thickness of 3.0 mm (Hybox 355). Both sections had an outer diameter of 48.3 mm. For each material,

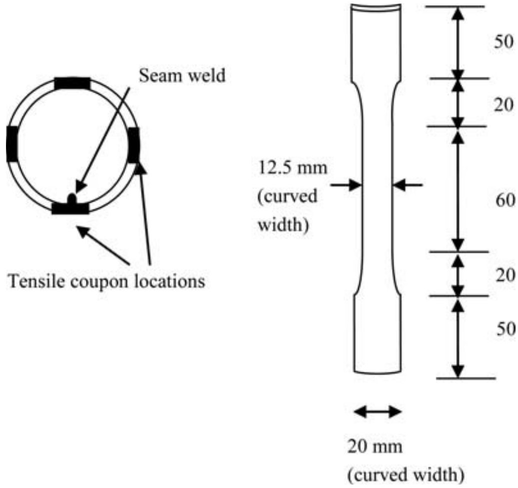

Figure 1. Tensile coupon locations and dimensions.

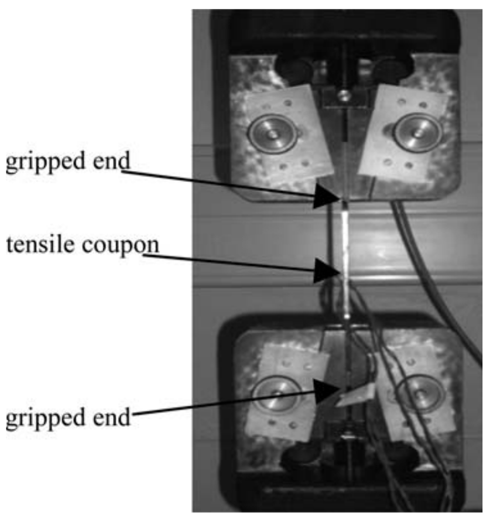

Figure 2. Tensile testing set-up.

4 longitudinal coupons were taken from different locations around the cross-section circumference. The coupon locations and dimensions are shown in Figure 1.

The test set-up is shown in Figure 2. The coupon ends were flattened prior to testing in order to fit inside the grips of the testing machine. While this process is thought to have locally work-hardened the end portions, the coupons were dimensioned so as to mitigate the effect of this hardening on the central region.

Typical stress-strain relationships obtained for both hot-rolled and cold-formed steel coupons are presented in Figure 3. The results correlate closely to those expected, with the hot-rolled steel exhibiting reasonably linear behaviour up to yield, followed by a plateau before advancing to the strain hardening region. The cold-formed steel on the other hand is

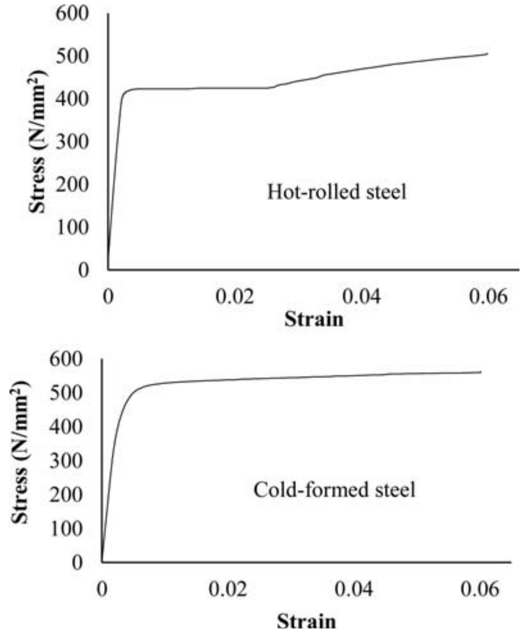

Figure 3. Stress-strain relationships from tensile coupon tests.

Table 1. Results of tensile coupon tests.

Steel	Yield stress/ 0.2% proof stress (N/mm^2)	Ultimate tensile Stress (N/mm^2)	Young's modulus (N/mm^2)	% elongation after fracture
Hot-rolled	415	546	206000	37
Cold-formed	499	573	184000	30

significantly more non-linear in the initial stages and does not display the same plateau as the hot-finished coupons.

The average yield stress (hot-rolled)/0.2% proof stress (cold-formed), ultimate stress, Young's modulus and percentage elongation after fracture are presented in Table 1 for both types of steel. In determining the values, the seam weld-coupon results were omitted.

2.3 *Concrete material tests*

A number of trial concrete mixes were carried out. Water-cement ratios and proportions of coarse and fine aggregate were varied in order to meet two objectives. The first objective was a compressive strength in the region of 20–25 MPa. This is to meet the minimum strength requirement of Grade 20 for seismic applications, specified in BS EN 1998-1. Also, it has been found that higher concrete strengths do not provide much benefit – this was shown by Broderick et al. (2005) for strengths greater than 28 MPa. The second objective was to achieve satisfactory compaction

Table 2. Concrete mix proportions by weight.

Water	Cement	Coarse aggregate	Fine aggregate
0.72	1	2.3	2.86

Table 3. Compressive strength and static elastic modulus.

7 day strength N/mm^2	28 day strength N/mm^2	Test date strength N/mm^2	Static elastic modulus N/mm^2
17.14	25.1	29.4	20100

for the long, slender tubes. Various methods of vibration were investigated and an effective procedure was developed using a beam-vibrator and a rubber mallet. Specimens were cast vertically, with the vibrator clamped onto a loosely bolted steel frame which was in direct contact with the test specimen. This arrangement was found to provide ample pulsation without leading to segregation and the method was aided by gently tapping the sides of the tube with the mallet. The tubes were filled in layers, with continuous vibration of the frame during casting and application of the mallet after each layer. After casting, the tops of the tubes were sealed with plastic to prevent the escape of moisture during curing. The design concrete mix is shown in Table 2.

The concrete mix used a maximum aggregate size of 6.35 mm had a high percentage of water and fine aggregate. The compressive strength was obtained in accordance with BS EN 12390-3 (2003) at 7 days, 28 days and the day of testing. In addition to this, the static elastic modulus on the test date was also measured. The values for these are given in Table 3.

2.4 *Column tests*

Cyclic axial tests were performed on six tubular columns, three of which consisted of hot-finished steel and the remaining three of cold-formed steel. For each steel type, one specimen was hollow, while the remaining two were filled with concrete.

2.4.1 *Specimen preparation*

All specimens were circular sections, with an outer diameter of 48.3 mm and a length of 1500 mm. All concrete-filled specimens were cast with the concrete mix given in Table 2 and compacted as described in Section 2.3. Following casting, both hollow and concrete-filled tubes were welded onto 25 mm thick steel end plates, and two outer stiffeners of dimensions 125 mm × 50 mm × 8 mm were welded onto each end as shown in Figure 4.

A small hole was drilled in the centre of the end-plates, in order to facilitate the escape of water vapour from the tube during welding. After manufacture,

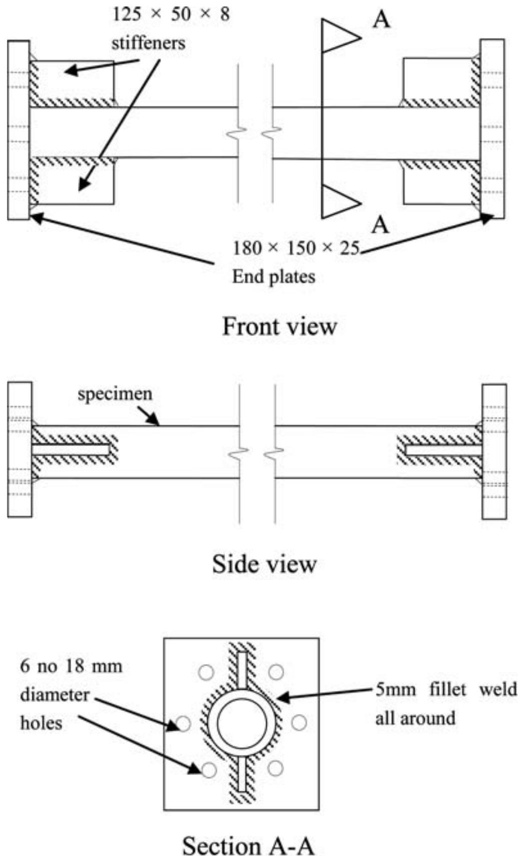

Figure 4. Cyclic test specimen details.

Table 4. List of test specimens and global imperfections.

Label	Steel	Infill	Global imperfection mm
HR-H	hot-finished	hollow	0.58
CF-H	cold formed	hollow	0.73
HR-F1	hot-finished	concrete	0.37
HR-F2	hot-finished	concrete	0.38
CF-F1	cold formed	concrete	0.73
CF-F2	cold formed	concrete	0.67

plaster was injected through the hole to fill the gap between the top surface of the concrete and the end-plate.

Specimen imperfections were measured at 30 mm intervals along each of four faces, in order to obtain the maximum global imperfection. A list of test specimens and corresponding maximum global imperfections is given in Table 4.

2.4.2 *Test procedure*

Specimens were tested in a purpose-built test rig, illustrated in Figure 5. The end plates were bolted

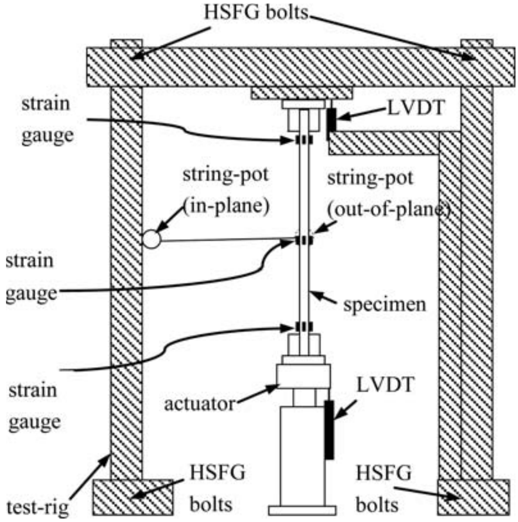

Figure 5. Test-rig and instrumentation.

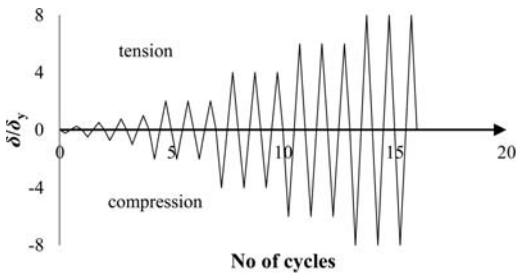

Figure 6. Cyclic loading protocol.

into the test-rig using six M16 bolts at each end and a cyclic load was applied using a 50-tonne hydraulic actuator.

The loading protocol used (Fig. 6) was that outlined in ECCS (1986), in which one compression and tension cycle is applied at each of the following displacement amplitudes: $0.25\delta_y$. $0.5\delta_y$. $0.75\delta_y$. $1.0\delta_y$. followed by three displacement amplitudes at each of the following $2\delta_y$. $4\delta_y$. $6\delta_y$. $8\delta_y$, etc. up to failure, where δ_y is the yield displacement of the specimen obtained from tensile coupon tests.

The axial load and displacement were monitored throughout the tests and in addition to this, the lateral displacement at mid-height was measured in two orthogonal directions, and axial strains at 12 points on the tube – four strain gauges on the four faces (Fig. 7), at the top, middle and bottom of the specimen. Some measures were taken to account for slip at connections and the flexibility of the test rig: HSFG bolts were utilized at the four corners, and the vertical displacement of the top beam was monitored throughout the test using an LVDT. This enabled axial displacement measurements to be adjusted accordingly.

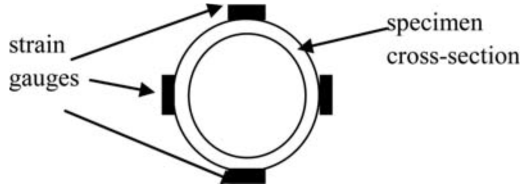

Figure 7. Strain gauge locations.

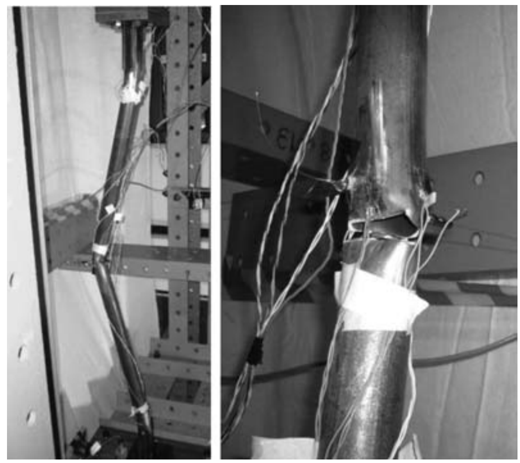

Figure 8. Deformation and failure of HR-H.

2.4.3 *Test results*

2.4.3.1 *Deformation and failure*

All specimens buckled predominantly about the unstiffened axis, regardless of the direction of the maximum imperfection. The hollow specimens, HR-H and CF-H exhibited overall member buckling during the 5th loading cycle, followed by local inward buckling at mid-height during greater displacement amplitudes. The extent of this local deformation increased as cycles progressed, until finally a crack propagated across this region during a tensile loading. Local buckling was mainly concentrated at the mid-height, with no noticeable buckling at the end regions, for either HR-H or CF-H. The failure of HR-H is depicted in Figure 8.

In the case of the concrete-filled tubes, overall buckling occurred in the 5th cycle, similarly to the hollow tubes. However, as the axial displacement increased, local inward buckling was delayed by the presence of the concrete. Curvature at the mid-height was less severe and distributed over a greater distance, as shown in Figure 9, allowing it to undergo larger displacement cycles. In contrast to the hollow tubes, in which the plastic hinge was confined to the mid-height, significant bending was also observed at the ends of the unstiffened length. Specimen HR-F1 showed both inward and outward local buckling at the mid-height and base, and eventually ruptured at these locations. In addition to the buckling, considerable necking was

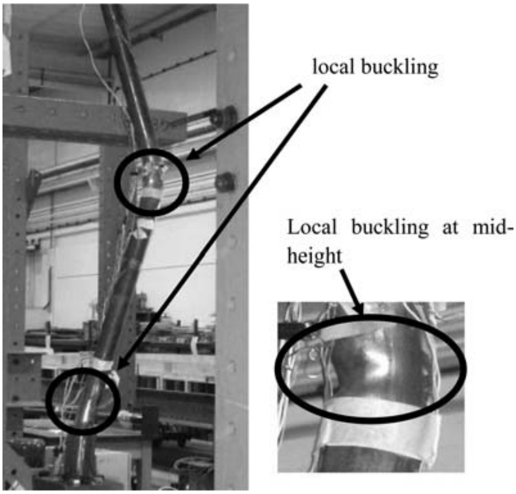

Figure 9. Deformation of HR-F1.

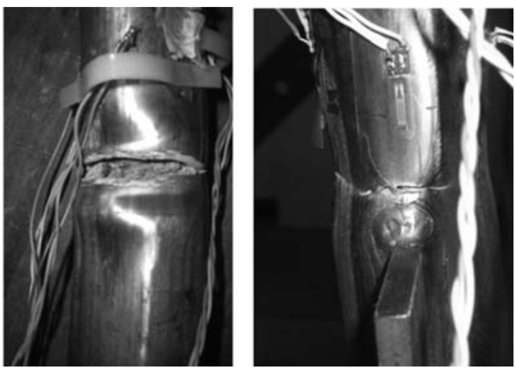

Figure 10. Failure at mid-height and base of HR-F1.

observed at the base of HR-F1, which can be seen in Figure 10.

Specimens HR-F2, CF-F1 and CF-F2 responded in a similar manner to HR-F1, developing plastic hinges near the top, middle and base of the specimens. The severity of local buckling and location of ultimate steel rupture varied from specimen to specimen, with HR-F2 failing near the top, and CF-F1 and CF-F-2 failing close to the base. Figure 11 shows the central and base regions of CF-F2. Here, the local bucking at mid-height (left) was not as severe as for HR-F1 and hence rupture occurred at the base.

A summary of the maximum compressive and tensile loads and number of cycles to failure is given in Table 5. Tensile forces ($N_{t,max}$) are normalized with respect to the expected yield force from the tensile coupon tests ($N_{t,y}$). The first cycle peak buckling loads ($N_{c,max}$) are normalized with respect to the predicted buckling loads ($N_{b,Rd}$) given in BS EN 1993-1-1 and BS EN 1994-1-1 for the hollow and filled specimens respectively. Non-dimensional slenderness ($\bar{\lambda}$) and buckling loads were calculated for hot-rolled and

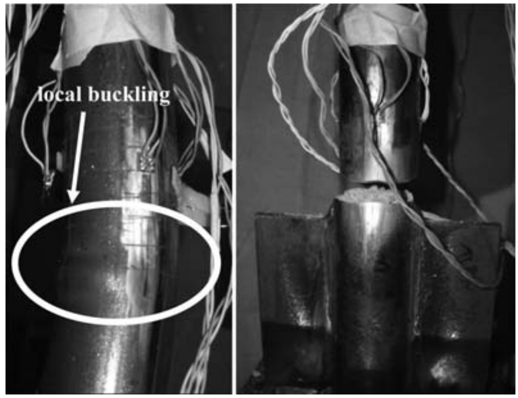

Figure 11. Mid-height region and base of CF-F2 at failure.

Table 5. Maximum numbers of cycles and loads.

ID	No of cycles to fracture	N_{tmax} kN	$N_{t,max}/N_{t,y}$	N_{cmax} kN	$\bar{\lambda}$	$N_{c,max}/N_{b,Rd}$ (EC3/EC4)
HR-H	17	180	0.96	155	0.78	1.17
CF-H	14	209	0.98	151	0.90	1.43
HR-F1	28	198	1.05	174	0.81	1.14
HR-F2	19	198	1.05	175	0.81	1.15
CF-F1	15	220	1.03	174	0.92	1.18
CF-F2	16	216	1.01	164	0.92	1.11

concrete-filled tubes using buckling curve 'a' and for the hollow cold-formed tube using buckling curve 'c'.

The maximum tensile loads for both hot-rolled and cold-formed hollow sections are slightly less than those predicted from the material tests, possibly owing to softening of the material from previous cycles, or from the residual out-of-straightness following elongation during buckling. The maximum tensile loads for concrete-filled specimens slightly exceed the predicted yield load, with the concrete infill providing average improvements of 9.4% and 4.1% for hot-rolled and cold formed filled tubes respectively in comparison with their hollow counterparts.

The first cycle buckling loads also exceed BS EN 1993-1-1 (2005)/BS EN 1994-1-1 (2004) predictions in all cases, with the hollow cold-formed section CF-H displaying a more noticeable increase than the hot-rolled or filled tubes.

2.4.3.2 *Ductility level and energy dissipation*

Load-displacement hysteresis curves for each specimen are presented in Figures 12–17.

Hot-rolled and cold formed members produced similar hysteresis curves, showing significant decreases in compressive and tensile peak loads during the second and third cycles at each displacement amplitude, and gradual degradations in compression and tension loads with increasing axial displacements. Concrete-filled tubes displayed noticeably

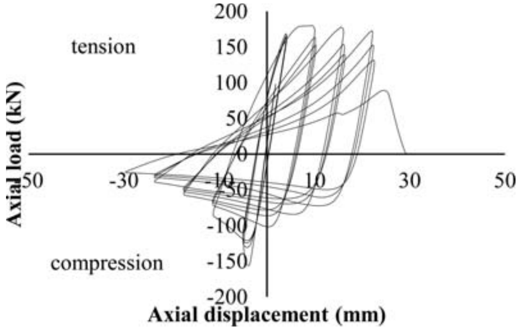

Figure 12. Load-displacement response for HR-H.

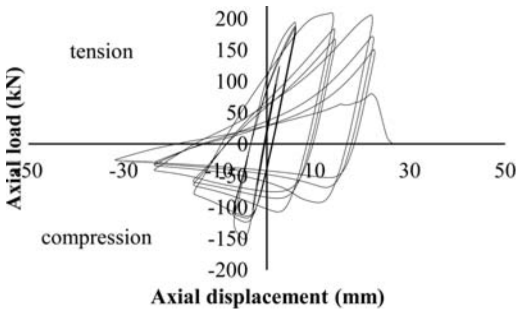

Figure 13. Load-displacement response for CF-H.

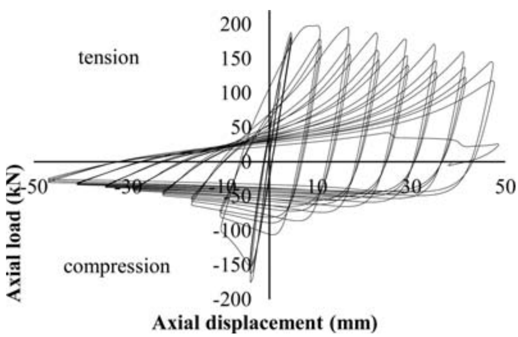

Figure 14. Load-displacement response for HR-F1.

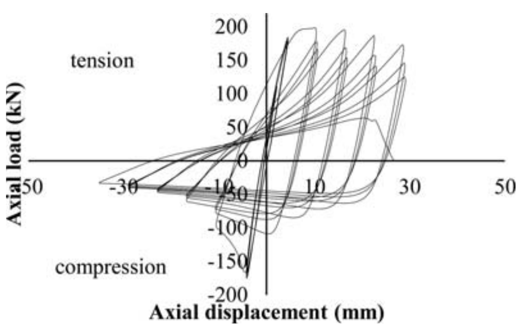

Figure 15. Load-displacement response for HR-F2.

fuller shaped curves than hollow members, and the curve for hot-rolled members was also a more rounded shape than for cold-formed. Also, concrete-filled tubes maintained a higher compressive resistance and more stable behaviour up to the maximum compressive displacement amplitude than hollow tubes. This is illustrated in Figures 18 and 19 for hot-rolled and cold-formed members respectively in their 13th cycles.

The load-displacement relationships show a low stiffness when loading in tension and a possible explanation for this is the elongation of specimens during compression cycles, which are then restraightened during tensile loading. Test data shows that a residual lateral deflection was always present after the initial buckling, which supports this explanation.

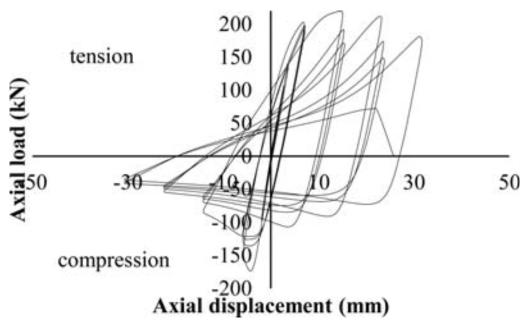

Figure 16. Load-displacement response for CF-F1.

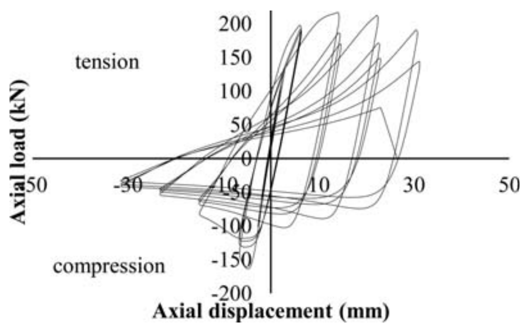

Figure 17. Load-displacement response for CF-F2.

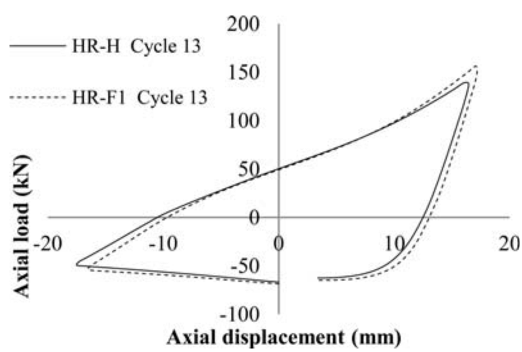

Figure 18. Load-displacement hysteresis for HR-H and HR-F1 in the 13th cycle.

Displacement ductility ratios are presented in Table 6 for each specimen, which is defined as $\mu_\Delta = \delta_{max}/\delta_y$, where δ_{max} is the maximum axial displacement.

Specimen HR-F1 exhibited significantly better ductility than the other five specimens. With the exception of this specimen, values for μ_Δ did not differ between hollow and concrete-filled specimens. Comparing hot-rolled and cold-formed steels, it is found that the former gave a superior performance to the latter in terms of ductility.

The energy dissipation for each member was evaluated using the area under the hysteresis curve and values are presented in Table 6 for the energy dissipated during the 8th, 11th and 14th cycles, and for the total energy dissipated per specimen up to failure.

Generally, cold-formed members dissipated more energy per cycle, as a results of a having a higher yield stress but did not endure as many cycles as the hot-rolled specimens, leading to lower overall amounts of energy dissipation. This is illustrated in Figure 20.

The presence of concrete does not appear to increase the energy dissipated per cycle, but prolongs the duration of the specimen enabling it to withstand a greater number of cycles prior to failure. This is particularly noticeable for specimen HR-F1, which dissipated a total of 96 kNm – almost three times greater than the hollow equivalent, HR-H. Figures 21 and 22 compare the energy dissipated between filled and hollow specimens for hot-rolled and void-formed steels respectively.

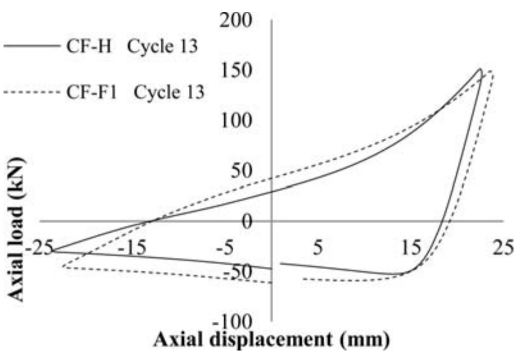

Figure 19. Load-displacement hysteresis for CF-H and CF-F1 in the 13th cycle.

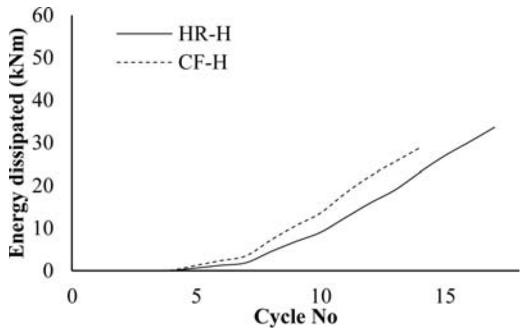

Figure 20. Energy dissipation for HR-H and CF-H.

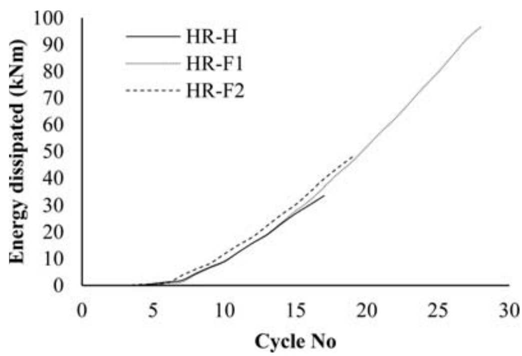

Figure 21. Energy dissipation for hot-rolled test specimens.

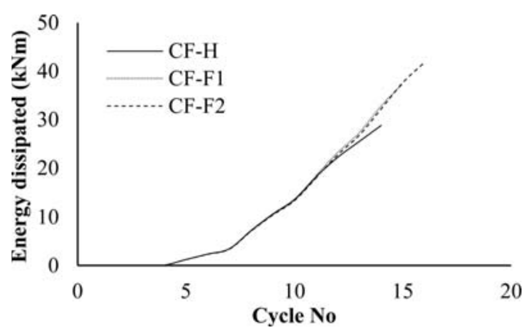

Figure 22. Energy dissipation for cold-formed test specimens.

Table 6. Energy dissipated at various stages of testing.

specimen	μ_Δ	Energy dissipated in 8th cycle kNm	Energy dissipated in 11th cycle kNm	Energy dissipated in 14th cycle kNm	Total energy kNm
HR-H	10	2.6	3.5	4.1	33.6
CF-H	8	4.4	5.3	2.5	28.8
HR-F1	16	3.2	4.1	4.8	96.7
HR-F2	10	2.4	3.3	4.0	48.0
CF-F1	8	4.5	5.5	6.1	37.4
CF-F2	8	4.4	5.4	6.1	41.8

3 CONCLUSIONS

It has been shown that concrete-infill enhances the performance of circular tubular steel members, although perhaps not to the same extent as rectangular hollow members. The uniformity of the cross-section ensures a more stable response, and provides superior durability under seismic loading.

Now that intermediate-length specimens have been tested, there is scope for further research looking at the resistance of longer members, with a non-dimensional slenderness in the region of 2. The effect of infill and cross-section shape for more slender circular members will need to be explored in a similar manner to establish relationships between non-dimensional slenderness and a variety of parameters, such as ductility, strength degradation and energy dissipation.

ACKNOWLEDGEMENT

The authors wish to thank TATA steel and Mr. Trevor Mustard for their support in this project. The authors would also like to thank Professors Roger Johnson and Toby Mottram from the University of Warwick and Professor Ahmed Elghazouli from Imperial College London for their technical guidance in carrying out this research.

REFERENCES

Broderick, B.M., Goggins, J.M. & Elghazouli, A.Y. 2005. Cyclic performance of steel and composite bracing members, *Journal of Constructional Steel Research* 61(4): 493–514.

Elchalakani, M., Zhao, X.L. & Grzebieta, R. 2003. Tests of cold-formed circular tubular braces under cyclic axial loading, *Journal of Structural Engineering* 129(4): 507–14.

Lee, C., Grzebieta, R.H. & Zhao, X.L. 2000. The importance of further studies on the capacity evaluation of concrete-filled steel tubes under large deformation cyclic loading, *Structural Failure and Plasticity*: 685–690, Oxford: Pergamon.

Liu, Z. & Goel, S.C. 1988. Cyclic load behavior of concrete-filled tubular braces, *Journal of Structural Engineering* 114(7): 1488–1506.

Martinez-Saucedo G., Tremblay, R. & Packer, J.A. 2008b. Seismic response if circular hollow section braces with slotted end connections. *Proceedings of the 12*th*International Symposium on Tubular Structures*: 227–233, Shanghai.

Nip, K.H., Gardner, L. & Elghazouli, A.Y. 2010. Cyclic testing and numerical modelling of carbon steel and stainless steel tubular bracing members, *Engineering Structures* 32(2): 424–41.

BS EN-1993-1-1. 2005. Design of steel structures, Part 1-1: General rules and rules for buildings. European Standard, CEN.

BS EN-1994-1-1. 2004. Design of composite steel and concrete structures, Part 1-1: General rules and rules for buildings. European Standard, CEN.

BS EN 1998-1. 2004. Design of structures for earthquake resistance – Part 1: General rules, seismic actions and rules for buildings. European Standard, CEN.

BS EN ISO 6892-1. 2009. Metallic materials – Tensile testing – Method of test at room temperature. European Standard, CEN.

BS EN 12390-3. 2002. Testing hardened concrete: Part 3: Compressive strength of test specimens. European Standard, CEN.

ECCS. 1986. Recommended Testing Procedure for Assessing the Behaviour of Structural Steel Elements under Cyclic Load. Brussels.

Tubular Structures XIV – Gardner (Ed.)
© 2012 Taylor & Francis Group, London, ISBN 978-0-415-62137-3

An experimental study of high-strength CFST columns subjected to axial load and non-constant bending moments

D. Hernández-Figueirido
Dpt. Ing Mecánica y Construcción, Universitat Jaume I, Castellón, Spain

M.L. Romero, J.L. Bonet & A. Hospitaler
Instituto de Ciencia y Tecnología del Hormigón, Universitat Politècnica de València, Valencia, Spain

ABSTRACT: This paper describes 49 experimental tests conducted on rectangular and square tubular columns filled with high strength concrete subjected to a non-constant bending moment distribution. The test parameters were the length (2, 3 and 4 m), the cross-section aspect ratio (square or rectangular), the wall thickness (4 or 5 mm), and the ratio of the top and bottom first order eccentricities $r = e_{top}/e_{bottom}$ (1, 0.5, 0 and −0.5). The effect of slenderness combined with the influence of variable curvature is compared with the design loads from Eurocode 4. The results show that for the slender elements of this experimental campaign the code presents an error close to 4%. It proves that this standard is applicable to high strength concrete, although the concrete tested is outside the upper bound of Eurocode 4 specifications.

1 INTRODUCTION

The use of normal strength concrete-filled tubular (CFT) columns has been widespread for some decades due to their high stiffness, ductility, and fire resistance, and has been well summarized by Shams & Saadeghvaziri (1997), Shanmugam & Lakshmi (2001), Gourley et al. (2008), and more recently by Zhao et al. (2010). Moreover, the use of high-strength concrete ($f'_c > 50$ MPa) has become more frequent due to advances in technology, mainly those affecting elements subjected to high compression. However, it was concluded from previous studies that further experimental tests for high strength concrete-filled (HSC) columns were necessary, Gourley et al. (2008).

Different authors stated that as high strength concrete is characterized by low dilatation, a substantial confinement effect does not occur (Johansson & Gylltoft 2001, Zeghiche & Chaoui 2005). Furthermore, for rectangular CFT columns the confinement is generally neglected due to non-uniform lateral pressure distribution across the section.

Several authors have presented studies for slender rectangular CFT columns where an axial load is applied in combination with an eccentricity in the load. In most cases the eccentricity is the same at both ends, producing a constant bending moment distribution, i.e. constant curvature. The first tests were performed by Knowles & Park (1969), followed later by Bridge (1976). Han (2000) studied tubular columns with a high slenderness ratio but with normal strength concrete, concluding that the strength of the concrete has very little influence on the ultimate capacity given that the failure load is governed by the flexural rigidity. Recently Yu et al. (2008) published the results of research on circular, square, short and long CFTs filled with high performance self-consolidating concrete. The results were in agreement with design values calculated using different design codes. Also, Han & Yao (2003, 2004), Lee (2007) and Zhang & Guo (2007) have performed experimental tests combining slender rectangular CFT columns with HSC and eccentricity.

Though a large body of research for CFT columns exists, it was found that cases where the eccentricity is different at both ends of the columns, producing a non-constant bending moment, were not well studied in the bibliography. Besides, if one of the eccentricities is positive and the other negative a double curvature in the element occurs. This problem directly affects slender, but not stub, columns as it changes the values of second order bending moments. Eurocode 4 (2004) provide an equivalent moment factor (β and C_m respectively) that depends on the type of bending diagram. Goode (2008) compiled the results of several tests, and compared them with Eurocode 4 (2004) provisions, reaching the conclusion that although for circular sections the provisions could be extended to a strength of concrete of 75 MPa, more tests are needed mainly for long circular tubular columns in combination with a bending moment. He did not present any results regarding double curvature.

For circular columns, only Kilpatrick & Rangan (1999), and Zeghiche & Chaoui (2005) have performed tests with different eccentricities at both ends. In the latter, the test parameters were slenderness, eccentricity, and single and double curvature. The comparison with EC4 provisions results on the unsafe side for variable curvature. They stated that more numerical and experimental tests should be performed to check the validity of the buckling design methods of Eurocode 4 (2004) in the case of high strength concrete for single and double curvature.

The authors compiled and updated the databases of Kim (2005) and Goode (2008) totaling close to 1400 rectangular experimental tests. From this new database, it was concluded that there is a lack, both for normal and high strength concrete, of tests for columns with non-constant bending moment.

For rectangular columns, Wang (1999) presented an experimental study where eight tests on normal strength concrete-filled columns were carried out with end eccentricities which produced moments other than constant curvature bending. He concluded that Eurocode 4 was safe but very conservative in some cases.

The authors (Hernandez-Figueirido et al. 2011) presented previously the first results of an experimental campaign for rectangular CFT columns for both constant and variable curvature with normal and high strength concrete but for columns with a length of 2 m and a medium slenderness.

This paper supplements this previous research with the results of the variable curvature tests for rectangular columns for cases with different lengths ($L = 2$, 3 and 4 meters) studying the effect of the slenderness on high strength concrete-filled columns. The test parameters were the length, the type of cross-section, the thickness (4 or 5 mm) and the ratio of the top and bottom first order eccentricities $r = e_{top}/e_{bottom}$ (1.0, 0.5, 0.0 and −0.5). In these tests the load eccentricity at the ends is fixed and the maximum axial load of the column is evaluated and compared with the design loads from Eurocode 4 (2004).

2 EXPERIMENTAL TESTS

2.1 *Introduction*

In this experimental program forty-six tests were carried out on high strength concrete-filled columns, referring to Table 1. Tests were repeated on three additional columns to demonstrate the reliability of the experiments, cases 2, 8 and 41, adding up to a total of forty-nine tests.

The aim of this test matrix was to investigate the effect that the slenderness of the column in combination with a variable bending moment has on their behavior, focusing on HSC. The effective buckling lengths of the columns (L_b) are the length of the tubes plus 135 mm, since to obtain the exact distance between the hinges it is necessary to add the special assembly length. The nominal cross-section of the tubes (height h × width b × thickness t) measured 100 × 100 × 4 mm, 100 × 150 × 4 mm, 100 × 150 × 5 mm, respectively. The thicknesses of the tubes were selected in order to avoid local buckling following Eurocode 4 (2004).

In this paper the nominal strengths of concrete are always 90 MPa and the axial load is applied with two different eccentricities at the top (20 or 50 mm) to strong axis bending to avoid any possible interaction between the strong and weak axes. The initial out-of-straightness of the steel tubes was not measured due to its difficulty. However, they accomplish the European fabrication standard EN 10219 what limits the maximum value to L/333.

All of the tests were performed in the laboratory of the Department of Mechanical Engineering and Construction of the Universitat Jaume I in Castellon, Spain.

2.2 *Material properties*

The hollow steel tubes were cold formed and supplied by a manufacturer. The nominal yielding strength of the steel was 275 MPa with an ultimate nominal strength of 330 MPa. However, the real strength (f_y) of the empty tubes was obtained by coupon test and compression stub section, referring to Table 1. The modulus of elasticity Es of the steel was set by European standards with a value of 210 GPa.

All columns were cast using concrete batched in the laboratory obtaining an approximate nominal concrete strength of 90 MPa (HSC). The concrete compressive strength f_c (termed also f'_c in ASIC code) was determined from a mean of three 150 × 300 mm cylinders using standard tests. All samples were tested on the same day as the column tests, 28 days, and the results are given in Table 1.

2.3 *Manufacture of the columns*

A 350 mm × 350 mm × 10 mm steel plate was welded to the bottom of each empty steel tube to facilitate the casting of the fresh concrete and to join the element to the pinned support assembly. The elements were then cast in a vertical position and the concrete was vibrated every 0.5 m with a needle vibrator. The tubes were overfilled with 1 cm of concrete and later covered with wet cloth. Prior to the test, the residual layer of concrete was smoothed and the columns were sealed off with another similar welded plate to ensure perfect contact between the plates and the steel and concrete core.

2.4 *Test setup and procedure*

The specimens were tested in a special 5000 kN capacity testing machine in a horizontal position, Figure 1.

The eccentricity of the compressive load applied was equal at both ends in some cases (20 mm or 50 mm), so the columns were subjected to constant curvature bending, whereas in the remaining cases a non-constant bending moment was produced.

Table 1. Tests properties and results.

Test	b	h	t	L (mm)	e_{top} (mm)	e_{bot} (mm)	r	f_y (MPa)	f_c (MPa)	N_{exp} (kN)
1	100	100	4	2135	20	−10	−0.5	346	92	737
2	100	100	4	2135	20	−10	−0.5	371	93	758
3	100	100	4	2135	20	0	0	363	89	652
4	100	100	4	2135	20	10	0.5	280	93	525
5	100	100	4	2135	20	20	1.0	375	88	490
6	100	100	4	2135	50	25	0.5	358	87	383
7	100	100	4	2135	50	50	1.0	358	91	321
8	100	100	4	2135	50	50	1.0	371	93	323
9	100	100	4	3135	20	−10	−0.5	353	97	502
10	100	100	4	3135	20	0	0	363	92	410
11	100	100	4	3135	20	10	0.5	280	86	363
12	100	100	4	3135	20	20	1.0	375	74	381
13	100	100	4	3135	50	−25	−0.5	358	96	357
14	100	100	4	3135	50	0	0	346	92	316
15	100	100	4	3135	50	25	0.5	358	90	218
16	100	100	4	3135	50	50	1.0	292	87	230
17	100	100	4	4135	20	−10	−0.5	280	88	367
18	100	100	4	4135	20	10	0	280	96	254
19	100	100	4	4135	20	20	1.0	280	94	220
20	100	100	4	4135	50	25	0.5	369	92	184
21	150	100	4	2135	20	−10	−0.5	268	93	945
22	150	100	4	2135	20	0	0	280	90	926
23	150	100	4	2135	20	10	0.5	342	90	850
24	150	100	4	2135	20	20	1	298	86	804
25	150	100	4	2135	50	25	0.5	424	90	463
26	150	100	4	2135	50	50	1	341	77	466
27	150	100	4	3135	20	−10	−0.5	280	91	690
28	150	100	4	3135	20	0	0	280	84	562
29	150	100	4	3135	20	10	0.5	342	89	501
30	150	100	4	3135	20	20	1.0	298	84	460
31	150	100	4	3135	50	−25	−0.5	308	92	502
32	150	100	4	3135	50	0	0	362	91	430
33	150	100	4	3135	50	25	0.5	312	91	287
34	150	100	4	3135	50	50	1	341	89	309
35	150	100	5	2135	20	−10	−0.5	304	93	104
36	150	100	5	2135	20	0	0	370	89	106
37	150	100	5	2135	20	10	0.5	424	86	981
38	150	100	5	2135	20	20	1.0	459	83	935
39	150	100	5	2135	50	25	0.5	293	85	526
40	150	100	5	2135	50	50	1.0	368	84	528
41	150	100	5	2135	50	50	1	336	92	458
44	150	100	5	3135	20	−10	−0.5	336	91	692
43	150	100	5	3135	20	0	0	370	79	690
44	150	100	5	3135	20	10	0.5	424	85	622
45	150	100	5	3135	20	20	1.0	459	91	573
46	150	100	5	3135	50	−25	−0.5	306	85	548
47	150	100	5	3135	50	0	0	396	87	456
48	150	100	5	3135	50	25	0.5	332	91	328
49	150	100	5	3135	50	50	1.0	368	82	381

It was necessary to build up special assemblies at the pinned ends to apply the load with different eccentricities while maintaining the column in a horizontal position, Fig 1.b, and c.

This figure presents a general view of the test for a 2-meter-long specimen where a special anti-torsion steel frame was built in order to avoid bottom hinge torsion rotation. Five LVDTs were used to symmetrically measure the deflection of the column at mid length (0.5 L) and also at four additional levels (0.25 L, 0.37 L, 0.625 L, 0.75 L).

Once the specimen was put in place, it was tested using a displacement control protocol in order to measure post-peak behavior.

3 RESULTS

3.1 *Force displacement*

Table 1 lists the maximum axial load (N_{exp}) for the forty-nine tests.

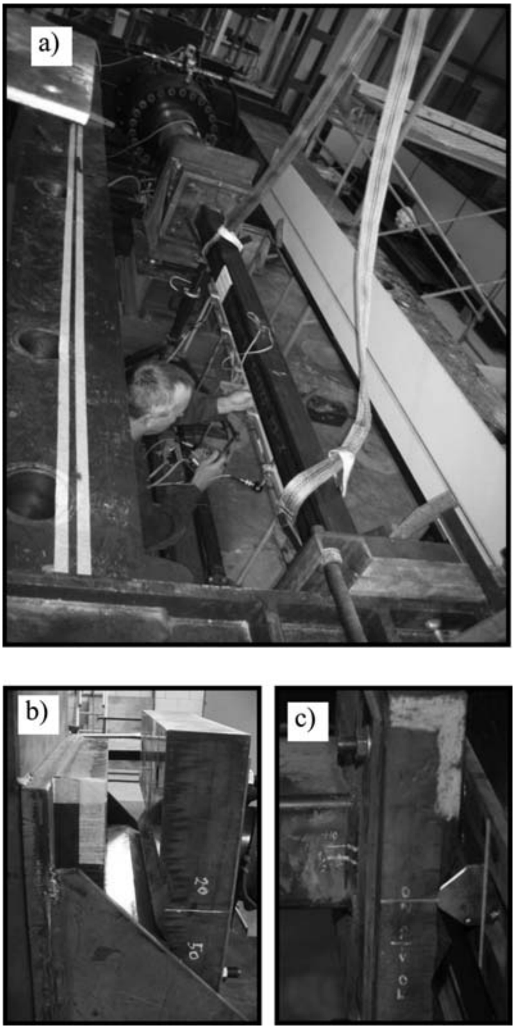

Figure 1. General view of the tests.

For a better understanding of the influence of the second order effects, Fig. 2 presents the force-displacement curves for square cross-section ($100 \times 100 \times 4$) and for tests with different lengths, but only with opposing eccentricity ratios $r = 1.0$ and -0.5 for simplicity.

The top eccentricity $e_{top} = 20$ mm is presented in Fig. 2a and the top eccentricity $e_{top} = 50$ mm is presented in Fig. 2b in order to study the effect of this parameter on global behavior. It is worth noting that there is a lower number of tests with $e_{top} = 50$ mm. In these tests, the general tendency of the curves is as expected: for a given length when the eccentricity at the bottom (minimum) is decreased (from $r = 1$ to $r = -0.5$), therefore producing variable curvature, Fig. 2a, the maximum load is increased (and the midspan lateral displacement reduced) because the second order bending moment is reduced. Also,

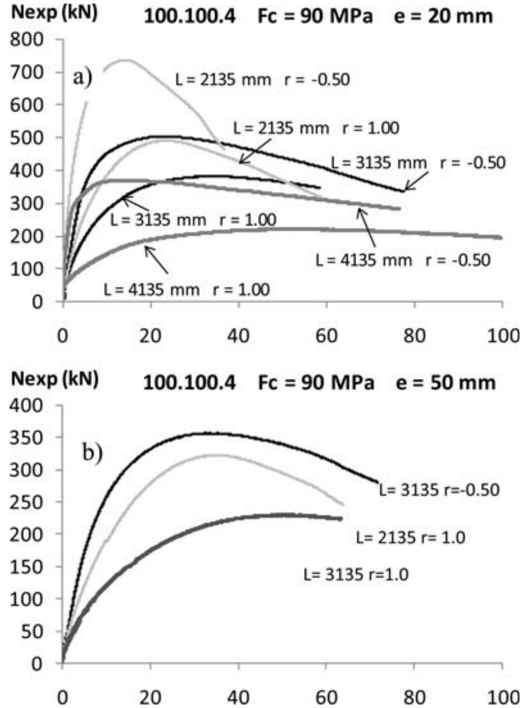

Figure 2. Axial load versus midspan displacement.

if cases with the same eccentricity ratio but different lengths are compared, the maximum axial load is higher if the length is lower.

It is interesting to observe that ductile post-peak behavior is achieved for all cases, but it is always slightly reduced for cases with lower length in comparison to those with higher length, that is, the slope of the descending branch is more pronounced for lower slenderness. Moreover, the cases with $r = -0.5$ differ from the cases with $r = 1.0$ in the descending branch. The slope is more gradual for cases with constant curvature than for those with variable curvature.

From Table 1, it can be observed that the load is obviously increased when the width or thickness of the tube is increased. The results show for the limited cases analyzed that the slenderness of the section, i.e. width to thickness ratio (B/t), has a lesser effect than directly increasing the area of concrete.

To complete the previous graph, Fig. 3 presents the maximum load N_{max} in terms of eccentricity ratio (e_{top}/e_{bot}) for all tests with the smaller section. From this figure it can be noted that the difference in the ultimate axial load is higher among the cases of 2 and 3 meters than among the cases of 3 and 4 meters.

It is also possible to observe that this difference is higher for the cases of $r = -0.5$ than for those where $r = 1.0$. This is because the problem is clearly governed by the second order effects and the variable bending moment has a higher effect in the cases with lower slenderness. A more in-depth examination of this

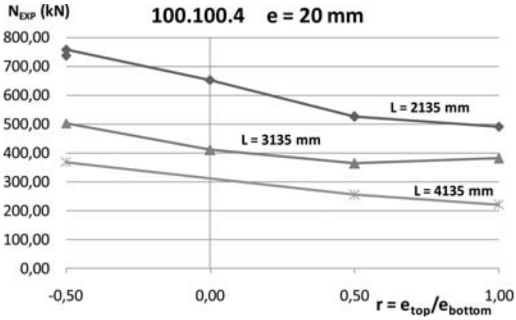

Figure 3. Axial load versus eccentricity ratio.

statement will be presented in the following sections comparing different cases of e_{top}/e_{bottom}.

3.2 *Observation of the deformed shape*

The deformed shape obtained from the 5 LVDTs is not presented in this paper for simplicity. However, from its study, it can be affirmed that the displacements are always in the same direction even in the case of double curvature ($r = -0.5$). It can be noted that for constant curvature the maximum displacement is achieved in the midspan section, producing a symmetrical deformed shape while for double curvature the maximum displacement is located to the left of the midspan section, i.e. closer to the higher eccentricity, producing an unsymmetrical deformed shape.

It is interesting to note that the behavior in terms of the length is different for constant and variable curvature. While for $r = 1$ the maximum displacement is achieved for L = 4135 mm and a lower one for L = 2135 mm, for $r = -0.5$ the maximum displacement is achieved for L = 3135 mm and a lower one for L = 4135 mm, which was initially surprising.

It can also be inferred that for the case of L = 4 meters with $r = -0.5$ the second order effects are lower and the first order curvature (variable) which depends on the length is higher in comparison with $r = 1.0$. This results in the element trying to bend in the negative direction, drastically reducing the lateral deflection.

4 COMPARISON WITH EUROCODE 4 (CEN 2004)

The design of normal-strength concrete-filled tubular columns has to be carried out in Europe following Eurocode 4 (2004) which limits the cylinder strength of concrete to 50 MPa for columns. The experiments in this study aim to clarify whether Eurocode 4 is still applicable to 90 Mpa, and also whether the second order effects, which depend on the slenderness and the eccentricity ratio, are correctly accounted for. This standard affirms that within the column length, second order effects may be allowed for by multiplying the greatest first order design bending moment ($M_{Ed} = N \cdot e_{top}$) by an amplification factor. In addition,

Table 2. Calculation of second order effects in Eurocode 4.

Eurocode 4 (CEN 2004)
$M_{tot} = k \cdot N \cdot e_{top} + k_2 \cdot N \cdot e_0$
$k = \dfrac{\beta}{1 - \dfrac{N_{Ed}}{N_{cr,eff}}}$ $k_2 = \dfrac{1}{1 - \dfrac{N_{Ed}}{N_{cr,eff}}}$
$\beta = 0.66 + 0.44 \cdot \dfrac{M_{top}}{M_{bot}} \geq 0.44$
$N_{cr,eff} = \dfrac{\pi^2 \cdot EI_{eff,2}}{L^2}$
$EI_{eff,2} = 0.9 \cdot (E_s I_s + 0.6 E_{cm} I_c)$
$e_0 = \dfrac{L}{300}$
$E_{cm} = 22000 \cdot \left(\dfrac{f_c}{10}\right)^{0.3}$ (MPa)

the value of the M_{Ed} is incremented in Eurocode 4 including the influence of the member imperfection, $e_0 = L/300$. Table 2 summarizes a comparison of the equations for calculating the second order effects. The remaining part of the description of the design method (interaction diagrams) is not included for simplicity.

Since these test specimens are rectangular, the increment in the resistance of the cross-section due to the confinement effect is ignored and the partial safety factor for steel and concrete is fixed at 1. Table 3 presents a comparison between the experiments (N_{exp}) and the design load of Eurocode 4 (N_{EC4}).

From Table 3 and Fig. 4 it can be stated that for Eurocode 4 (2004) some of the cases are on the unsafe side ($N_{exp}/N_{AISC} < 1$) and others are on the safe side ($N_{exp}/N_{AISC} > 1$), reaching a mean value of 1.04 and a standard deviation of 0.10 was obtained.

It is worth noting that the concrete tested is outside of the upper bound of Eurocode 4 specification. It can be also observed that the cases with higher axial load are always on the safe side.

From a detailed study of Table 3 it can be inferred that Eurocode 4 is safer for $r = -0.5$ than for $r = 1.0$ if the same length is studied. Also the ratio (N_{exp}/N_{code}) error increases in the unsafe side if the length or the eccentricity increases. However there are particular cases for Eurocode 4 code which present excessive unsafe errors. It corresponds to the cases where the second order effects are more important and are due to an overestimation of the flexural stiffness E·I. This indicates that the equation of the stiffness of the section E·I needs correction. Some authors as for instance Tikka and Mirza (2006) have proposed that

Table 3. Error of Eurocode 4.

T	b	h	t	L (mm)	e_{top} (mm)	e_{bot} (mm)	r	N_{exp} (kN)	N_{EC4} (kN)	N_{exp}/N_{EC4}
1	100	100	4	2135	20	−10	−0.5	737	655	1.12
2	100	100	4	2135	20	−10	−0.5	758	655	1.15
3	100	100	4	2135	20	0	0	652	611	1.06
4	100	100	4	2135	20	10	0.5	525	522	1.00
5	100	100	4	2135	20	20	1.0	490	511	0.95
6	100	100	4	2135	50	25	0.5	383	347	1.10
7	100	100	4	2135	50	50	1.0	321	293	1.09
8	100	100	4	2135	50	50	1.0	323	301	1.07
9	100	100	4	3135	20	−10	−0.5	502	450	1.11
10	100	100	4	3135	20	0	0	410	409	1.00
11	100	100	4	3135	20	10	0.5	363	356	1.01
12	100	100	4	3135	20	20	1.0	381	345	1.10
13	100	100	4	3135	50	−25	−0.5	357	332	1.07
14	100	100	4	3135	50	0	0	316	303	1.04
15	100	100	4	3135	50	25	0.5	218	256	0.85
16	100	100	4	3135	50	50	1.0	230	208	1.10
17	100	100	4	4135	20	−10	−0.5	367	287	1.27
18	100	100	4	4135	20	10	0	254	257	0.98
19	100	100	4	4135	20	20	1.0	220	254	0.86
20	100	100	4	4135	50	25	0.5	184	194	0.94
21	150	100	4	2135	20	−10	−0.5	945	829	1.14
22	150	100	4	2135	20	0	0	926	798	1.16
23	150	100	4	2135	20	10	0.5	850	777	1.09
24	150	100	4	2135	20	20	1	804	669	1.20
25	150	100	4	2135	50	25	0.5	463	503	0.92
26	150	100	4	2135	50	50	1	466	402	1.15
27	150	100	4	3135	20	−10	−0.5	690	576	1.19
28	150	100	4	3135	20	0	0	562	522	1.07
29	150	100	4	3135	20	10	0.5	501	515	0.97
30	150	100	4	3135	20	20	1.0	460	453	1.01
31	150	100	4	3135	50	−25	−0.5	502	431	1.16
32	150	100	4	3135	50	0	0	430	403	1.06
33	150	100	4	3135	50	25	0.5	287	335	0.85
34	150	100	4	3135	50	50	1	309	308	1.00
35	150	100	5	2135	20	−10	−0.5	104	962	1.08
36	150	100	5	2135	20	0	0	106	959	1.11
37	150	100	5	2135	20	10	0.5	981	888	1.10
38	150	100	5	2135	20	20	1.0	935	838	1.11
39	150	100	5	2135	50	25	0.5	526	515	1.02
40	150	100	5	2135	50	50	1.0	528	475	1.11
41	150	100	5	2135	50	50	1	458	475	0.96
44	150	100	5	3135	20	−10	−0.5	692	673	1.02
43	150	100	5	3135	20	0	0	690	615	1.12
44	150	100	5	3135	20	10	0.5	622	593	1.04
45	150	100	5	3135	20	20	1.0	573	581	0.98
46	150	100	5	3135	50	−25	−0.5	548	499	1.09
47	150	100	5	3135	50	0	0	456	485	0.93
48	150	100	5	3135	50	25	0.5	328	404	0.81
49	150	100	5	3135	50	50	1.0	381	359	1.06
									Avg.	1.04

the flexural stiffness E·I must dependent not only on the material and geometry but also on the eccentricity and the slenderness.

5 CONCLUSIONS

The paper describes forty-nine experimental tests conducted on rectangular and square tubular columns filled with high strength concrete subjected to axial load and a non-constant bending moment distribution.

The following conclusions can be summarized:

– For a given length, when the eccentricity at the bottom (minimum) is decreased (from $r = 1.0$ to $r = -0.5$), therefore producing variable curvature, the maximum load is increased (and the midspan lateral displacement reduced) since the second order bending moment is reduced. It is interesting

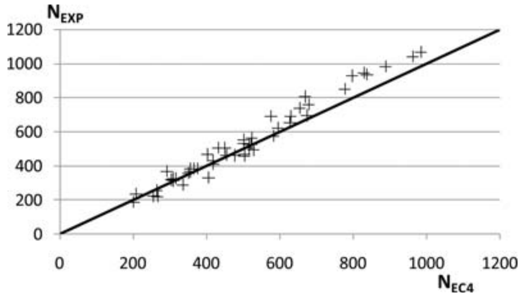

Figure 4. Predicted load of Eurocode 4 versus experimental load.

to observe that ductile post-peak behavior is achieved for all cases, but is always slightly reduced for cases with lower length in comparison with higher length, that is, the slope of the descending branch is more pronounced for lower slenderness. Moreover, the cases with $r = -0.5$ differ from those with $r = 1.0$ in the descending branch. The slope is more gradual for cases with constant curvature than for those with variable curvature.

– For longer elements, the problem is clearly governed by the second order effects and the variable bending moment has a higher effect for lower slenderness.
– It is interesting to observe that the behavior in terms of the length is different for constant and variable curvature. While for $r = 1$ the maximum displacement is achieved for $L = 4135$ mm and the lower one for $L = 2135$ mm, for $r = -0.5$ the maximum displacement is achieved for $L = 3135$ mm and the lower one for $L = 4135$ mm, which was initially surprising. But it can be inferred that for the case of $L = 4$ meters with $r = -0.5$ the second order effects are lower and the first order curvature (double), which depends on the length, is higher in comparison with $r = 1.0$. This results in the element attempting to bend in the negative direction drastically reducing the lateral deflection.
– Second order effects depend not only on the slenderness but also on the eccentricity and the first order bending moment, which agrees with the proposal by other authors (Tikka and Mirza 2006) to combine all the effects together inside the definition of the stiffness E·I, making this dependent not only on the materials and the section, but also on the slenderness and the eccentricity.
– The experimental ultimate load of each test was compared with the design loads from Eurocode 4, presenting an average error close to 5%. The results show for the limited cases tested that this code is applicable to high strength concrete.
– However there are particular cases which present excessive unsafe errors. It corresponds to the cases where the second order effects are more important and are due to an overestimation of the flexural stiffness EI. This result indicates that the equation of the flexural stiffness of the section E·I in combination with the equivalent moment factors (β) need correction.

ACKNOWLEDGEMENTS

The authors wish to express their gratitude to the Spanish Ministry of Science and Innovation for help provided through project BIA2009_9411, to the Spanish Ministry of Education through BIA2005-255, and the European Union for FEDER Funds.

REFERENCES

Bonet, J.L., Miguel, P.F., Fernandez, M.A., Romero, M.L. 2004, Biaxial bending moment magnifier method, Engineering Structures, 26(13): 2007–19.

Bridge, R. Q. 1976, Concrete Filled Steel Tubular Columns, Report No. R283, School of Civil Engineering, University of Sydney, Sydney, Australia.

European Committee of Standardization (CEN). 2004. Eurocode 4: Design of composite steel and concrete structures Part 1-1: General rules and rules for buildings", EN 1994-1-1:2004, Brussels.

Goode, C.D. 2008, Composite columns-1819 tests on concrete filled tube columns compared with Eurocode 4, The Structural Engineer, 86(16): 33-38.

Gourley, B. C., Tort, C., Denavit, M. D., Schiller, P. H., and Hajjar, J. F. 2008. A Synopsis of Studies of the Monotonic and Cyclic Behavior of Concrete-Filled Steel Tube Beam-Columns", Report No. UILU-ENG-2008-1802, Newmark Structural Laboratory Report Series (ISSN 1940-9826), Department of Civil and Environmental Engineering, University of Illinois at Urbana-Champaign, Urbana, Illinois.

Han, L.H., Yao, G.H. 2003, Influence of concrete compaction on the strength of concrete-filled steel RHS columns, Journal of Construction Steel Research, 59(6): 751–67.

Han, L.H, Yao,G.H. 2004, Experimental behaviour of thin-walled hollow structural steel (HSS) columns filled with self-consolidating concrete (SCC), Thin-Walled Structures 42: 1357–1377.

Han, L.H. 2000, Tests on concrete filled steel tubular columns with high slenderness ratio, Advances in Structural Engineering, 3(4): 337–344.

Hernández-Figueirido, D., Romero, M.L., Bonet, J.L., Montalvá, J.M. 2012, Ultimate capacity of rectangular concrete-filled steel tubular columns under unequal load eccentricities", Journal of constructional steel research, 68(1): 107–117.

Johansson, M., Gylltoft, K. 2001, Structural behaviour of slender circular steel-concrete composite columns under various means of load application, Steel and Composite Structures, 1(4): 393–410.

Kilpatrick, A.E., Rangan, B.V. 1999, Tests on High-Strength Concrete-Filled Steel Tubular Columns, ACI Structural journal, 96 (2): 268–275.

Kim, D.K. 2005, A database for composite columns, Ms Thesis. Georgia Tech University. U.S.A.

Knowles, R. B., Park, R. 1969, Strength of Concrete Filled Steel Tubular Columns, Journal of the Structural Division, ASCE, 95(12): 2565–2587.

Lee, S.J. 2007, Capacity and the moment-curvature relationship of high-strength concrete filled steel tube columns under eccentric loads, Steel and Composite Structures, 7(2), 135–160.

Perea, T. 2010. Analytical and experimental study on slender concrete-filled steel tube columns and beam-columns. Ph.D. thesis, Georgia Institute of Technology, Georgia, GA.

Portoles, J.M., Romero, M.L., Bonet, J.L., Filippou, F.C. 2011, Experimental study of high strength concrete-filled circular tubular columns under eccentric loading, Journal of constructional steel research, 67(4): 623–633

Shams, M., Saadeghvaziri, M.A. 1997, State of the art of concrete-filled steel tubular columns, ACI Structural Journal, 94 (5): 558–571.

Shanmugam, N.E., Lakshmi, B. 2001, State of the art report on steel-concrete composite columns, Journal of constructional steel research, 57 (10): 1041–1080.

Tikka, T.K., Mirza, S.A. 2006, Nonlinear equation for flexural stiffness of slender composite columns in major axis bending, Journal of structural engineering, 132 (3): 387–399.

Wang, Y.C. 1999, Tests on slender composite columns, Journal of constructional steel research, 49(1): 25–41.

Yu, Q., Tao, Z., Wu, Y.X. 2008, Experimental behaviour of high performance concrete-filled steel tubular columns, Thin-Walled Struct, 46: 362–370.

Zeghiche, J. and Chaoui, K. 2005. An experimental behaviour of concrete-filled steel tubular columns, Journal of constructional steel research, 61(1): 53–66.

Zhang, S., Guo, L. 2007, Behaviour of High Strength Concrete-Filled Slender RHS Steel Tubes, Advances in Structural Engineering, 10(4): 337–351.

Zhao, X.L., Han, L.H. and Lu, H. 2010. Concrete-filled tubular members. 1st Ed. Oxon: Spon Press.

Tubular Structures XIV – Gardner (Ed.)
© 2012 Taylor & Francis Group, London, ISBN 978-0-415-62137-3

Static behavior of T-shaped concrete-filled steel tubular columns subjected to eccentric compressive loads

H. Yang & S.M. Zhang
Harbin Institute of Technology, Harbin, China

Y.L. Yang
Key Laboratory of Mechanics on Disaster and Environment in Western China Ministry of Education, Lanzhou, China; Lanzhou University, Lanzhou, China

ABSTRACT: Special-shaped column frame structures improve residential architectural space, by eliminating the exposure of column corners to indoor space. Due to improvement in constraint effect for concrete, special-shaped Concrete-Filled Steel Tubular (CFST) columns are expected to have advantages in mechanical behavior. In the meanwhile, steel plates' premature local buckling and concave corner's separation between steel tube and concrete should be given more attention. The tensile bar stiffener, welded on inside tube surfaces, was introduced in this paper. Experimental study of 4 T-shaped columns subjected to eccentric compressive loads was carried out. Parametric impact analysis was emphasized on the constraint effect, the eccentricity and the specimen type. Failure modes and static mechanical properties were investigated. Experimental results showed that: the tensile bar stiffener effectively restrains the deformation at welds of steel plates and concave corners; the CFST specimens are provided with better comprehensive mechanical performance, especially for the stiffened CFST specimens.

1 INTRODUCTION

Columns in traditional frame structures, with corners extended into indoor space, normally have larger cross-sectional depths than those of adjacent infilled walls, leading to the reduction of usable utilization area and disturbance to indoor environment (Figure 1). Recently, special-shaped columns, as an improved architectural approach, have been increasingly introduced into residential and commercial buildings. Smooth jointing of special-shaped columns and adjacent infilled walls guarantees the efficiency of indoor space and useability of corner locations (Figure 2).

Systematic research and extensive engineering practice is mainly on the RC special-shaped column. Early studies focused on the static behavior of T-shaped and L-shaped stubs, subjected to axial compressive load and biaxial eccentric compressive load, based on which, resistance interaction curves for practice were proposedby Joaquin (1979), Cheng & Hsu (1989), Mallikarjuna & Mahadevappa (1992), Dundar & Sahin (1993) and Yau (1993). Since 2000, with the development of housing industry in China, further study carried out extensively by Chinese researchers, such as Zhang & Ye (2003), Cao (2005) and Wang & Shen (2006), has concentrated on the comprehensive static and seismic behavior, especially for members in structural systems, directly for engineering applications.

The irregularity in cross section of special-shaped column brings about disadvantages in mechanical behavior, and leads to limitations in its seismic

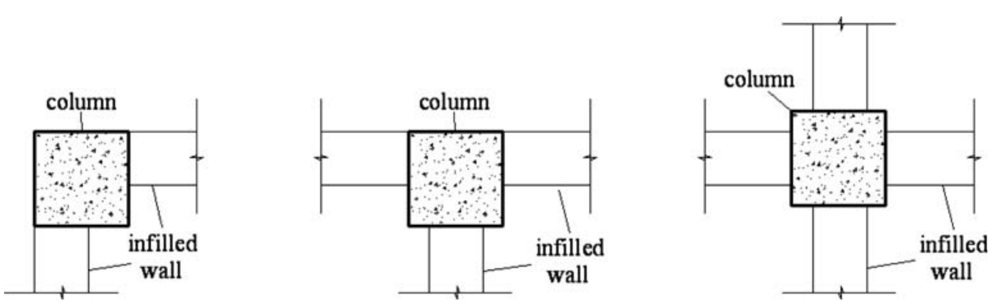

Figure 1. Joints in frame structure with rectangular columns.

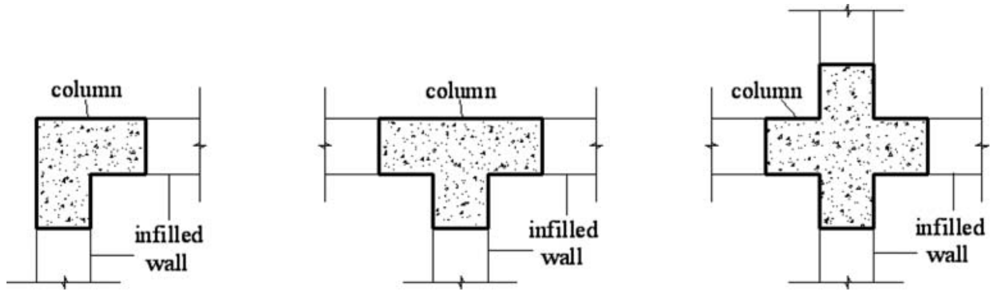

Figure 2. Joints in frame structure with special-shaped columns.

performance: only apply to 8-degree seismic fortification zone (0.2 g) or below, and subjected to rigorous applicable maximum building height restrictions, compared with that of rectangular columns. These limitations are based on the China National code – Technical specification for concrete structures with specially shaped columns (JGJ 149-2006/JGJ 514-2006), which focuses on the special-shaped columns.

Scholars in China have engaged in research and promotion of special-shaped composite columns to improve their seismic behavior, e.g. CFST and steel reinforced concrete (SRC) columns. Research on special-shaped CFST columns have focused on postponing the buckling of steel tubes and the constraint effect for concrete, therefore stiffeners were employed in the special-shaped tube. Pulled binding bars by Cai & He (2008) and ribs by Chen (2003) were adopted in axially loaded test research on T-shaped, L-shaped CFST stubs; bar stiffeners researched by Wang et al. (2009) and Yang et al. (2010) were introduced in static and pseudo static experiments, and preliminary achievements were made. The research mentioned above, nevertheless, is inadequate for engineering application and complementary systematic research should be carried out.

An experiment on T-shaped CFST columns subjected to eccentric compressive load was carried out in this paper. Tensile bar stiffeners were introduced in CFST specimens to postpone the tubes' buckling. Failure modes and static behavior of the specimens were investigated, and mechanical behavior of specimens was properly evaluated.

2 EXPERIMENTAL STUDY

2.1 *Details of specimens*

An experiment on T-shaped columns subjected to eccentric compressive load was carried out. Specimens, basic information of which is summarized in Table 1, consist of 4 eccentrically loaded specimens. Except for specimen type, the eccentricity parameter, deviating toward the web, was investigated. Restricted by loading device and measuring apparatus, specimens were designed with similarity ratio of 1:2, with the length of specimens being 1500 mm. The cross sectional dimensions and constituents are demonstrated in Figure 3.

Table 1. Parameters of specimens.

Specimen	Specimen type	Eccentricity (mm)
TEC	Reinforced concrete	50
TES	Concrete-filled steel tube	50
TESS-1	Stiffened concrete-filled steel tube	25
TESS-2	Stiffened concrete-filled steel tube	50

To postpone or restrain local buckling of T-shaped tubes, tensile bars as stiffeners were welded on the internal tube surfaces and concave corners, with longitudinal weld spacing of 100 mm and with cross sectional distribution shown in Figure 3c. The tensile bar employs straight hot-rolled plane bars. Holes, on the tube, with diameters slightly larger than those of the stiffeners, were drilled and reserved for the stiffeners to pass through and to be welded at both ends.

2.2 *Material properties*

According to the Chinese National standard – Metallic materials-tensile testing at ambient temperature (GB/T228-2002), mechanical properties of the steel plate and reinforcement bar were tested, and their material properties are collected in Table 2 and Table 3.

2.3 *Experimental devices and measuring apparatus*

The experiment was carried out at the Structural and Seismic Test Research Center, Harbin Institute of Technology. A 500t computerised OSD hydraulic pressure press was used as the loading device, with two articulated rigid loading pads at the top and bottom, in which the bottom pad lifted the specimen and the top kept motionless.

In the eccentrically loaded specimen experiment, a knife-edge articulation system was sandwiched between the loading pad and specimen, to simulate articulated boundary conditions. The knife-edge articulation system consists of two close engaged parts: one rigid steel plate with a centered triangular convex

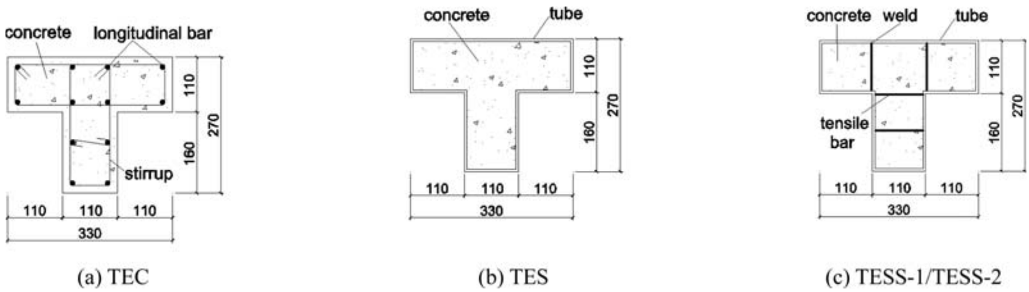

Figure 3. Cross-sectional dimensions of specimens.

Table 2. Material mechanical properties of RC specimens.

Specimen	Longitudinal bar Yielding strength (N/mm^2)	Longitudinal bar Diameter (mm)	Stirrup Yielding strength (N/mm^2)	Stirrup Diameter (mm)	Concrete Prismatic compressive strength (N/mm^2)
TEC	353	12.1	373	6.5	37.5

Table 3. Material mechanical properties of CFST specimens.

Specimen	Steel tube Yielding strength (N/mm^2)	Steel tube Thickness (mm)	Stiffener Yielding strength (N/mm^2)	Stiffener Diameter (mm)	Concrete Prismatic compressive strength (N/mm^2)
TES	315	3.49	—	—	37.5
TESS-1/2	315	3.49	304	8.0	37.5

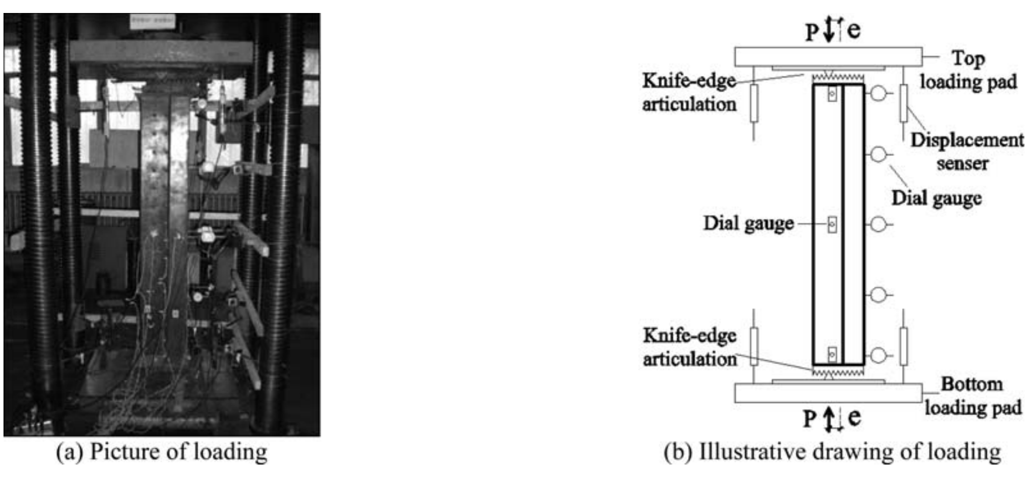

Figure 4. Loading devises and measuring apparatus in eccentric compressive test.

fixed on the loading pad and another rigid steel plate with saw-tooth triangular concaves fixed on the specimen. The magnitude of eccentricity is adjusted with different engaged location of triangular convex on the saw-tooth triangular concaves (shown in Figure 4).

The actual load was real-time monitored on the pressure press and recorded every loading step. Displacement sensors were arranged to measure vertical displacement (shown in Figure 4). Five dial gauges were arranged in a deforming plane, quartering the